4. Kinetics of Gasification Reactions and Reactor Design

In the previous section, the reactor performance was discussed mainly from the thermodynamic viewpoint. In this section, the kinetics of each of the reactions taking place in the gasifier is discussed first. In the subsequent section, the reaction kinetic model developed is combined with reactor flow models for the simulation and optimization of the gasifier performance. A detail discussion of models of solid-gas reactions system can be found elsewhere [34-37, 39, 40].

Most coals are made up of a number of macerals. Carbons derived from different macerals differ in reactivity. As gasification progresses, a decline in rate is usually observed since carbon of progressively lower reactivity remains. It has been observed that, upon heating, coal first becomes metaplastic and gives off volatile matter leaving a rather stable coke. Thus, coal or char may be regarded to be composed of two distinguished portions differing greatly in reactivity. The highly reactive portion is related to the volatile portion of coal characterized by the aliphatic hydrocarbon side chain, and to oxygenated functional groups present. The low reactive portion is the residual carbonaceous coke. Thus, the gasification of coal at elevated temperatures can be divided into the first and second phase reactions; each reaction represents one of the two distinctly different reactivities of carbon present in coal.

4.1 Oxygen-Steam System

As has already been discussed in detail, many reactions are

possible in a gasifier. In oxygen-steam gasifiers, the following reactions are most important:

$$C + aO_2 = (2-2a)CO + (-1+2a)CO_2$$

$$C + H_2O = CO + H_2$$

$$H_2O + CO = H_2 + CO_2$$

The stoichiometric coefficient "a" in the carbon-oxygen reaction depends on the temperature as well as the type of coal. It has been shown [19] that when the temperature is low, the coefficient "a" is approximately unity, producing mostly carbon dioxide. On the other hand, at high temperatures "a" decreases to 0.5 producing mostly carbon monoxide. The rate of oxidation of carbon is studied by many investigators, and is summarized in the book "Combustion of Pulverized Coal" by Field, Gill, Morgan, and Hawksley [8]. Since this reaction takes place much faster than the other reactions, the reaction practically reaches the completion. Thus, the kinetics of this reaction does not materially affect the reactor performance. However, the carbon-steam reaction is a rather slow reaction, and its kinetics does affect the reactor performance.

The kinetics of the carbon-steam reaction is discussed in detail by Von Fredersdorff [24]. The rate expression based on Langmuir's adsorption mechanism is widely applied for the carbon-steam reaction.

$$\text{Rate} = \frac{kP_{H_2O}}{1 + aP_{H_2O} + bP_{H_2}}$$

Although the reactor flow model developed [see Appendix A] is capable of adopting this type of rate expression without difficulty, the Langmuir type expression proved to be too complicated to justify the accuracy of rate data available. The rate expression involves at least three adjustable constants, all of which vary widely depending on the investigator [19]. The reaction of steam with coal is much more complicated than with pure carbon introducing additional uncertainties into the already complex form of rate expression based on the adsorption mechanism. Accordingly, the following simpler rate equation with only one rate constant was adopted in this study.

$$\text{Rate} = k_v\left(C_{H_2O} - \frac{C_{H_2} \cdot C_{CO} RT}{K}\right) \left[\frac{\text{mole-carbon reacted}}{(\text{mole carbon left})(\text{sec})}\right]$$

The values of k_v are computed from rates reported in the literature shown in Table IV-7 and represented in Figure IV-24. Since, in some cases, k_v was calculated from adsorption type expression, the constants for these cases became dependent on hydrogen and/or steam partial pressure. The pressures represented by the lines shown in Figure IV-24 are listed in Table IV-7. The rate constants for lines 6,7,8,10, and 11, which make one group, are much lower than those of line 1 to 5, and 9, which constitute another group. In the former group, carbons employed in the reactions were more graphatized resulting in low rate constants. Furthermore, the experiments of the former group were performed mostly at high pressures so that the rate was retarded by higher hydrogen partial pressure and steam partial pressure.

Steam-char reaction at high pressures containing a large

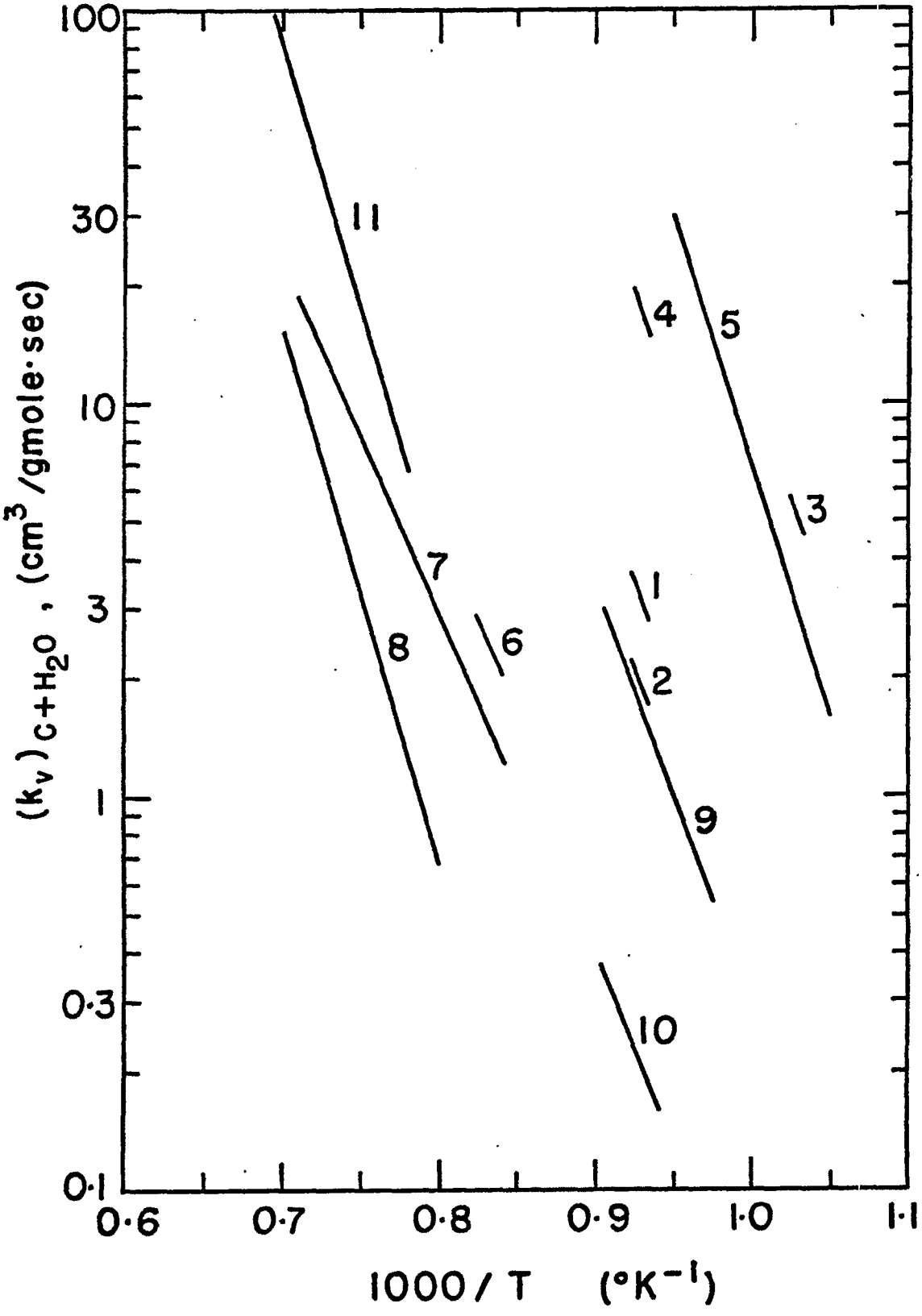

Figure IV-24 Summary of Rate Constants for Carbon-Steam Reaction from the Previous Investigators.

Table IV-7 Summary of Investigation of Steam Reactions With Coal, Char, and Carbon

Line	Investigators	Material	Total Pressure (atm)	Reference
1,2,	Jolly & Pohl	coke	1	14
3,4,	Gadsby, Hinshellwood, & Sykes	nut char coal char	1	10
5	Long & Sykes	coconut shell charcoal	0.2∿1	18
6	Feldkirchner & Linden	low temperature bituminous coal char	103	6
7	Feldkirchner & Huebler	low temperature bituminous coal char	69	5
8	Von Fredersdorff	coal tar, pitch, coke	1∿3.5	24
9,10,	Blackwood & McGrory	coconut carbon	1∿50	1
11	Ergun & Metsen	foundry coke	1	4

fraction of steam seems to show that the reaction is nearly independent of the steam concentration [25] in line with adsorption mechanism.

The water-gas shift reaction on the coal surface, which takes place simultaneously with steam carbon reaction, has not been studied in detail. Thus, a similar rate expression as used in catalytic shift reaction is adopted in this study. Accordingly,

$$\text{Rate} = k_v\left(C_{CO} - \frac{C_{H_2} C_{CO_2}}{K C_{H_2O}}\right)$$

The rate constant "k_v" is computed based on line 2 of Figure IV-25. The values of equilibrium constants are given in Figure V-1 of Chapter V.

4.2 Hydrogen-Steam System

In the hydrogen-steam system, the methane forming reaction becomes as important as the carbon-steam and water-gas shift reactions.

$$\text{Char} + aH_2 = CH_4$$

$$C + H_2O = CO + H_2$$

$$H_2O + CO = H_2 + CO_2$$

Here, the stoichiometric coefficient "a" in the char-hydrogen reaction varies from about 1.4 to 2.0 depending on the hydrogen content in the char and the level of carbon conversion. The rates of hydrogen reaction with the pretreated char and coal are compared in Figure IV-26. Char prepared by pretreatment in an oxidizing atmosphere to prevent agglomeration exhibits much higher density than coal reacted in a reducing atmosphere. When raw coal is reacted with hydrogen, the coal particles undergo softening and rapid swelling very much like the way popcorn explodes upon heating. Pretreated char also develops a "cheese" like

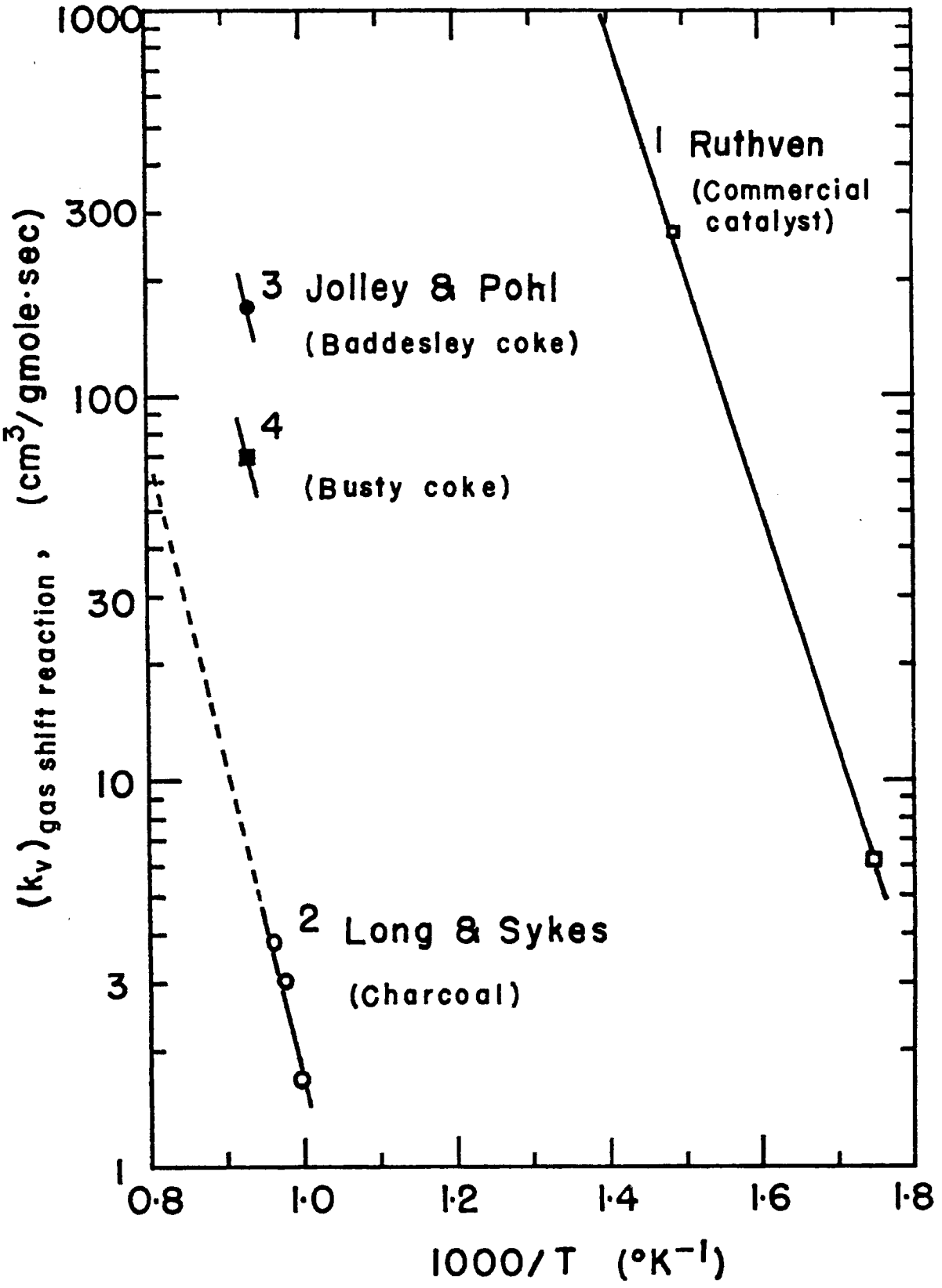

Figure IV-25 Summary of Water-Gas Shift Reaction Rate Constants of the Previous Investigations.

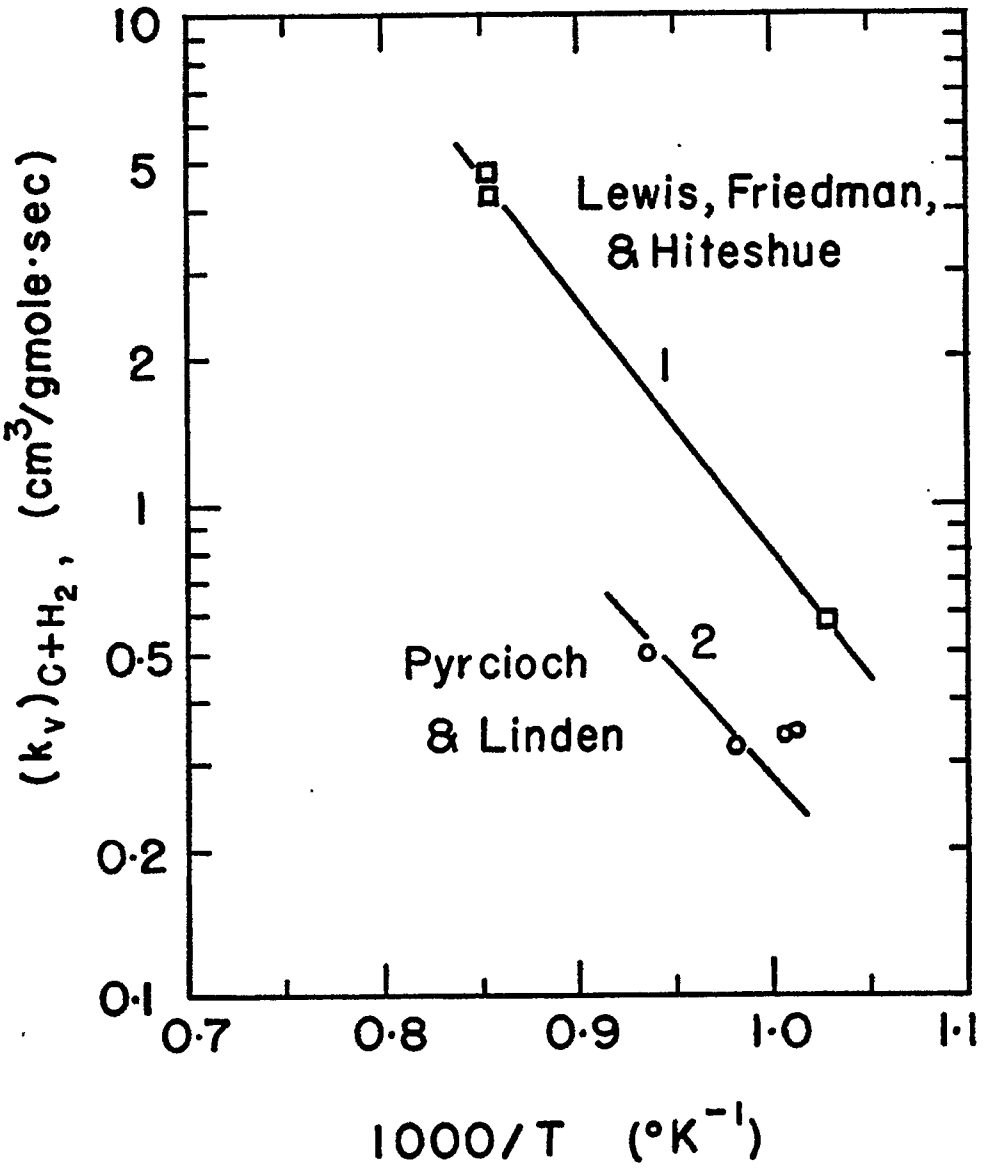

Figure IV-26 Summary of Rate Constants of Char-Hydrogen Reaction in the Second Phase from Previous Investigations.

structure upon reacting with hydrogen, but to a much lesser extent in comparison to the untreated coal. Thus, the reaction rate and percent weight of carbon present are much lower for pretreated char than that with raw coal.

Thus, the hydrogen reaction associated with the initial phase of coal conversion is by way of pyrolysis and devolatilization followed by the vapor phase hydrogenation. This first phase of reaction is very rapid and is practically complete when carbon conversion is about 20% [26]. On the other hand, the second phase reaction, the reaction of hydrogen with residual carbon, takes place at the surface of the particle at a much slower rate than the first phase reaction [27]. For simplicity, the forms of rate expression used in this study are chosen to be the same for both phases, but the values of the rate constants are greatly different. Thus, for bituminus coal and pretreated char, we have:

First Phase Reaction.

$$\frac{dX}{dt} = k_v(1-X)(C_{H_2} - C_{H_2}^*)$$

where X is the overall carbon conversion.

raw coal: $k_v = 950$ [cm^3/mole-sec.]

pretreated char: $k_v = 9.0$[cm^3/mole-sec.]

Second Phase Reaction

$$\frac{dx}{dt} = k_v(1-x)(C_{H_2} - C_{H_2}^*)$$

where $x = \frac{X-0.2}{0.8}$ is the carbon conversion in the second phase reaction.

The values of k_v used in the second phase reaction for the raw coal and the pretreated char are shown as line 1 and line 2, respectively, in Figure IV-26 based on the data of previous investigators [12,21].

There are a number of other rate expressions for gasification reactions available depending on the investigators [32]. However, for the purposes of the present study, the equations presented are believed to be of adequate accuracy without introducing unnecessary complications to calculation procedure in reactor design.

4.3 Coal-Hydrogen-Methane Equilibrium

It has been well documented [26,27] that coal-hydrogen reaction exceeds the carbon-hydrogen-methane equilibrium at low conversion and reaches closely to the carbon-hydrogen equilibrium at nearly complete conversion. A pseudo-equilibrium constant "K_p" defined as:

$$(K_p)_{1300°F} = \frac{P^*_{CH_4}}{(P^*_{H_2})^2}$$

for coal-hydrogen-methane system as a function of carbon conversion at 1300°F is shown in Figure IV-27. An empirical relationship has been developed to convert the pseudo-equilibrium constant from 1300°F to other temperatures as follows:

$$(K_p)_T = (K_p)_{1300°F} \cdot 2.881 \times 10^{-5} \exp\left(\frac{18,400}{T}\right)$$

where T is temperature in °R.

Hence, from the above relations, the equilibrium hydrogen concentration which appeared in the rate expression "$C^*_{H_2}$" can be calculated.

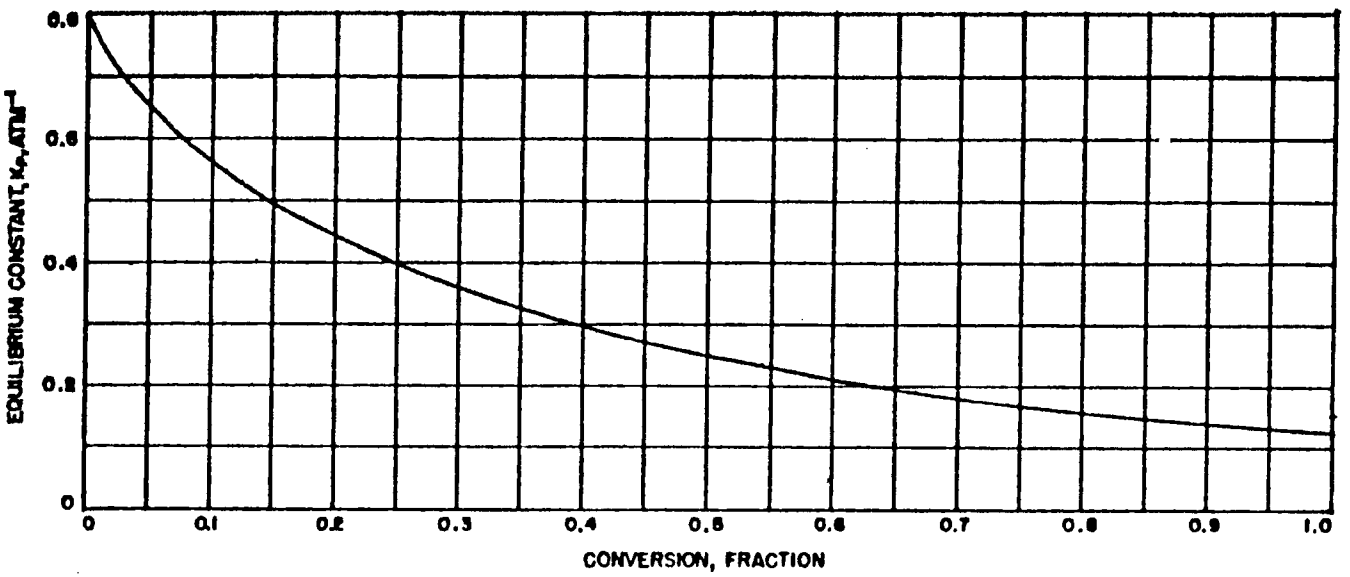

Figure IV-27 Approximate trend of the Equilibrium Constant as a Function of Conversion for the Char-Hydrogen Reaction at 1300°F and 2000 PSIG Total Pressure

4.4 Fluidized Bed Reactor Design

Fluid bed reactors are among the most commonly used contacting devices for solid gas reactions. Fluid bed reactors have both desirable and undesirable characteristics. The fluid bed is particularly suitable for coal gasification because of the good gas-solid contact, good heat transfer, the rapid solid mixing leading to nearly isothermal operating conditions, and its capability of transporting large quantities of heat to or from the reactor bed. However, because of the rapid solid mixing, the residence times of solids are not uniform, and gas bypasses in the form of bubbles leading to poor conversion efficiency. Particles are also subject to attrition and elutriation as the result of rapid solids mixing. At high temperatures, ash may be softened causing particle agglomeration, which necessitates lowering the reaction temperature reducing reaction rate considerably.

For simulation of a fluidized bed catalytic reactor, Kato and Wen [16] proposed the bubble assemblage model and showed that the performance of a fluidized bed reactor can be estimated by a flow model consisting of bubbles of various sizes and an emulsion phase with an interchange of gas and solids between them. Yoshida and Wen [29] extended the bubble assemblage model to fluidized beds with non-catalytic solid-gas reactions. The detail description of this model and the pertinent parameters characterizing the model is presented in the Appendix A.

To determine the diameter and bed height needed for fluidized bed reactors, the gas velocity required to provide the onset of fluidization or minimum fluidization must be known.

A generalized correlation of minimum fluidization velocity based on a comprehensive study by Wen and Yu [28] is available:

$$(N_{Re})_{mf} = \sqrt{(33.7)^2 + 0.408N_{Ga}} - 33.7$$

where

$$(N_{Re})_{mf} = \frac{U_{mf}\rho_f d_p}{\mu}$$

$$N_{Ga} = \frac{d_p^3 \rho_f (\rho_s - \rho_f) g}{\mu^2}$$

This correlation is applicable for nonvesicular particles and does not provide accurate prediction for the coal chars with popcorn like structure.

An empirical correlation proposed by Feldman et. al. [7] for coal char is used to calculate U_{mf}.

$$(N_{Re})_{mf} = 0.0135\ (N_{Ga})^{0.730}$$

This equation gives a larger U_{mf} than that from the Wen-Yu correlation.

Unlike catalytic reactions, reactivities of solids in gasification reactions change depending on the solid conversion level within the reactor. Thus, for simulation of gasification reactor performance, a relation between the carbon conversion and char reactivity is needed. Yoshida and Wen employed the so-called unreacted-core shrinking model for a certain class of solid-gas reaction systems. In this study, the rate expressions presented in the previous section are used, namely, the rate per unit particle is assumed to be proportional to the weight of the residual carbon left in the particle.

In order to represent the behavior of solids and gas, the bubble assemblage model provides the bubble phase and the emulsion phase, with each phase represented by a number of complete mixing compartments connecting together in series as shown in Figure IV-28. The bulk flows as well as the interchanges of solid and gas are shown in the diagram by arrows. Knowing the concentration C_A of gaseous component, A, from the material balance, the extent of reaction of component, A, can be calculated. Under the steady state operation, the extent of gaseous reaction must be related to the extent of solid conversion via stoichiometric relation. Thus, for a counter-current operation, the material balance around any compartment except the top and bottom compartments can be written as:

Emulsion Phase:

$$F_e Y_{2j+1} + F_m Y_{2j} = (F_e+F_m) Y_{2j-1} + k_v W Y_{2j-1} (C_{A2j-1} - C_A^*)$$

Bubble Phase:

$$F_b Y_{2j-2} + F_m Y_{2j-1} = (F_b+F_m) Y_{2j} + k_v W Y_{2j} (C_{A2j} - C_A^*)$$

For Top Compartment of Emulsion Phase:

$$F_S + (F_b+F_m) Y_{2J} = (F_e+F_m) Y_{2J-1} + k_v W Y_{2J-1} (C_{A2J-1} - C_A^*)$$

For Bottom Compartment of Bubble Phase:

$$(F_b+F_m) Y_1 = (F_b+F_m) Y_2 + k_v W Y_2 (C_{A2} - C_A^*)$$

These equations are linear with respect to Y_i and therefore are easily solved.

The computer program combining the rate expression and the bubble assemblage model for the fluidized bed reactor used in the simulation

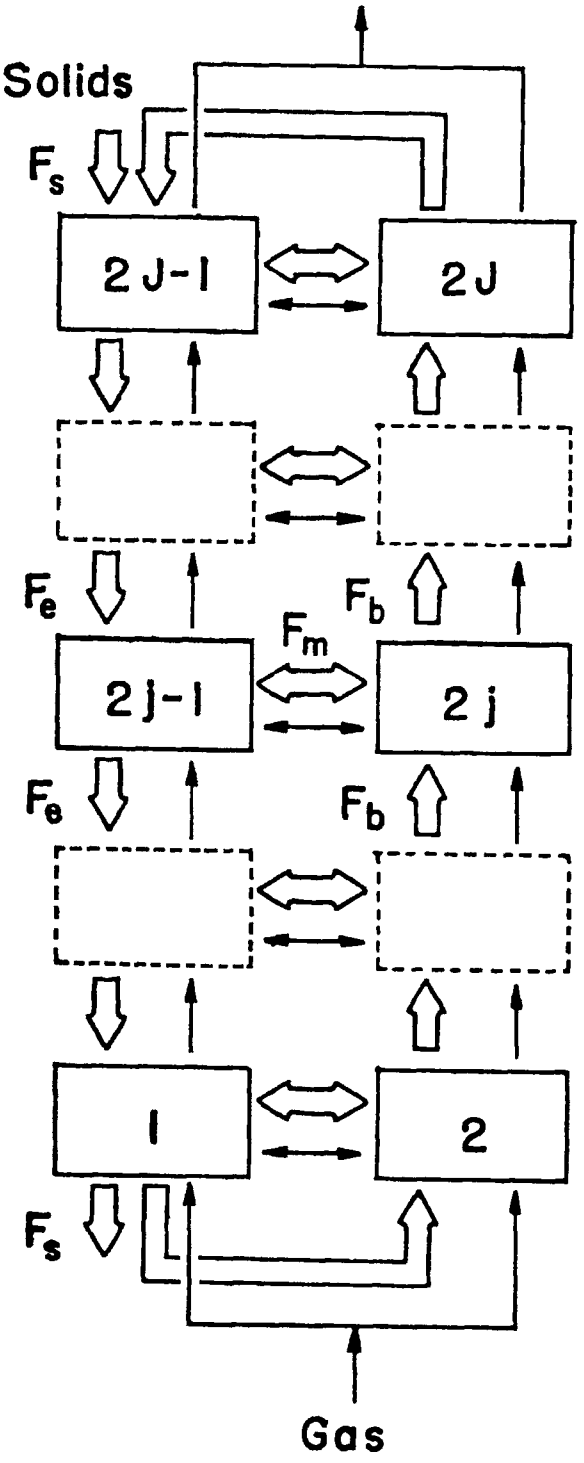

Figure IV-28 Schematic Diagram Representing the Movements of Gas and Solid in a Counter-Current Fluidized Bed Based on Bubble Assemblage Model.

of oxygen-steam and hydrogen-steam gasifiers is presented in the Appendix B. Although in this program the number of reactions and the number of gaseous components are specified as 3 and 5, respectively, the program can handle any number of reactions and gas components with proper modification. The logic diagram for the calculation procedure is presented in Figure IV-29.

Evaluations of bubble sizes, bubble velocities, gas and solids exchange coefficients, bed expansion, etc., that are characteristic parameters of the bubble assemblage model are described in detail in the Appendix A, and therefore will not be repeated here.

Examples of fluidized bed reactor designs based on the bubble assemblage model and effects of operating conditions on reactor configuration are shown in Figures IV-30 and IV-31. The operating conditions for these cases are:

Bed Temperature	1700°F
Bed Pressure	1100 psig
Char (Pretreated) Flow Rate	500 tons per hour
Inlet Gas Flow Rate	95,700 moles per hour
Inlet Gas Composition:	

H_2	25.6%
H_2O	30.2
CO	34.3
CO_2	9.9
	100.0%

Figure IV-30 shows the effects of char particle size and gas velocity

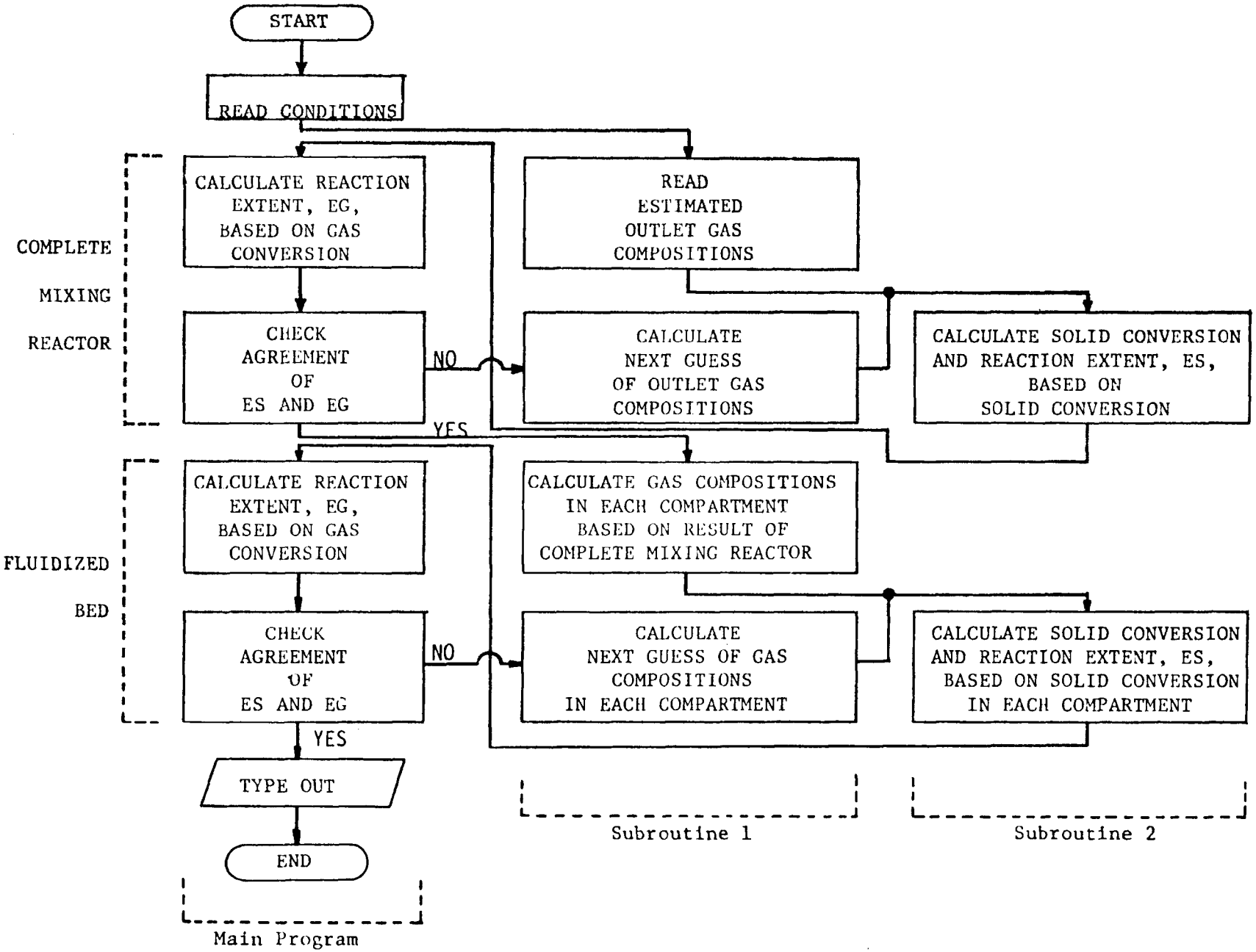

Figure IV-29 Computer Logic Diagram For Calculation of Fluid Bed Coal Gasifier.

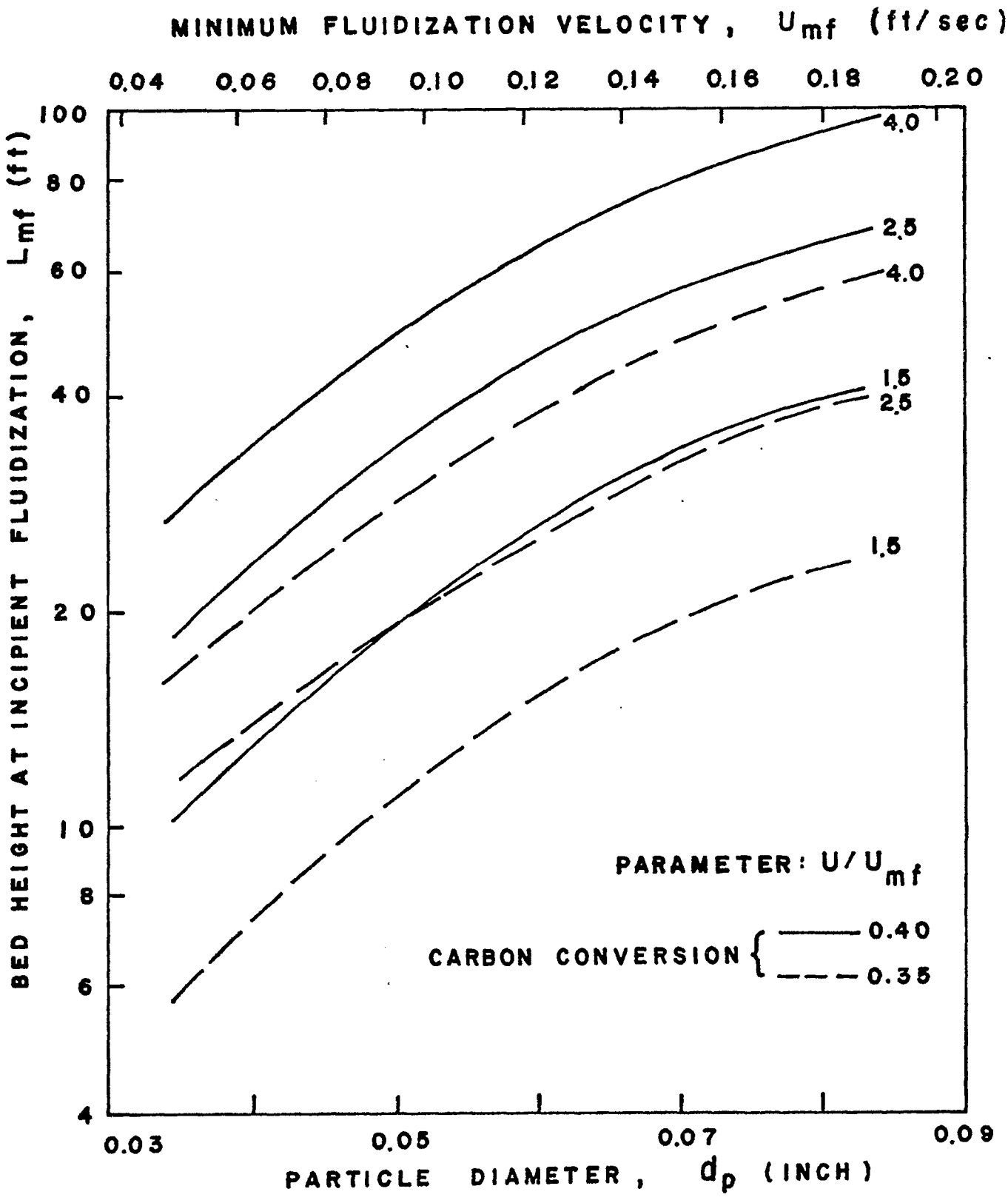

Figure IV-30 Example of the Design of Fluidized Bed Gasifier showing the effects of coal particle diameter and gas velocity on the reactor height.

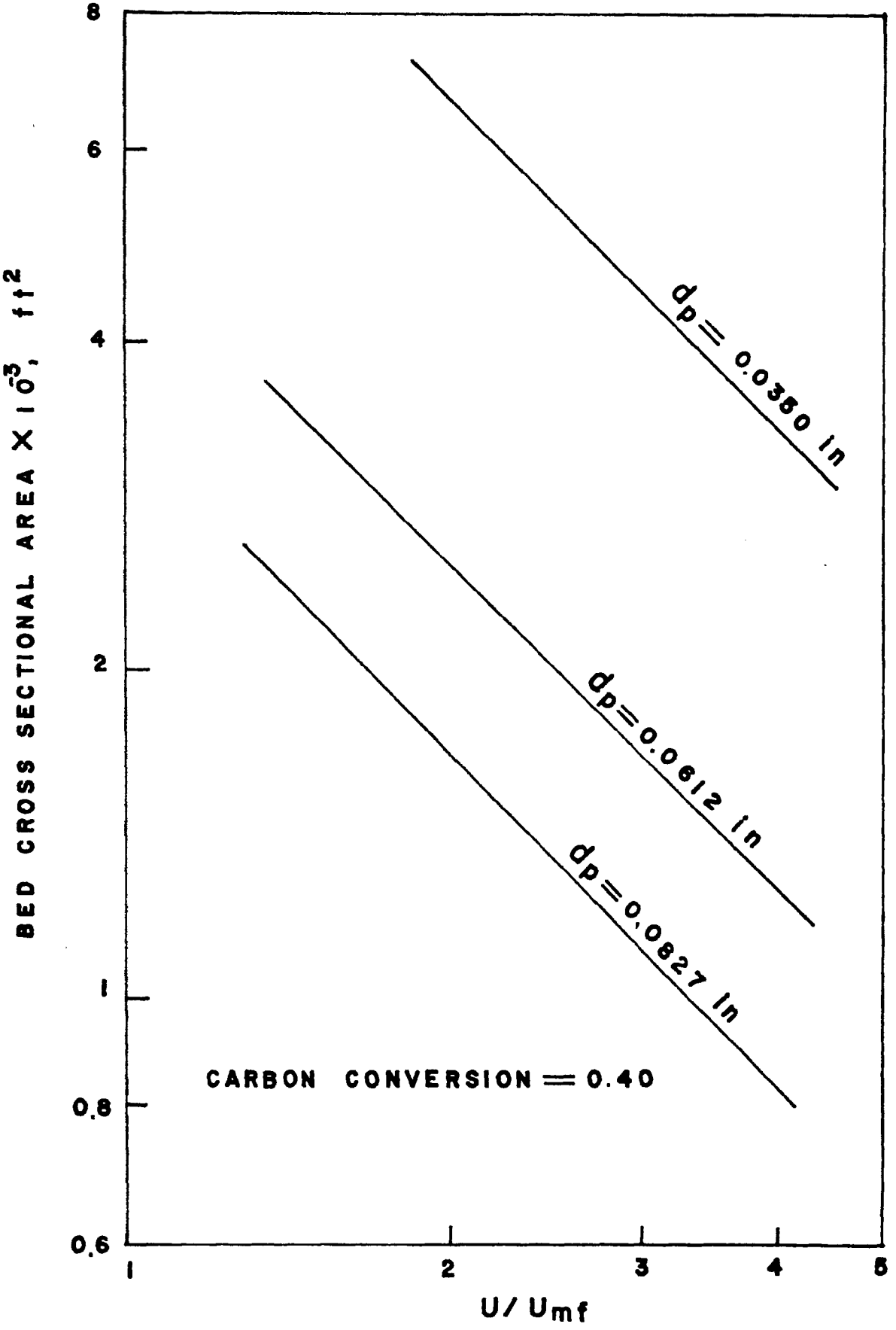

Figure IV-31 Example of the Design of Fluidized Bed Gasifier indicating the effects of coal particle diameter and gas velocity on the reactor cross sectional area.

on the bed height corresponding to the incipient fluidization at two carbon conversion levels. It is seen that both particle size and gas velocity affect the size of the reactor considerably. Figure IV-31 shows the effect of gas velocity and particle size on the reactor cross-sectional area at the 40% carbon conversion level. As can be seen from these figures, small particle size and low gas velocity favor a low bed height, but require a large bed diameter reactor.

Therefore, optimum conditions selected must be based on economic optimization of the reactor system. Although the reactor height is shorter at lower gas velocities, in order to assure good solid mixing and good heat transfer, the gas velocities corresponding to U/U_{mf} of at least 2.0 are selected. The expanded bed height and the transport disengaging height (free board) required are computed. These results are obtained for each of the alternate gasification processes and are shown in the next section.

In the fluidized bed hydrogasification where hydrogen rich gas is employed, the excess heat of the reaction must be removed through the heat transfer surface provided in the bed in order to maintain the bed at a desired temperature. This is accomplished by feeding pressurized water through heat transfer tubes which are embedded in the reactor. Part of the water is boiled off in the tubes, while the remainder is separated from steam, and is returned to the feed point to be combined with the make-up water. The generated saturated steam is then passed through the superheater located above the bed. The required heat transfer area and the cost of the heat exchanger are computed and presented in the next section.

4.5 Entrained Bed Reactor Design

In order to directly feed the raw coal without agglomeration in the gasifier, reactions of coal particles with its carrier gas in a relatively dilute phase, or an entrained bed reactor, has been considered. The extent of conversion of coal is limited by the relatively short solid residence time available in the reactor. The relationships between the gas velocity and the solid velocity can be obtained by the following equation which is based on the drag force consideration in a multiparticle system [30]:

$$\varepsilon^{4.7} \cdot \frac{d_p^3 \rho_f (\rho_s - \rho_f) g}{\mu^2} =$$

$$18 \frac{d_p (U - \varepsilon U_p) \rho_f}{\mu} + 2.7 \left[\frac{d_p (U - \varepsilon U_p) \rho_f}{\mu}\right]^{1.687}$$

where $$1 - \varepsilon = \frac{4 G_s}{\pi D_t^2 \rho_s U_p}$$

The kinetic information together with the heat transfer relation are then integrated to obtain the residence time, and the length of reactor required for the desired carbon conversion.

4.6 Slag Bed Reactor Design

At a temperature substantially higher than ash softening point, the bed material slags and thus can flow out of the reactor. Lacking quantitative performance data of slag beds, the design is based on a simple flow model; namely, the molten solids are in complete mixing while the gas is in plug flow blowing through the bed in forms of jets and bubbles. Since at such a high temperature the reaction rate is

extremely rapid the mass transfer plays a significant role in the rate determining step. The apparent rate of reaction and the size of the reactor required are calculated based on the mass transfer mechanism.

5. Optimization of Gasification Phase Equipment Costs

The size of a fluidized bed gasification reactor is calculated based on the bubble assemblage model and the kinetics data given previously. To account for the transport disengaging height (TDH), the overall reactor height is determined by adding 30 feet to the calculated expanded bed height or by applying a multiplication factor of 2.6 to the calculated expanded bed height; whichever results in smaller overall height.

In the case of the entrained bed reactor in Alternate II-3, the bed height is calculated by assuming a plug flow of both gas and solids.

The results of gasification phase optimization are presented in the next section for each of the alternates separately.

For each alternate, a schematic diagram showing the gasification phase is given. This is followed by a figure showing the total installed cost of gasification equipment as a function of the number of units required. The cost estimations are based on the formulas given in Chapter II. Finally, a table summarizes the optimum sizes and numbers of reactors that give the minimum total installed equipment cost.

The reactor sizes and the total cost of gasification equipment for Alternate V are not calculated because of the insufficient kinetics information.

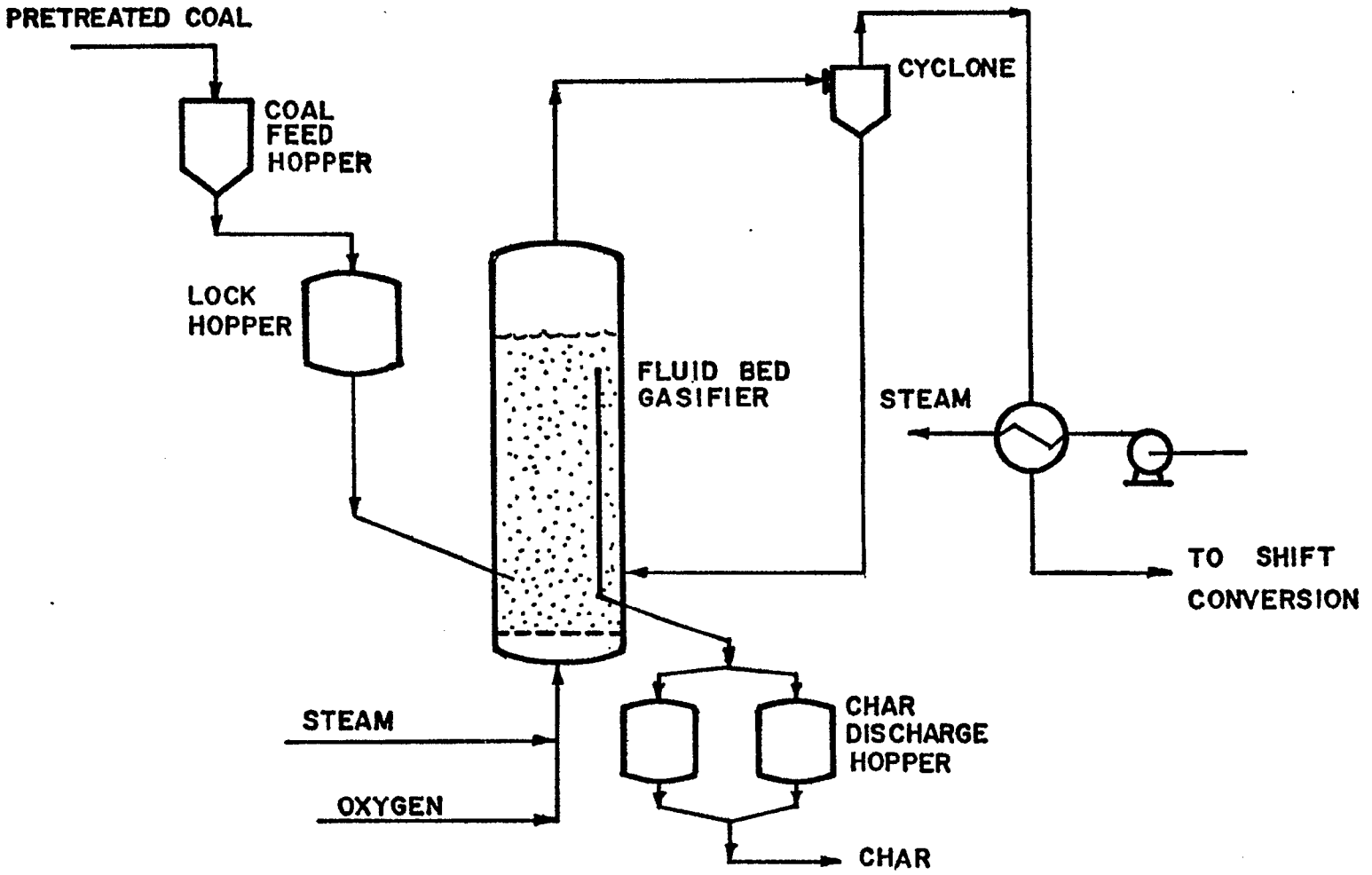

Figure IV-32 Gasification Phase Of Alternate I

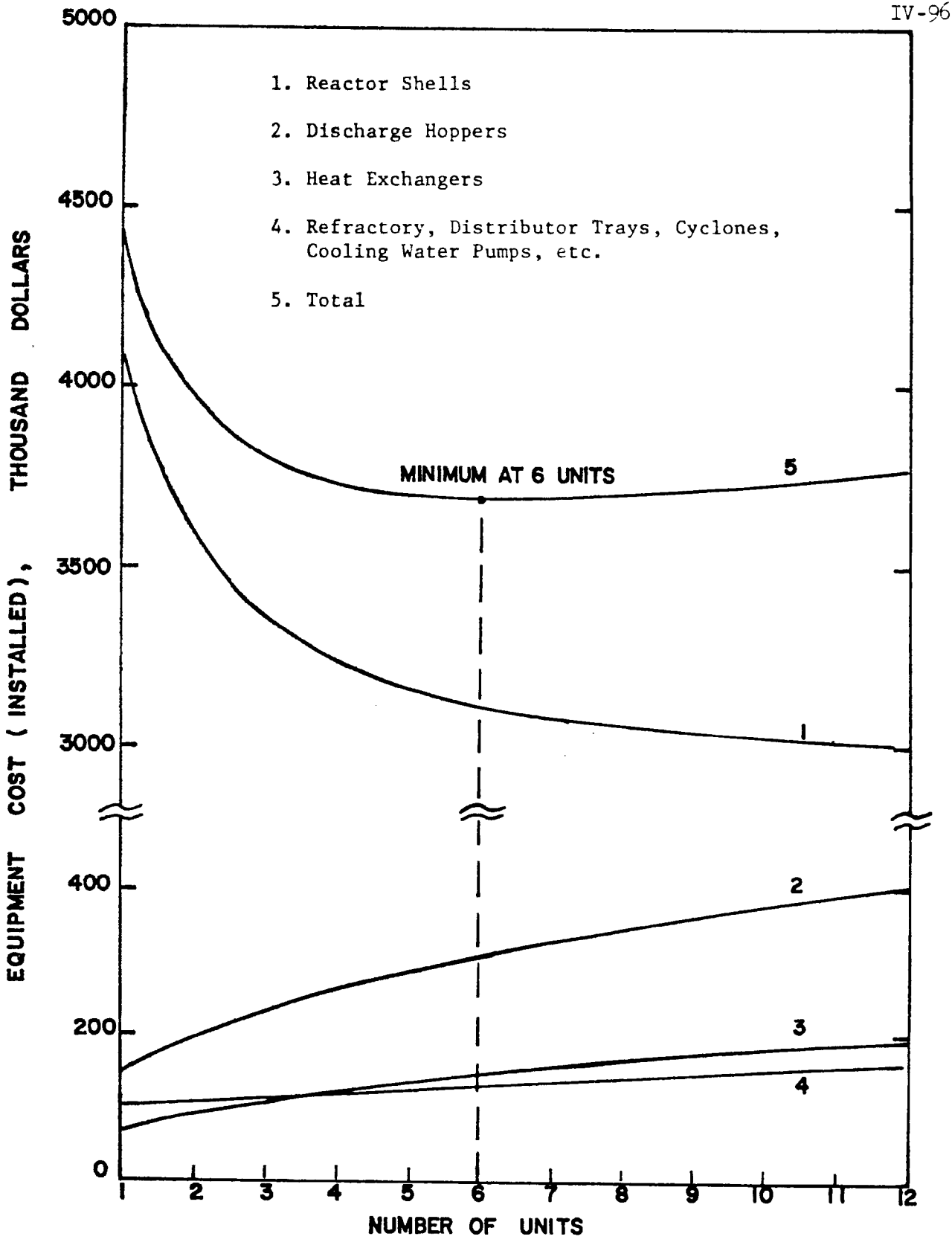

Figure IV-33 Equipment costs as a function of number of units for Alternate I

Table IV-8 Optimum Size and Number of Fluid Bed Gasifiers for Alternate I

Number of Units Required	6
Height, ft.	20.8
Inside Diameter of Refractory, ft.	13.2
Inside Diameter of Shell, ft.	13.9
Thickness of Shell, in.	6.35

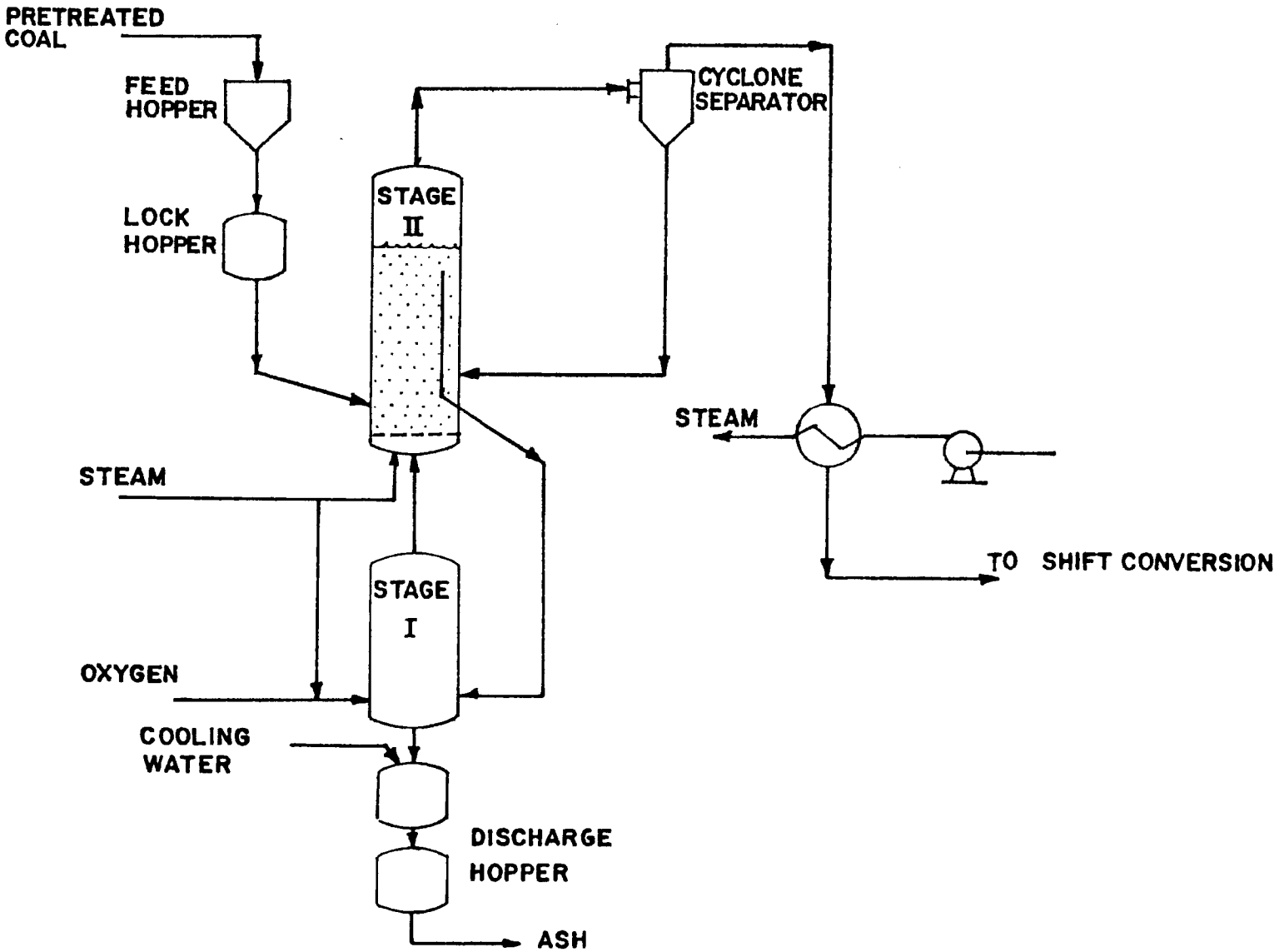

Figure IV-34 Gasification Phase Of Alternate II-1

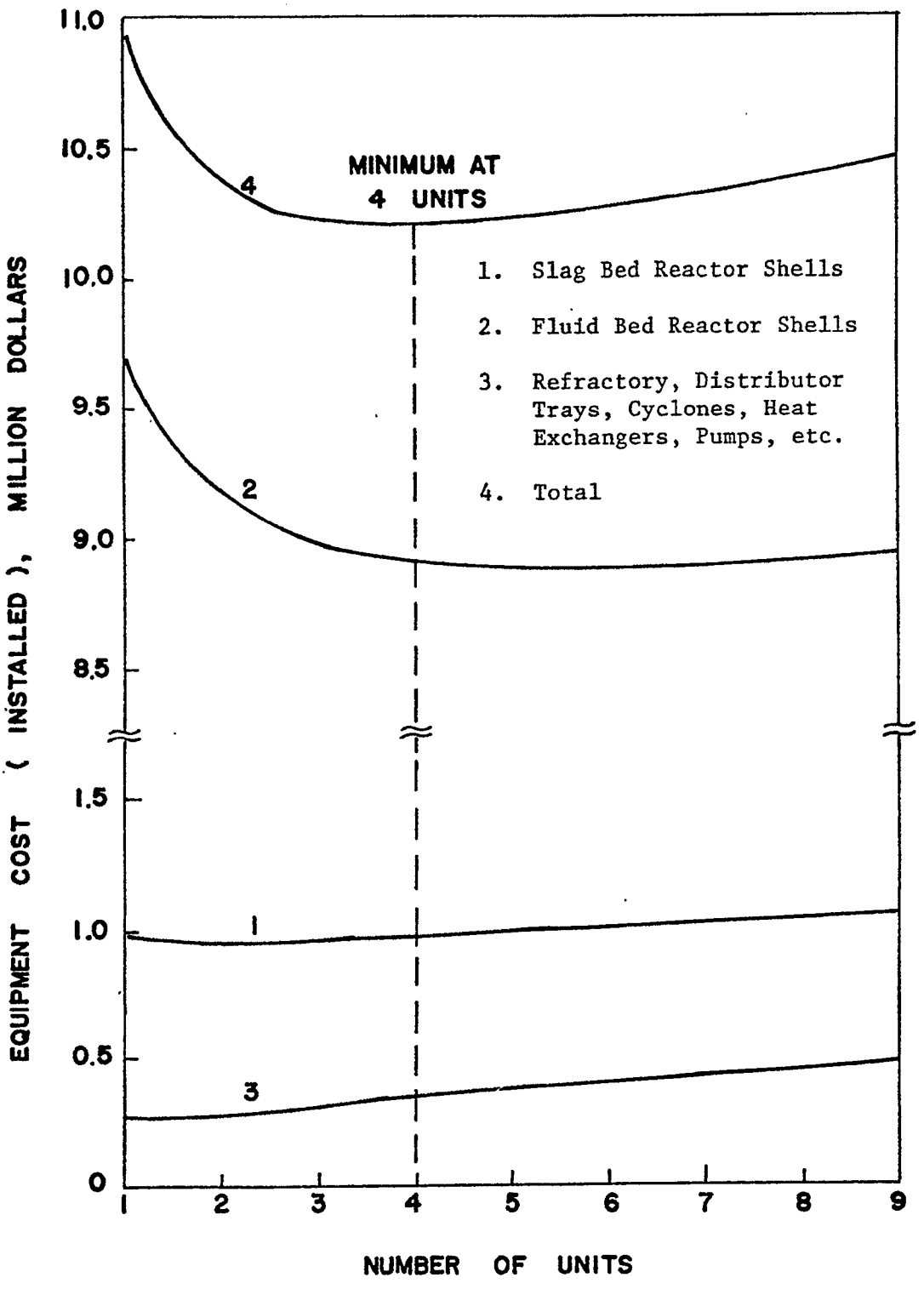

Figure IV-35 Equipment Costs as a Function of Number of Units for Alternate II-1

Table IV-9 Optimum Size and Number of Gasification Reactors for Alternate II-1

	Stage I (Slag Bed)	Stage II (Fluid Bed)
Number of Units Required	4	4
Height, ft.	20.0*	66.3
Inside Diameter of Refractory, ft.	8.5	17.3
Inside Diameter of Shell, ft.	10.0	18.1
Thickness of Shell, in.	4.67	8.14

* Including 13 feet for slag quenching and removal

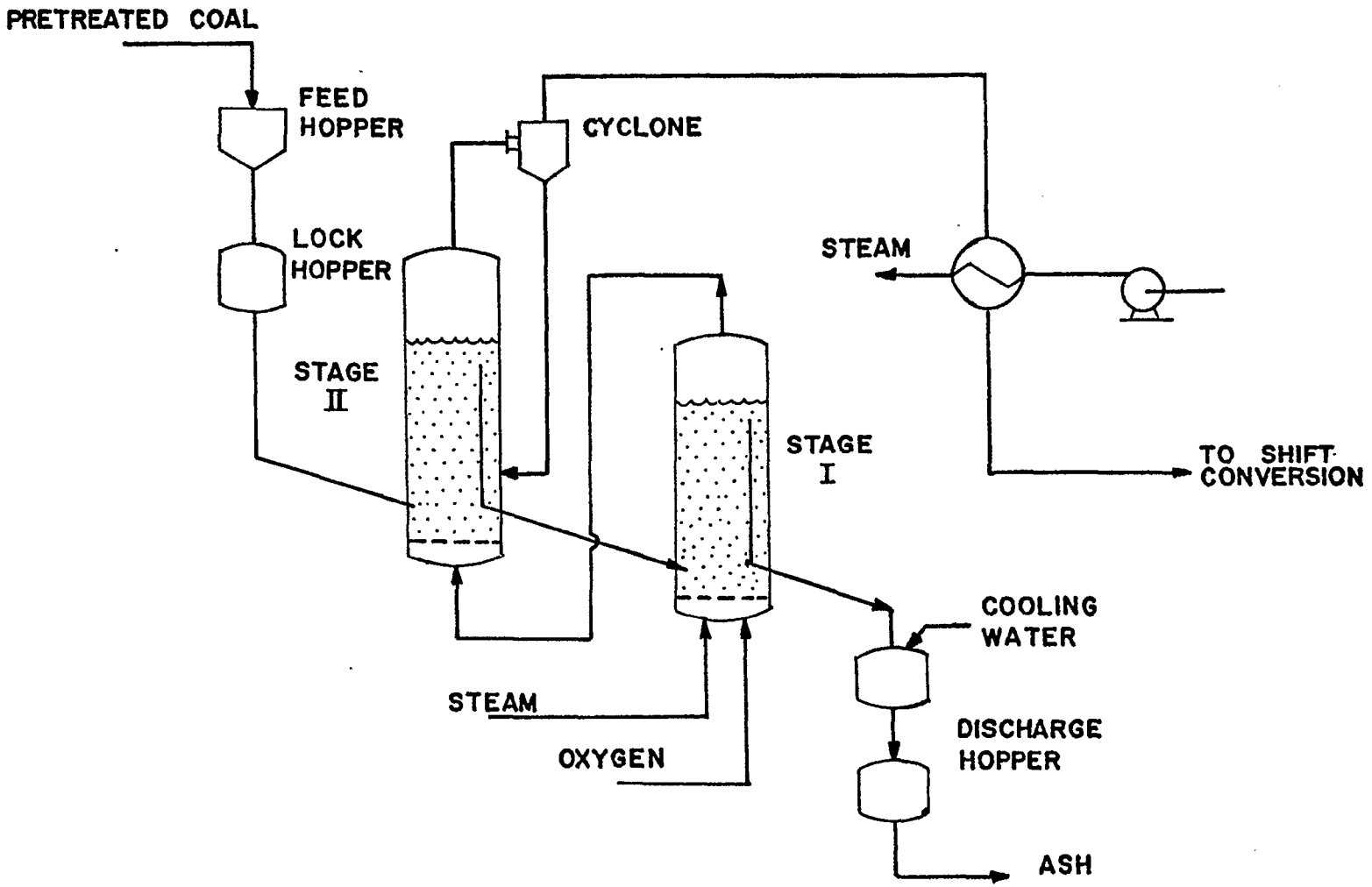

Figure IV-36 Gasification Phase Of Alternate II-2

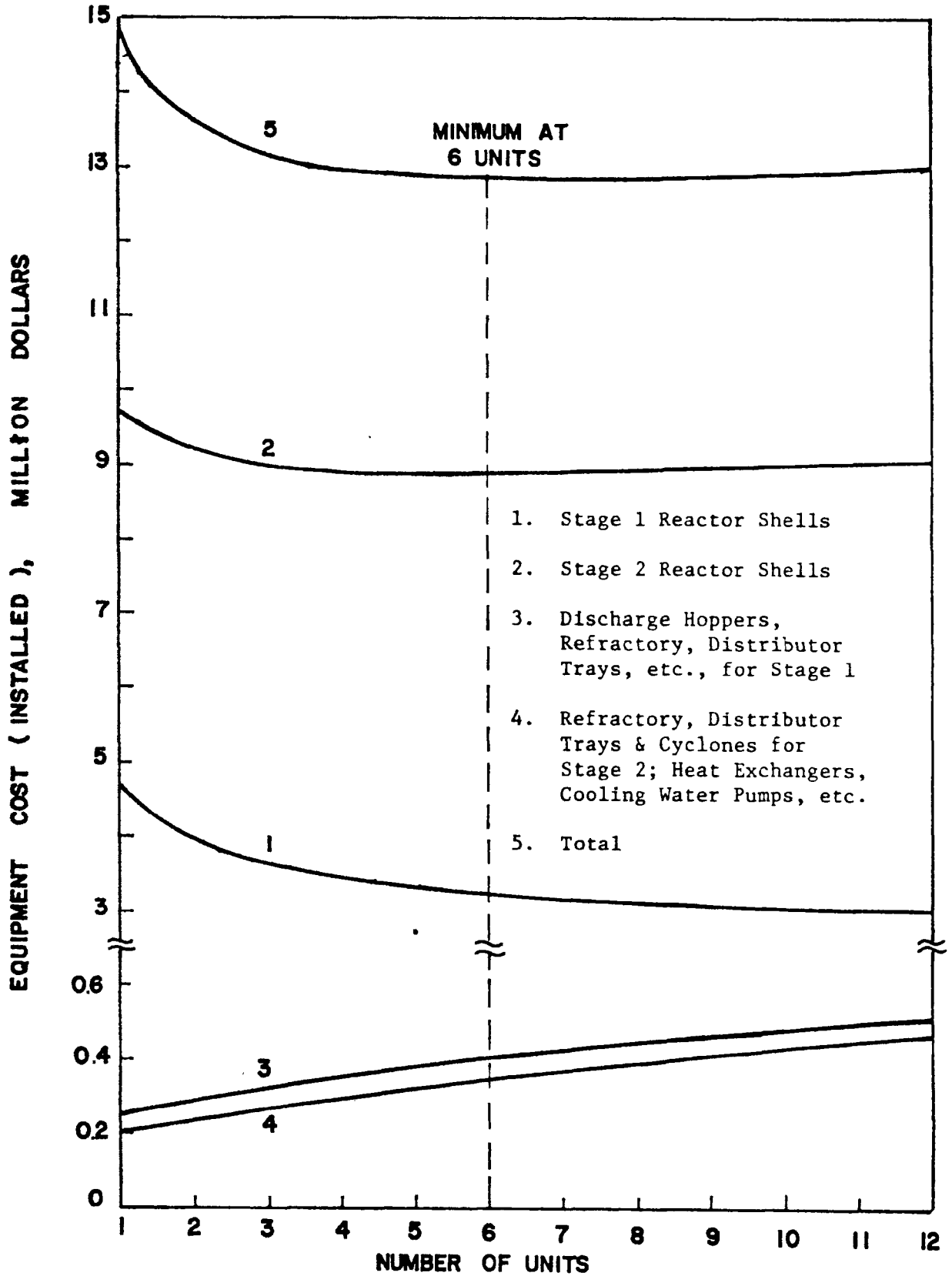

Figure IV-37 Equipment Costs As a Function Of Number of Units For Alternate II-2

Table IV-10 Optimum Size and Number of Gasification Reactors for Alternate II-2

	Stage I (Fluid Bed)	Stage II (Fluid Bed)
Number of Units Required	6	6
Height, ft.	15.0	66.3
Inside Diameter of Refractory, ft.	14.7	14.1
Inside Diameter of Shell, ft.	15.4	14.9
Thickness of Shell, in.	7.05	6.76

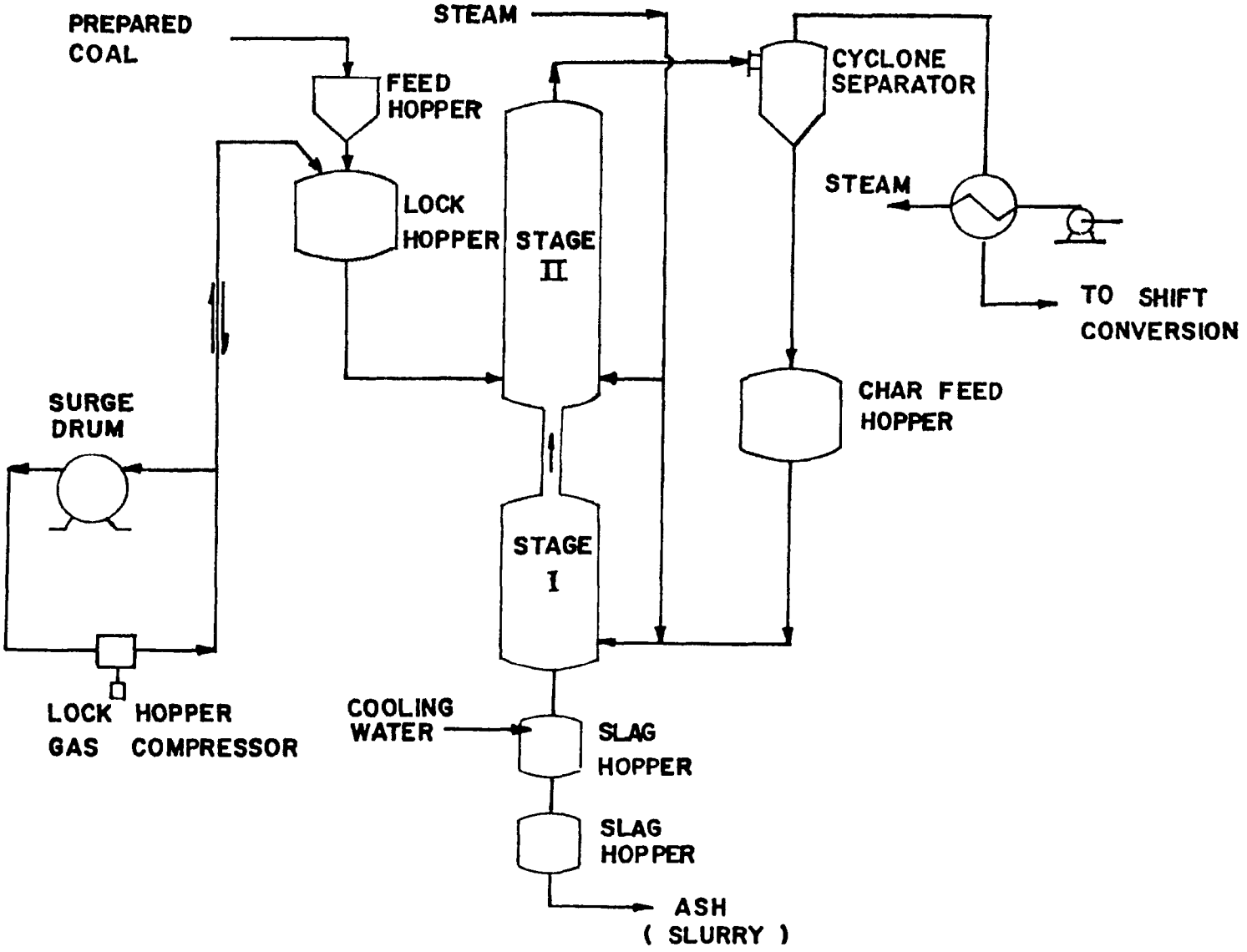

Figure IV-38 Gasification Phase Of Alternate II-3

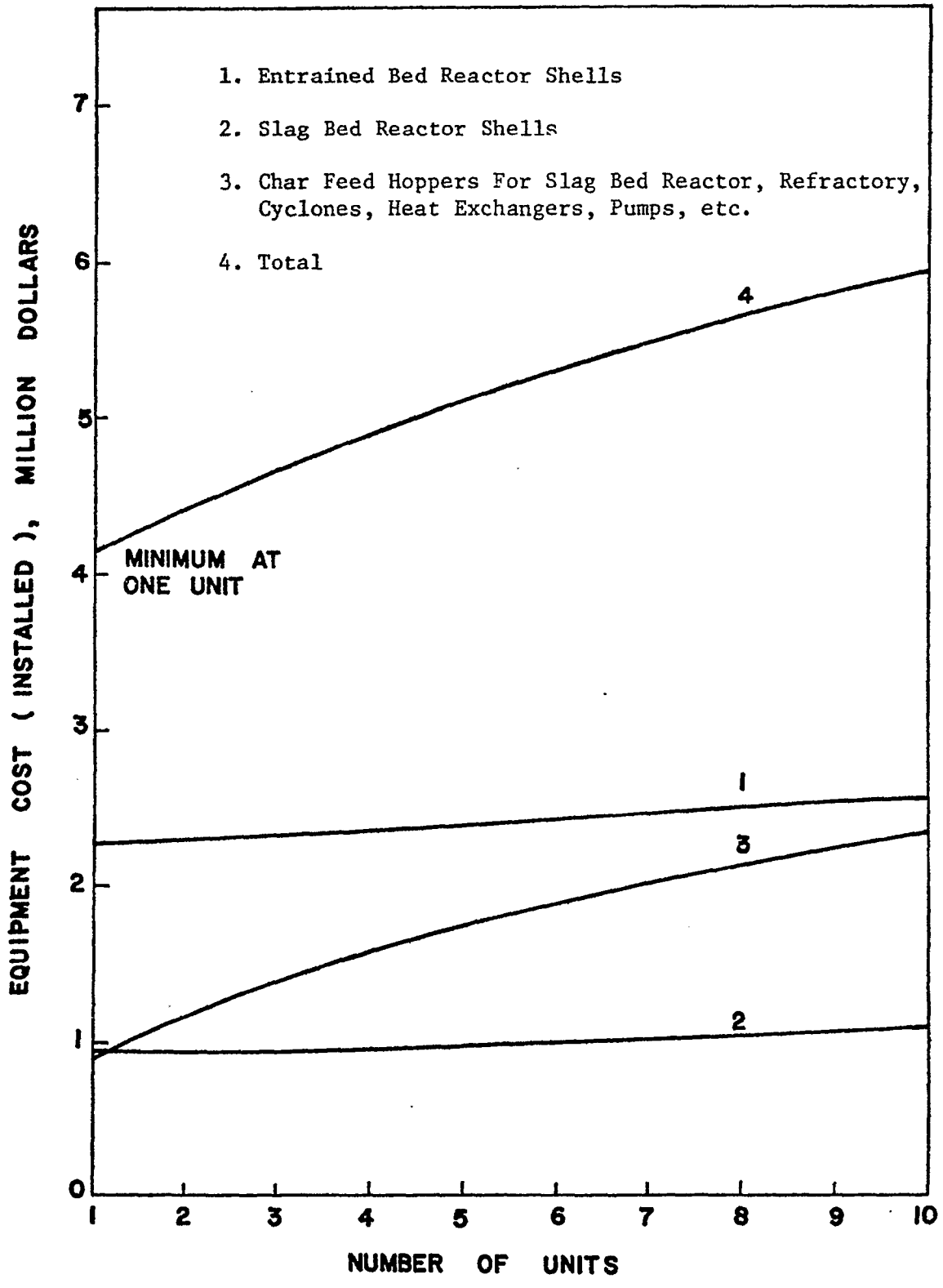

Figure IV-39 Equipment costs as a function of number of units for Alternate II-3

Table IV-11 Optimum Size and Number of Gasification Reactors for Alternate II-3

	Stage I (Slag Bed)	Stage II (Entrained Bed)
Number of Units Required	1	1
Height, ft.	20.0*	70.0
Inside Diameter of Refractory, ft.	17.0	17.0
Inside Diameter of Shell, ft.	18.5	17.8
Thickness of Shell, in.	8.42	8.01

* Including 13 feet for slag quenching and removal.

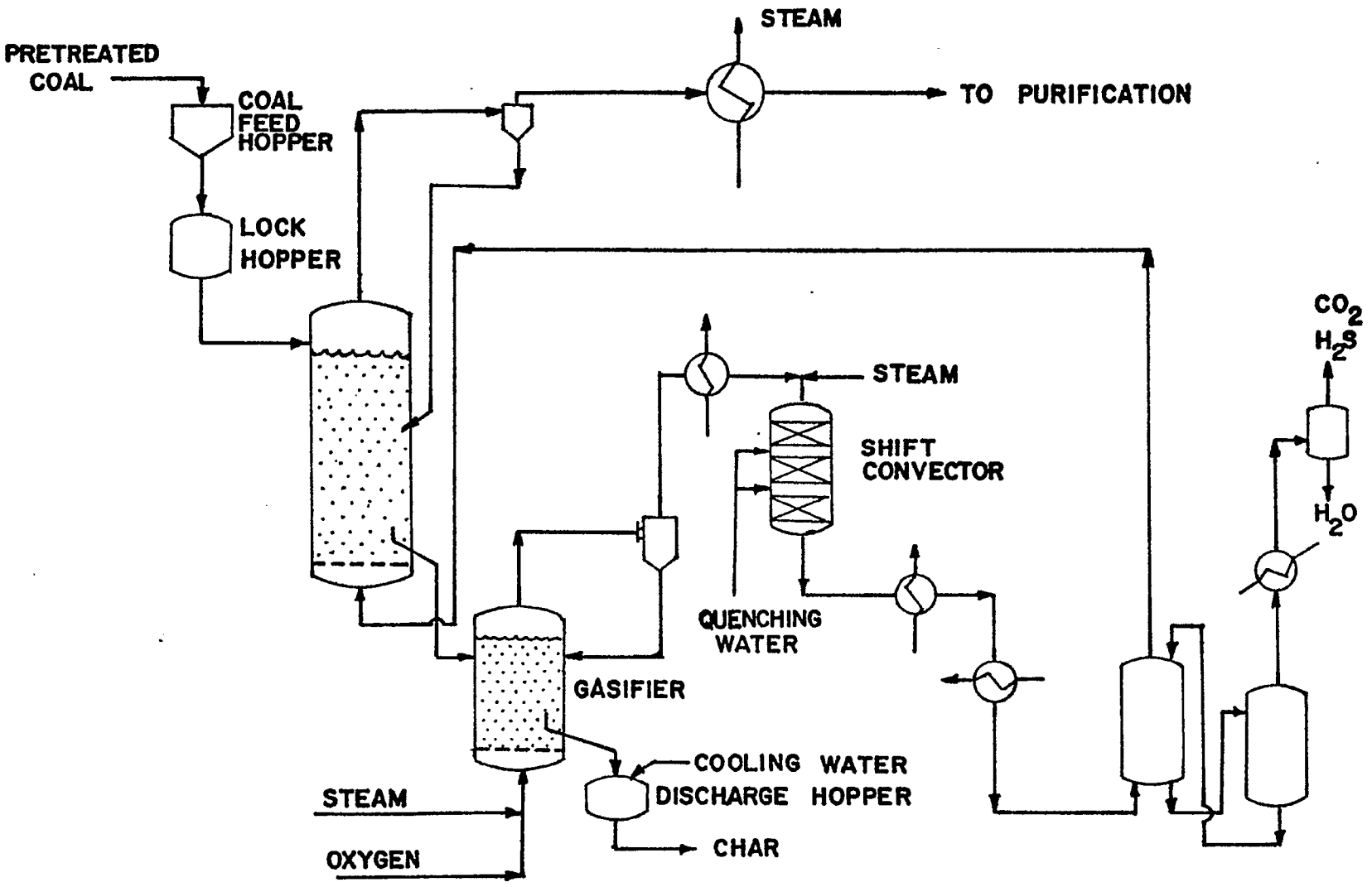

Figure IV-40 Gasification Phase Of Alternate III

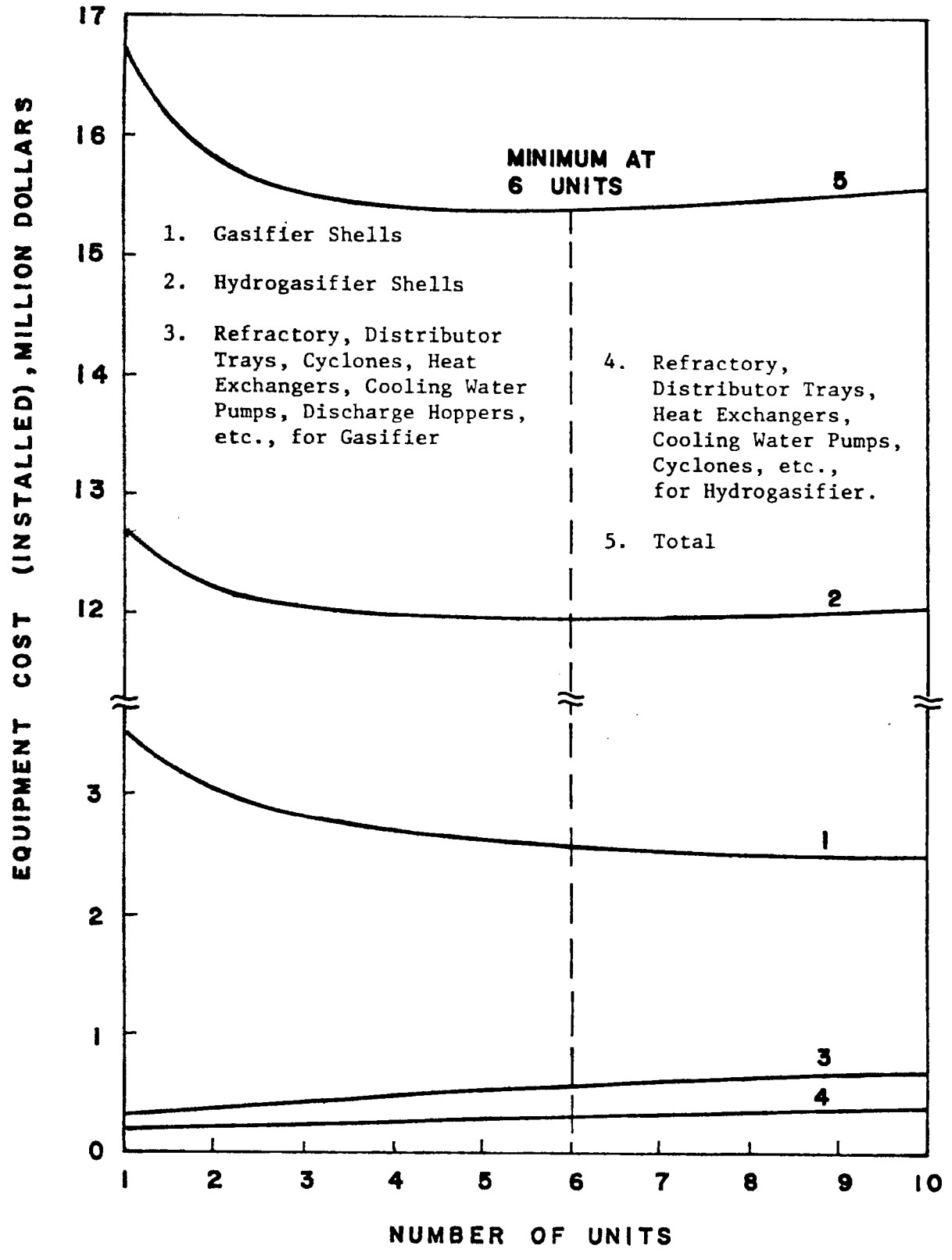

Figure IV-41 Equipment Costs As a Function of Number of Units For Alternate III.

Table IV-12 Optimum Size and Number of Gasification Reactors for Alternate III

	Gasifier (Fluid Bed)	Hydrogasifier (Fluid Bed)
Number of Units Required	6	6
Height, ft.	16.5	90.9
Inside Diameter of Refractory, ft.	12.9	13.9
Inside Diameter of Shell, ft.	13.7	14.6
Thickness of Shell, in.	6.24	6.32

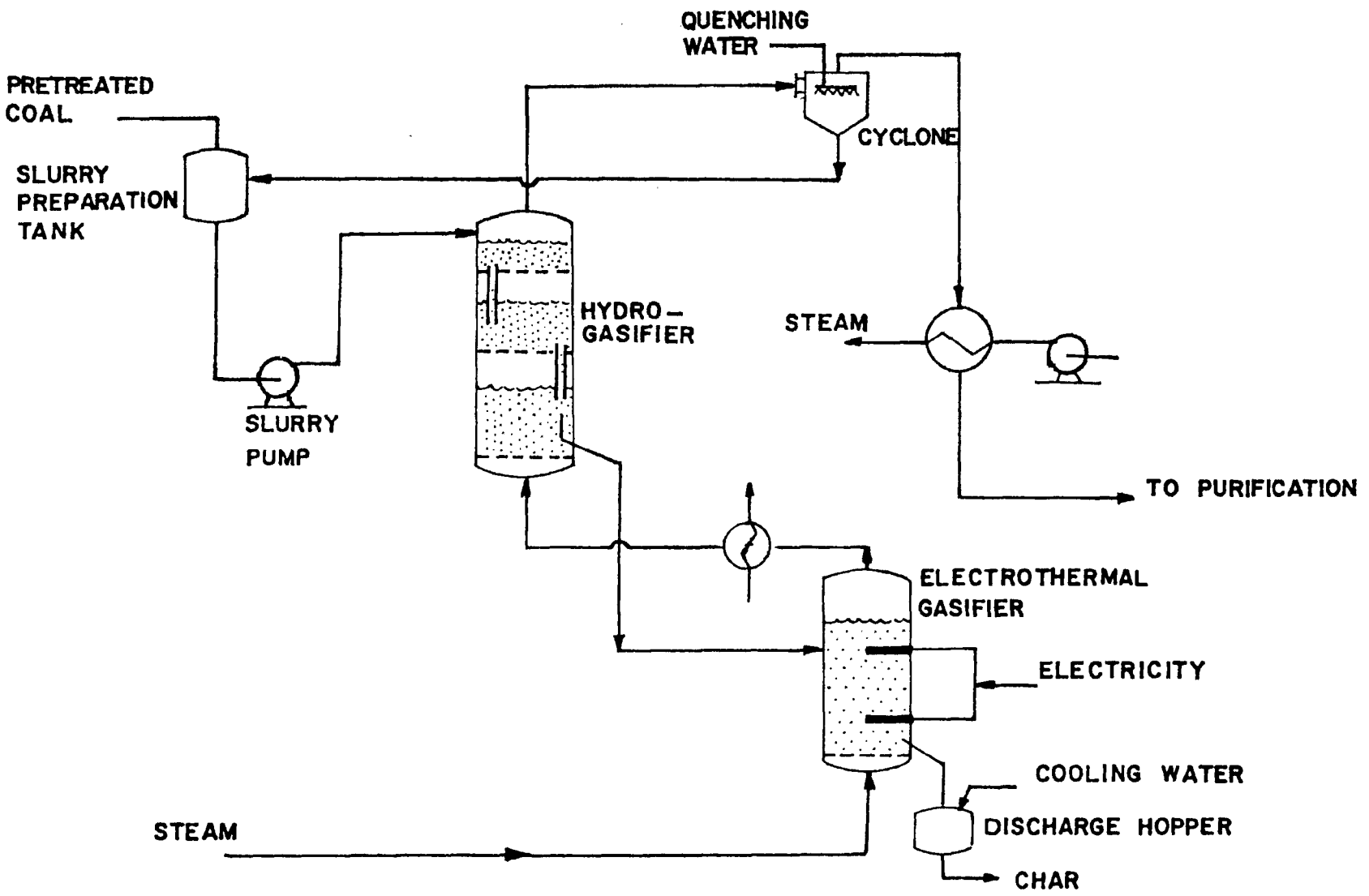

Figure IV-42 Gasification Phase Of Alternate IV

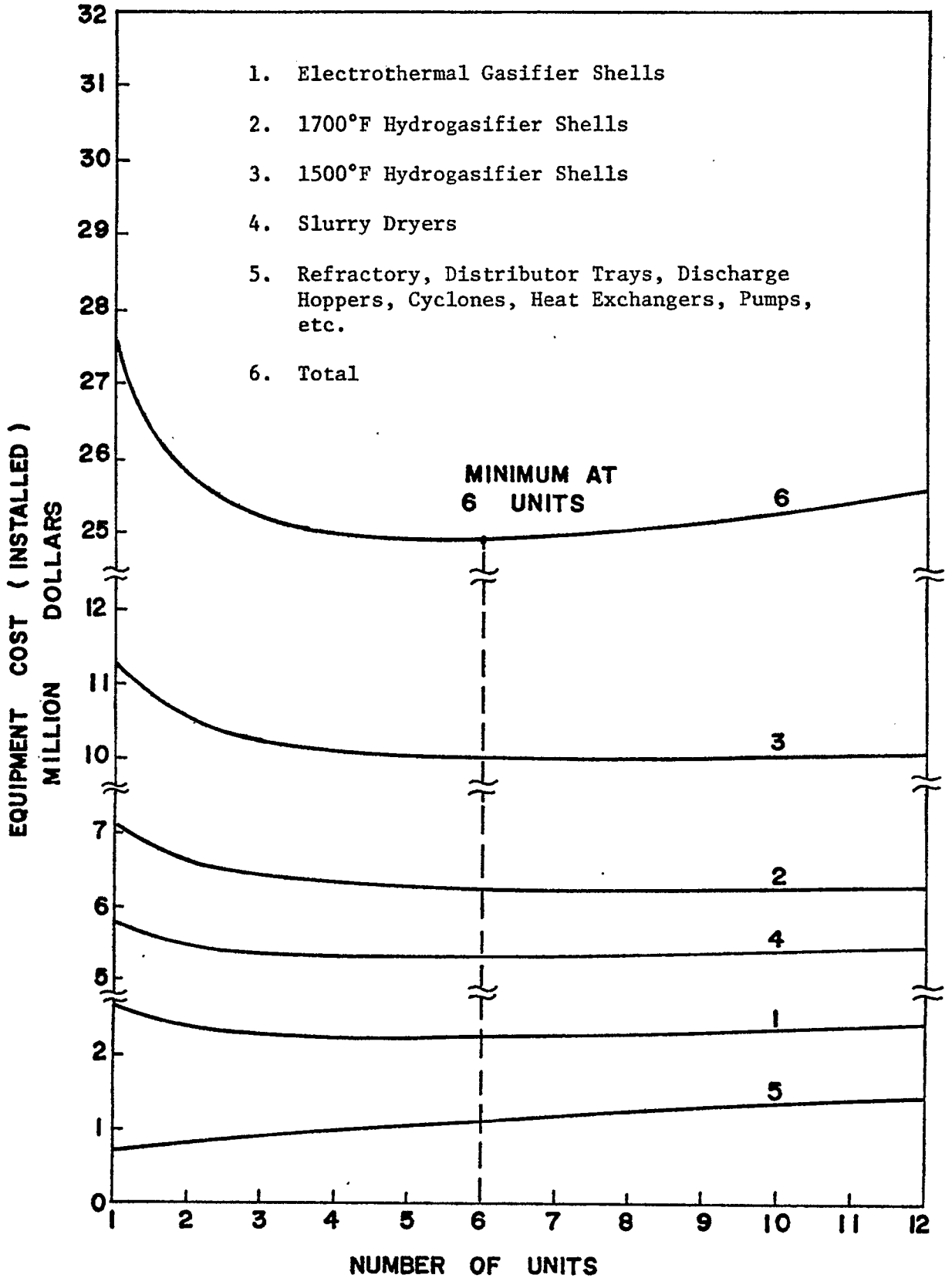

Figure IV-43 Equipment Costs as a Function of Number of Units for Alternate IV.

Table IV-13 Optimum Size and Number of Gasification Reactors

for Alternate IV

	Electrothermal Gasifier (Fluid Bed)	Hydrogasifier (1700°F Fluid Bed)	Hydrogasifier (1500°F Fluid Bed)	Slurry Dryer
Number of Units Required	6	6	6	6
Height, ft.	19.7	38.4	68.5	54.0
Inside Diameter of Refractory, ft.	17.4	18.0	17.0	11.9
Inside Diameter of Shell, ft.	18.2	18.8	17.7	12.6
Thickness of Shell, in.	8.40	8.63	8.10	5.83

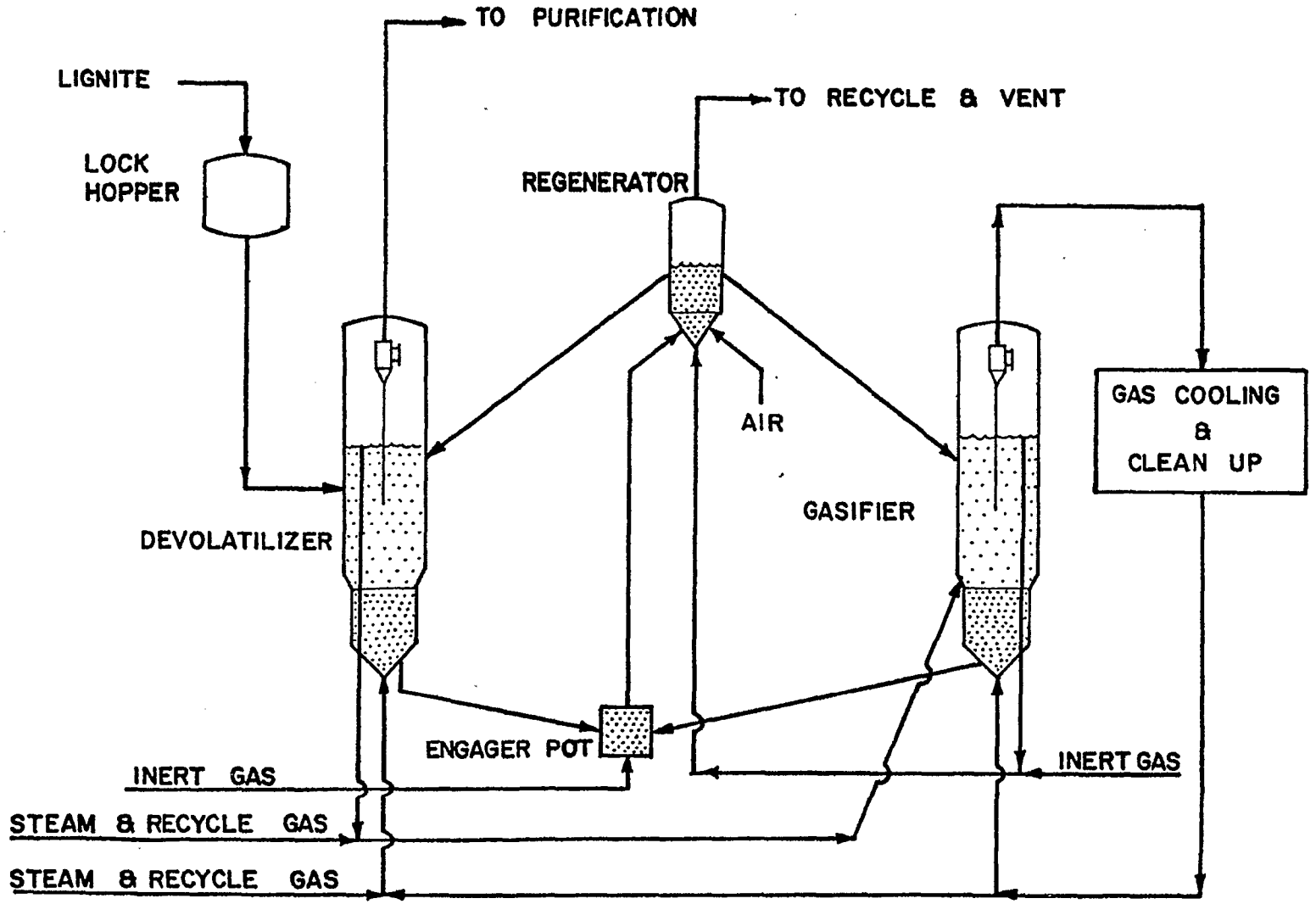

Figure IV-44 Gasification Phase of Alternate V

Page Intentionally Left Blank

NOTATION

a', b'	constants
C_A	concentration of component A(moles/cu.ft. or moles/cm^3)
$\overline{C}_p$	mean specific heat of gas (BTU/lb-mol °F)
d_p	particle diameter (ft.)
D_t	reactor diameter (ft.)
F_b	upward solid flow rate in bubble phase (moles/sec)
F_e	downward solid flow rate in emulsion phase (moles/sec)
F_m	solid flow rate between bubble phase and emulsion phase (moles/sec)
F_S	solid feed rate (moles/sec)
G_s	solid flow rate in entrained bed (moles/sec)
H_a	heat input based on unit amount of coal (BTU/lb-mol)
H_{CO_2}, H_{CO}, H_{H_2}	
H_{N_2}, H_{CH_4}, H_{H_2O}	enthalpies of CO_2, CO, H_2, N_2, CH_4 and water vapor respectively (BTU/lb-mol)
H_ℓ	heat loss based on unit amount of coal (BTU/lb-mol)
H_{pf}, H_{pg}, H_{ps}	amount of preheat for coal, dry gas and superheated water vapor, respectively (BTU/lb-mol)
H_w	enthalpy of liquid water (BTU/lb-mol)
k_v	reaction rate constant (cc/gmole/sec)
K	equilibrium constant
L_{mf}	bed height at incipient fluidization (ft.)
M_C, M_H, M_O, M_W	quantities of carbon, hydrogen, oxygen, and liquid water respectively, based on unit quantity of coal (lb-mol/lb-mol)
M_{O_2}, M_{CO_2}, M_{N_2}	
M_{H_2}, M_{H_2O}, M_{CH_4}	quantities of O_2, CO_2, N_2, H_2, water vapor, CH_4, CO, respectively in gaseous medium based on
M_{CO}	unit quantity of coal (lb-mol/lb-mol)

m_{CO_2}, m_{CO}, m_{H_2}, m_{N_2}, m_{H_2O}, m_{CH_4}	quantities of CO_2, CO, H_2, N_2, H_2O, CH_4 respectively based on unit quantity of coal (lb-mol/lb-mol)
Q_C, Q_{CO}, Q_{CH_4}, Q_w	heat of combustion for solid carbon and gaseous CO, CH_4, H_2 respectively. (BTU/lb-mol)
Q_g	gross calorific value of coal or coke (BTU/lb-mol)
Q_g^*	gross calorific value of coal or coke (BTU/lb)
Q_H	heating value of outlet gas per lb-mol of coal (BTU/lb-mol)
q_{CH_4}	heat of formation for CH_4 (BTU/lb-mol)
q_w	heat of formation for feed stock (BTU/lb-mol)
ν_w	latent heat for vaporization of water (BTU/lb-mol)
t_i, t_s	preheat temperature of gasification medium and of superheated steam (°F)
t_g	temperature of exit gas (°F)
t_o	temperature of circumstance (°F)
U_o	gas velocity (ft/sec)
U_{mf}	minimum fluidization velocity (ft/sec)
U_p	particle velocity (ft/sec)
V_{H_2}	amount of H_2 introduced (ft^3/lb)
v_{H_2}, v_{CO}, v_{CH_4}	amount of H_2, CO and CH_4 produced at standard state (ft^3/lb)
W	quantity of solid in a compartment (moles)
X	carbon conversion
Y	1 - X
α	ratio of the heat generated by conversion η_C to that of 100% conversion
β	amount of preheat

γ	amount of heat accompanying the exit gas
δ	heat loss
ε	voidage
η_C	conversion of carbon
η_G	gasification efficiency
μ	gas viscosity(lb/ft.hr)
ρ_f	gas density (lb/cu.ft.)
ρ_s	solid density (lb/cu.ft.)

superscript * represents amount based on lb-coal

Literature

1. Blackwood, J. D. and McGrory, F., Australian Journal of Chemistry, 11 16 (1958).

2. Engineering Study and Technical Evaluation of BCR "Two-Stage Super-pressure Gasification Process", prepared by Air Products and Chemicals, Inc., Sept. 15, 1970.

3. Gas Generator Research and Development, Survey and Evaluation (BCR Report L-156) (1964-1965)

4. Ergun, S., U.S.B.M. Bulletin 598 (1962).

5. Feldkirchner, H. L. and Huebler, J., IEC Process, Design & Develop. 4 134 (1965).

6. Feldkirchner, H. L. and Linden, H. R., IEC Process, Design & Develop. 2 153 (1963).

7. Feldman, H., Kiang, K. D. and Yavorsky, P. M., ACS Div. of Fuel Chem. Preprints, Vol 15, No. 3, pp. 62-76, Sept. 1971.

8. Field, M. A., Gill, D. W., Morgan, B. B. and Hawksley, P. G. W., "Combustion of Pulverized Coal" The British Coal Utilization Research Association, Leatherhead, 1967.

9. Forney, A. J., Kenney, R. F., Gasior, S. J. and Field, J. H., Fluid Bed Gasification of Pretreated Pittsburgh Seam Coals, "Fuel Gasification" (Advanced in Chem. Series 69) p. 128, Amer. Chem. Soc. Pub. (1967).

10. Gadsby, J., Hinshelwood, C. N. and Sykes, K. W., Proc. Royal Soc. (London) A187, 129 (1946).

11. Henry, J. P. and Louks, B. M., An Economic Comparison of Processes for Producing Pipeline Gas (Methane) from Coal. Prepared for Amer. Chemical Society Meeting, Chicago, September 1970.

12. Hiteshue, R. W., Proceedings of the Synthetic Pipeline Gas Symposium, Pittsburgh, Pa., Nov. 15, 1966, pp. 13-23.

13. Janka, J. C. and Malhotra, R., "Estimation of Coal and Gas Properties for Gasification Design Calculations, I.G.T. Report, January 1971.

14. Jolly, L. J. and Pohl, A., J. Inst. Fuel 26 33 (1953)

15. Katell, Sidney and Wellman, P., An Evaluation of Tonnage Oxygen Plants., Bureau of Mines, U. S. Department Of The Interior, Morgantown, W. Va.

16. Kato, K. and Wen, C. Y., Chem. Eng. Sci., 24 1351 (1961).

17. Kunii, D., Performance Characteristics of Hydrocarbon Cracker and Gas Generators, Chem. Eng. (Japan) 29, 286 (1965).

18. Long, F. J. and Sykes, K. W., Proc. Royal Soc. (London) A193 377 (1948).

19. Lowry, H. H., "Chemistry of Coal Utilization", Supplementary Volume, John Wiley & Sons, Inc., New York 1963.

20. Newman, L. L., Oxygen in the Production of Hydrogen or Synthesis Gas, Ind. Eng. Chem., 40 599 (1948).

21. Pyrcioch, E. J. and Linden, H. R., Ind. Eng. Chem. 52 590 (1960).

22. Rossini, F. D., et. al.,"Selected Values of Physical and Thermodynamic Properties of Hydrocarbons and Related Compounds" Carnegie Press, Pittsburgh, Pa., (1953).

23. Segeler, C. G., "Gas Engineering Handbook", The Ind. Press, New York (1966).

24. Von Fredersdorff, C. G., Inst. Gas Technology Research Bulletin No. 19 (1955) p. 75.

25. Wen, C. Y., Abraham, D. C. and Talwalker, A. T., "A Kinetic Study of Reaction of Coal Char with Hydrogen-Steam Mixture", Fuel Gasification, Advances in Chemistry Series. 253 (1967).

26. Wen, C. Y., Huebler, J., Ind. Eng. Chem. Process, Design & Develop. 4 142 (1965).

27. Wen, C. Y., and Huebler, J., Ind. Eng. Chem. Process Design & Develop. 4 147 (1965).

28. Wen, C. Y. and Yu, Y. S., CEP Symposium Series 62 100 (1966).

29. Yoshida, K. and Wen, C. Y., Chem. Eng. Sci. 25 1395 (1970).

30. Wen, C. Y., Chap. 16, Dilute Phase System "Fluidization" Academic Press 1971.

31. Chang, T. M. and Wen, C. Y., Ind. Eng. Chem. Fundamental, 7, 422 (1968)

32. Feldman, H. F., Simons, W. H., Mima, J. A. and Hiteshue, R. W., ACS Division of Fuel Chem. Preprints, Vol. 14, No. 4, part II, pp. 1-13, Sept. 1970

33. Ishida, M. and Wen, C. Y. Ind. Eng. Chem. Proc. Des. Dev., 10 164 (1971)

34. Ishida, M., and Wen, C. Y., Chem. Eng. Sci., 26, 1031 (1971)

35. Ishida, M., Wen, C. Y. and Shirai, T., ibid., 26, 1043 (1971)

36. Wen, C. Y., Ind. Eng. Chem., 60, (9), 34 (1968)

37. Wen, C. Y. and Wang, S. C., Ind. Eng. Chem., 62 (8), 30 (1970)

38. Wen, C. Y. and Chang, T. M., Ind. Eng. Chem. Proc. Des. Dev., 7, 49 (1968)

39. Wen, C. Y. and Wei, L. Y., A.I.Ch.E. Journal, 16, 848 (1970)

40. Wen, C. Y. and Wei, L. Y., ibid., 17, 272 (1971)

Chapter V. SHIFT CONVERSION

Page Intentionally Left Blank

SHIFT CONVERSION

As was described in the gasification section, different gas compositions were obtained from the effluents of different types of gasifiers. These effluent gases were then introduced to the water-gas shift conversion system after certain treatments, i.e., light oil vaporization, dust removal, etc.

The objective of the present study is to search for the most economical scheme for shift conversion by which the effluent gases from gasifiers can be processed to achieve a proper hydrogen-to-carbon monoxide ratio for methanation at a later stage. For the purpose of demonstrating techniques used in design, simulation and optimization, the effluents from the gasifiers are classified into three typical cases which are used in this chapter and the subsequent chapters.

Among the three cases, Case I already contains enough hydrogen for methanation, and, therefore, only Case II and Case III are treated by the subsequent purification and methanation processes. However, considering the varieties of gas compositions appearing in commercial water-gas shift conversion processes, two other special cases, namely, Case S-1 and Case S-2 are also selected and optimized. Case S-1 represents the intermediate-CO-concentration case for methanation under low operating pressure range, and Case S-2 is for the production of pure hydrogen associated with the primary coal gasification phase. Table V-1 lists the specific conditions of each case.

In this study, two most likely operational schemes, adiabatic reactor system and cold-quenching reactor system, are considered. Because of the relatively low heat of reaction, it is obvious that the system employing internal heat removal is unnecessary.

The optimization is based on the combined three stages of operation: waste heat boiler, reactor, and product gas cooler. The pseudo first order

Table V-1. Flow Rates and Compositions of Feed and Product Gases

Case II

	Feed		Product	
	lb mole/hr	mole %	lb mole/hr	mole % (dry basis)
CO	9210.	11.7	6450.	10.4
H_2O	19160.	24.4	-	-
H_2	17820.	22.7	20580.	33.1
CO_2	11570.	14.7	14330.	23.0
CH_4	19720.	25.1	19720.	31.7
C_6H_6	140.	0.2	140.	0.2
N_2	720.	0.9	720.	1.2
H_2S	230.	0.3	230.	0.3
Total	78570.	100.0	62170.	100.0

Inlet Temperature = 1000°F Pressure = 1100 psia

Case III

	Feed		Product	
	lb mole/hr	mole %	lb mole/hr	mole % (dry basis)
CO	31850.	35.0	12420.	12.6
H_2O	11770.	12.9	-	-
H_2	19220	21.1	38650.	39.1
CO_2	12000.	13.2	31430.	31.9
CH_4	14590.	16.0	14590.	14.8
C_6H_6	200.	0.2	200.	0.2
N_2	780.	0.9	780.	0.8
H_2S	590.	0.7	590.	0.6
Total	91000.	100.0	98660.	100.0

Inlet Temperature = 1700°F Pressure = 1050 psia

Case S-1 [9]

	Feed lb mole/hr	mole %	Product lb mole/hr	mole % (dry basis)
CO	20930.	16.9	18500.	19.4
H_2O	30690.	24.8	-	-
H_2	54590.	44.1	57010.	59.6
CO_2	8450.	6.8	10880.	11.4
CH_4	8830.	7.1	8830.	9.2
N_2	370.	0.3	370.	0.4
Total	123860.	100.0	95590.	100.0

Inlet Temperature = 1600°F Pressure = 380 psia

Case S-2 [13]

	Feed lb mole/hr	mole %	Product lb mole/hr	mole % (dry basis)
CO	14700.	36.7	1370.	2.8
H_2O	4200.	10.5	-	-
H_2	19170.	48.0	32500.	66.2
CO_2	1710.	4.3	15040.	30.6
CH_4	140.	0.4	140.	0.3
N_2	40.	0.1	40.	0.1
Total	39960.	100.0	49090.	100.0

Inlet Temperature = 1127°F Pressure = 1200 psia

rate equation which includes the catalyst pore diffusion effect is used for the present optimization, but other types of rate equations are also discussed. The objective function, which is the production cost, is formulated based on the Utility Gas Production General Accounting Procedure[26].

1. Thermodynamics and Reaction Kinetics

1.1 Simultaneous Reactions

The possible reactions involved in water-gas shift conversion process with feed gas components containing CO, H_2O, H_2, CO_2, CH_4 and N_2 are:

(1) $CO + H_2O = CO_2 + H_2$

(2) $CO + H_2 = C + H_2O$

(3) $CH_4 = C + 2H_2$

(4) $2CO = C + CO_2$

(5) $CO_2 + 2H_2 = C + 2H_2O$

(6) $CO + 3H_2 = CH_4 + H_2O$

(7) $2CO + 2H_2 = CH_4 + CO_2$

(8) $CO_2 + 4H_2 = CH_4 + 2H_2O$

Although only three of the above reactions are independent reactions, it will be worthwhile to consider their general tendency within the range of operating conditions.

If a reaction is written in the form

$$\Sigma \nu_i M_i = 0 \qquad (V-1)$$

the equilibrium constant, K_y based on mole fraction of gaseous components can be expressed as

$$K_y = K_\chi^{-1} P^{-\Sigma \nu_i} K_f \qquad (V-2)$$

where

M_i is the chemical component i

ν_i is the stoichiometric coefficient for component i

P is the total pressure of the system

$K_\chi = \prod_i x_i^{\nu_i}$, $K_f = \prod_i f_i^{\nu_i}$

χ_i and f_i are the fugacity coefficient and the fugacity of component i, respectively.

The values of K_y obtained from the Bureau of Standards [21] are plotted in Figure V-1 , for the estimation of possible carbon deposition and other reactions. Reactions (2) to (5) accompany the carbon deposition, and (6) to (8) involve the methane formation. Among the several techniques usually applied to control the selectivity of simultaneous reactions, the method of adjusting the reactant concentrations and selecting the proper catalyst seems most promising. As can be seen from Figure V-1 , all values of equilibrium constants, except that of reaction (3), decrease as the temperature is increased. The necessary steam concentration, to prevent the carbon deposition and methane formation, may be calculated from these values. However, at a temperature below 700°K (800°F), the amount of steam required computed this way is too large to be practical for cost consideration.

Since the determination of the amount of steam required depends on the rate of reaction and the type of catalyst used, the thermodynamic equilibrium consideration alone is not sufficient. In practice, a large amount of steam is used in most water-gas shift conversion processes, and therefore reactions (2), (5), (6) and (8) are largely suppressed. On the other hand, reactions such as (3), (4) and (7) should be regulated by other conditions. The problem of carbon deposition and methane formation has been one of the major reasons for developing a highly selective water-gas shift catalyst. According to the report by Girdler [29,8], the carbon deposition and methane formation can be avoided without difficulty by using the commercial iron-chromium-oxide catalyst under the suitable steam to gas ratio. Despite its importance however, the determination of the steam to

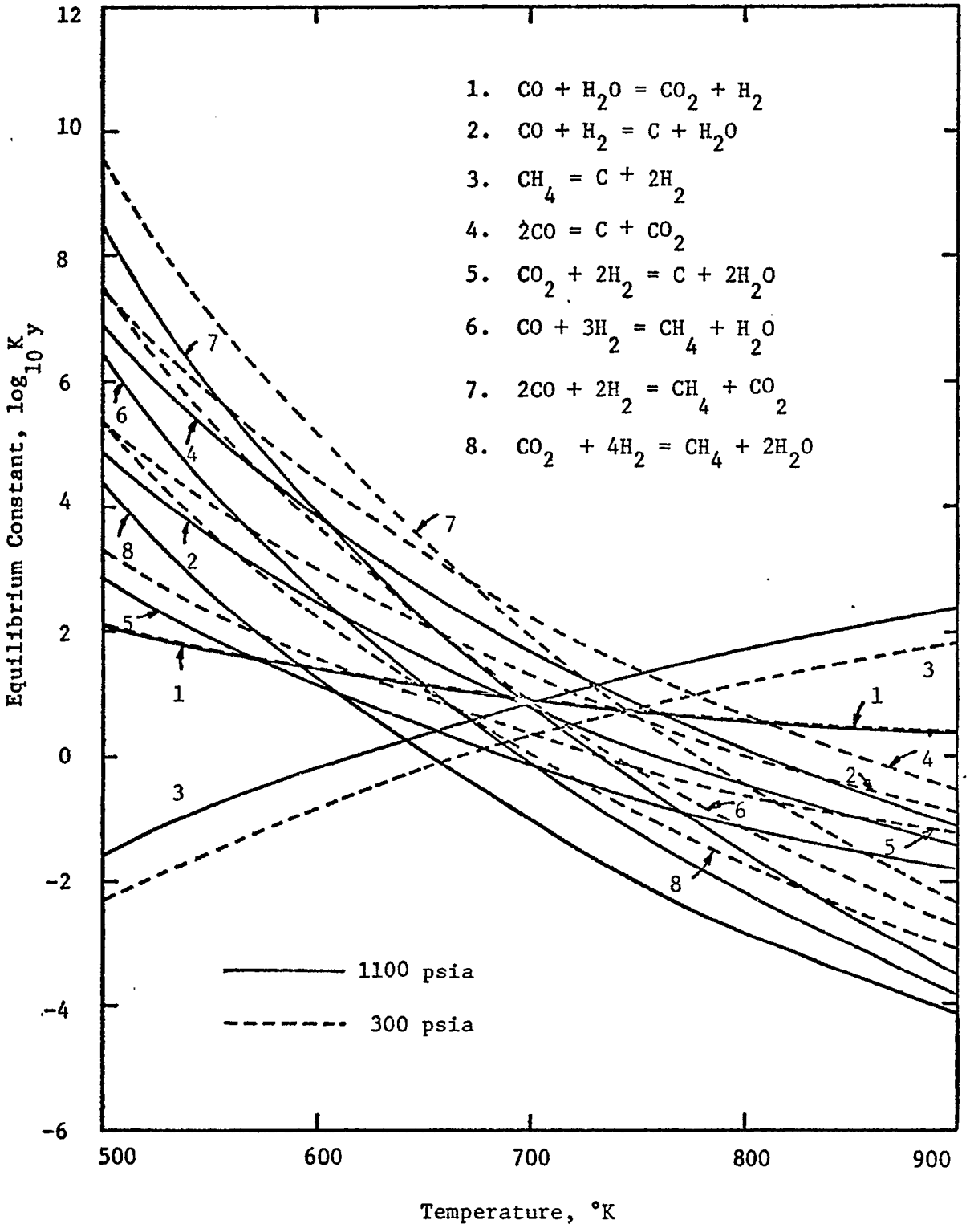

Figure V-1 Equilibrium Constants of Possible Reactions in Water-Gas Shift Process As a Function of Temperature

gas ratio is not straightforward. Girdler [29] reported that the steam to gas ratio is approximately between 1.0 to 3.0, depending mainly upon the concentration of CO. In this study therefore, the steam to gas ratio is selected by a rather simple approach[27], satisfying roughly the criteria recommended by Girdler for negligible carbon deposition and other side reactions.

1.2 Rate Equation

The stoichiometric relation of water-gas shift reaction is expressed as

$$CO + H_2O \rightleftharpoons CO_2 + H_2 \qquad (V\text{-}3)$$

Among many different types of water-gas shift rate equations proposed so far, the first order equation of Laupichler [14], and Mars [16], the second order equation of Moe [18], and the exponential form of the equation of Bohlbro, et. al. [5] are noteworthy. The recent paper of Ruthven [22] reviewed the experimental results obtained by previous investigators, and concluded that the pseudo-first order rate equation is quite adequate in most cases. This equation seems to have more flexibility than others since it includes the pore diffusion effect of catalyst, which is particularly important at high temperatures. In the present study, the pseudo-first order rate equation is consistently used regardless of operating conditions. However, the result obtained from the second order equation of Girdler [8] is also presented for comparison. The two types of rate equations are summarized as follows:

(1). Second order rate equation

$$r'_{CO} = k(C_{CO}\, C_{H_2O} - C_{H_2}\, C_{CO_2}/K_y) \qquad (V\text{-}4)$$

$$k = \exp(15.95 - 17500/RT) \qquad (V\text{-}5)$$

where r'_{CO} is the reaction rate of CO in cu.ft.CO/(cu.ft.cat.)(hr.)

C_i is the concentration of component i in mole fraction.

k is the reaction rate constant and K_y is the equilibrium constant.

R is gas constant and T is the temperature in degree Rankines.

2. Pseudo-first order rate equation

$$-dp_{CO}/dt = k_o(p_{CO} - p_{CO_e}) \qquad (V-6)$$

or in an integrated form

$$-\ln\left(1 - \frac{X_{CO}}{X_{CO_e}}\right) = k_o t = k_{ap}/S_v \qquad (V-7)$$

where

p_{CO} and p_{CO_e} are partial pressures of CO at any time and at equilibrium, respectively [psi].

k_o is apparent first order rate constant based on the unit catalyst bed volume [hr^{-1}].

X_{CO} and X_{CO_e} are fractional conversions of CO at any time and at equilibrium, respectively.

k_{ap} is apparent catalyst activity at pressure p [hr^{-1}].

S_v is the space velocity at N.T.P. basis [hr^{-1}].

The value of k_{ap} is obtained from intrinsic catalyst activity, k_s as follows:

$$k_s = 199.6 \exp(-49140/RT) \qquad (V-8)$$

$$k_{V_1} = \rho_p s_p RT k_s \qquad (V-9)$$

$$D_{e_1} = 0.069 \left(\frac{T}{673}\right)^{1.5} \qquad (V-10)$$

$$\phi_1 = \frac{d_p}{2}\sqrt{k_{V_1}/D_{e_1}} \qquad (V-11)$$

$$\eta_1 = \frac{3}{\phi_1}\left(\frac{1}{\tanh\phi_1} - \frac{1}{\phi_1}\right) \qquad (V-12)$$

$$k_{a_1} = \frac{492}{T} k_{V_1} \eta_1 (1 - \varepsilon) \qquad (V-13)$$

$$k_{ap} = k_{a1} [(P/14.7)^{0.35} - 1/\phi_1]/(1 - 1/\phi_1) \qquad (V\text{-}14)$$

where

k_{V_1} is intrinsic rate constant at 1 atm. [hr^{-1}]

ρ_p and S_p are the pellet density [lb./cu.ft.] and surface area [sq.ft./lb.] of catalyst

D_{e_1} is effective diffusivity of CO in catalyst pores at 1 atm. [sq.ft./hr.]

ϕ_1 is Thiele modulus at 1 atm.

η_1 is effectiveness factor at 1 atm.

ε is voidage of catalyst bed

k_{a_1} is apparent catalyst activity at 1 atm. [hr^{-1}]

The profiles of reaction rate under specified conditions using pseudo-first order and second order equation are shown in Figure V-2.

1.3 Effect of Pressure on Catalyst Activity and Pore Diffusion

As it is apparent from the rate equation, the catalyst activity increases with increasing pressure. Since most of the water-gas shift conversions are carried out at elevated pressure, many experiments performed by earlier workers show the effect of pressure on catalyst activity. According to the report of Moe [16], beyond 400 psig the activity of water-gas shift catalyst increases more than four times that at an atmospheric pressure.

Figure V-3 shows the effect of pressure on catalyst activity using pseudo-first order rate equation with catalyst pellets sizes and temperatures as parameters. Although the range of pressure has been investigated up to 1000 psig in this figure, the values above 450 psig may not be accurate because of the uncertainty of rate equation at high pressures.

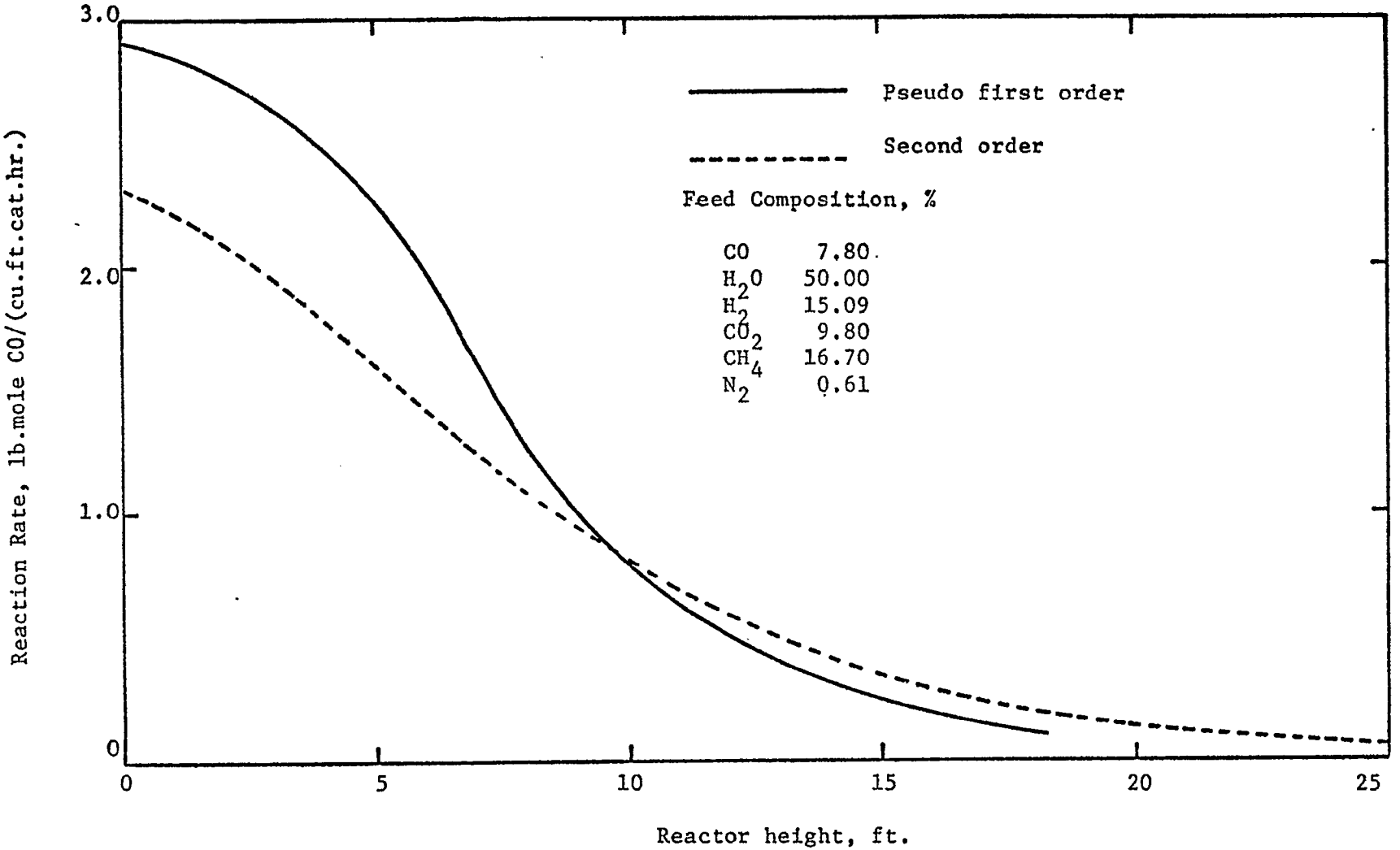

FIGURE V-2 Comparison of Pseudo First Order and Second Order Rate Equation with Inlet Temperature at 750°F

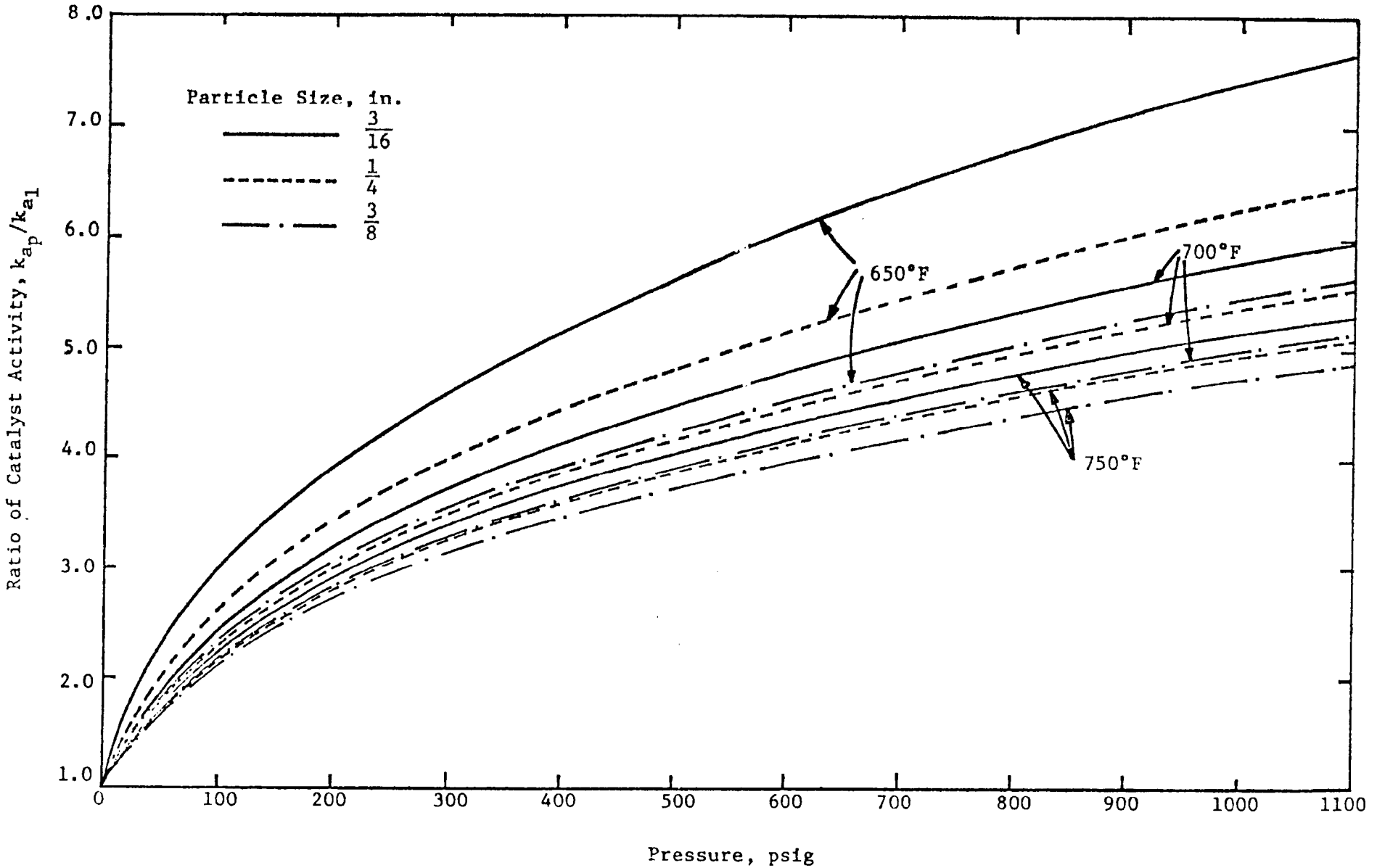

FIGURE V-3 Effect of Pressure on Catalyst Activity With Temperature and Particle Size as Parameters

From Figure V-3, the effect of pressure on catalyst activity appeared to be more pronounced for the smaller catalyst pellets and at lower temperatures. The effect of pore diffusion on the reaction rate can be evaluated from the dimension of catalyst pellets and the effective diffusivity through catalyst pores in terms of the Thiele modulus. Values of Thiele modulus and the effectiveness factor versus temperature are shown in Figure V-4 for various pressures and various sizes of catalyst pellets. Evidently the effect of diffusion becomes more important as the temperature increases and as the pellet size becomes larger.

1.4 Mass Heat Transfer Within Catalyst Bed

Since the rates of water-gas shift reaction and the heat generation are comparatively moderate, the difference in temperature and concentration between the bulk phase of the gas and the catalyst surface is not very large. This can be shown numerically.

The temperature difference may be estimated by:

$$T_c - T_b = \frac{r_s \Delta H}{h_p \pi d_p^2} \qquad \text{(V-15)}$$

where h_p is the heat transfer coefficient between the particle surface and bulk phase, and can be calculated from[28]

$$J_H = (N_{Pr})^{2/3} h_p/(C_p G) = 0.989\ (d_p G/\mu)^{-0.41} \qquad \text{(V-16)}$$

The maximum temperature difference will result from the maximum reaction rate. The calculation based on the reaction rate of 6 lb-mole CO/(hr.) (cu.ft.cat.), and with gas velocity, G, of 7000 lb/(hr.)(sq.ft.), shows that the temperature difference is approximately 3°F. Such a negligibly small value of temperature

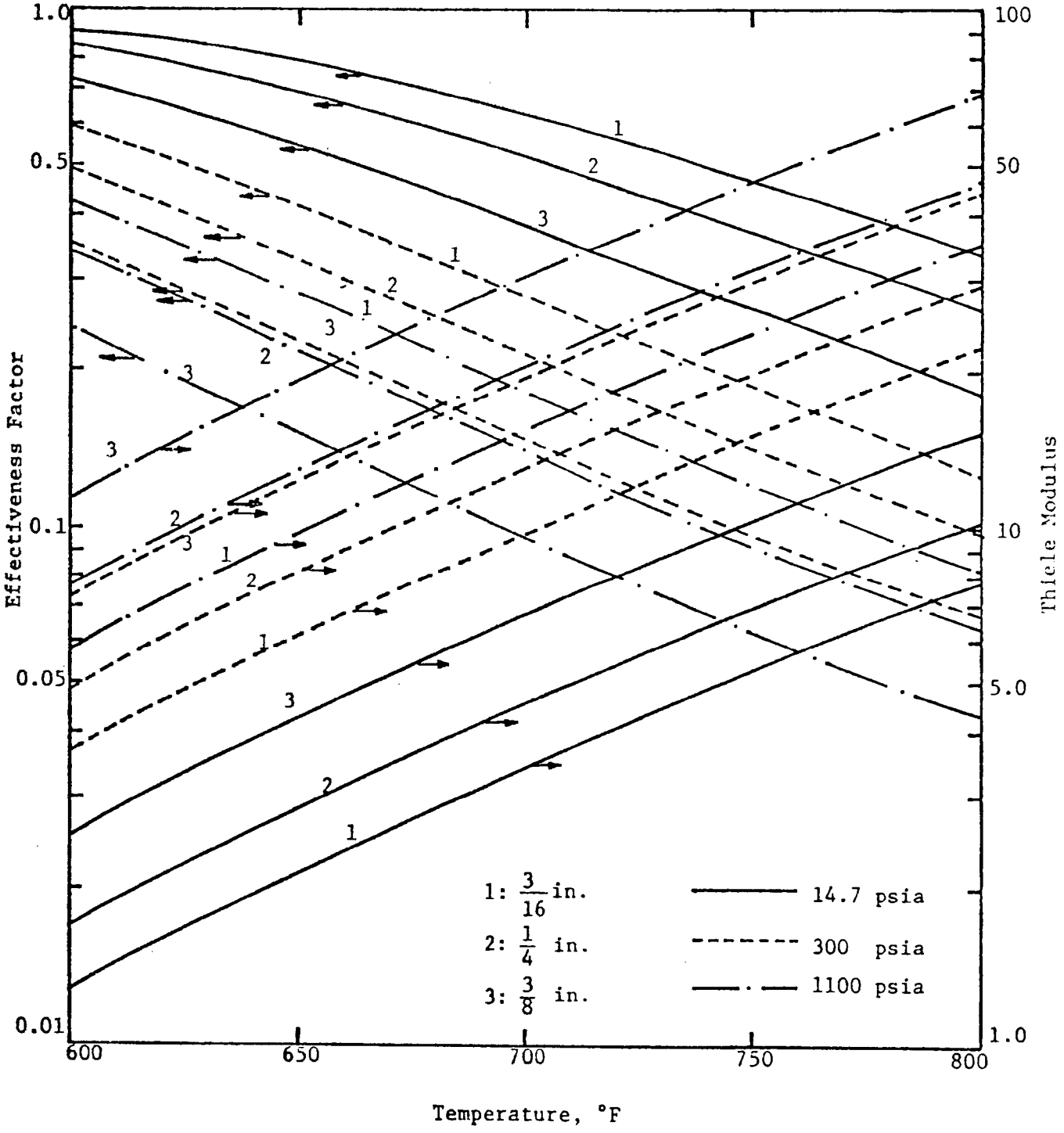

FIGURE V-4 Effectiveness Factor and Thiele Modulus with Particle Size and Pressure as Parameters

difference was also reported earlier[14],[16]. The temperature gradient within a catalyst pellet can be calculated by the following heat balance equation, assuming an uniform reaction in the catalyst.

$$\frac{d^2T}{dr^2} + \frac{2}{r}\frac{dT}{dr} = \frac{r_{CO}}{k_e}\Delta H \qquad \text{(V-17)}$$

where k_e, the effective thermal conductivity may be calculated from

$$1/k_e = 1/[(1-\zeta)k_c + \zeta k_g] \qquad \text{(V-18)}$$

where ζ is the internal porosity of catalyst

k_c is the thermal conductivity of the catalyst material

k_g is the thermal conductivity of reacting gases

The solution of the above equation using proper boundary condition is

$$T = T_c + \frac{1}{6}(-\frac{r_{CO}}{k_e}\Delta H)[(\frac{d_p}{2})^2 - r^2] \qquad \text{(V-19)}$$

Again, r_{CO} = 6 lb mole/(hr. $ft.^3$) is used for the calculation of temperature difference within the pellet, giving $(T-T_c)\Big|_{r=0} < 4^oF$.

In a similar manner, the concentration difference between the bulk phase and the surface of the catalyst is approximated by

$$C_c - C_b = r_s/(k_f \pi d_p^2) \qquad \text{(V-20)}$$

where k_f is the fluid-particle mass transfer coefficient in the bed, and may be evaluated from [11] (V-21)

$$J_M/(1-\varepsilon)^{0.2} = 1.46\,[d_p G/\mu(1-\varepsilon)]^{-0.41}$$

The numerical calculation indicates that the maximum difference in concentration corresponds to only 2% of that of bulk phase.

In summary, it may be safely assumed that the differences in temperature and concentration between the bulk phase and the catalyst surface are negligibly small.

2. Reactor Performance Equation

2.1 Flow Model for Fixed Bed Reactor

Flow patterns of fluid in a fixed bed reactor are describable by the dispersed plug flow model or compartment-in-series model. This is shown for the present system of the study as follows. The dispersed plug flow model is characterized by the reactor dispersion number such that [15]

$$D_a/vL = (D_a/vd)(d/L) < 0.01 \qquad \text{(V-22)}$$

where D_a is the axial dispersion coefficient

v is the axial mean velocity

d is the characteristic length in the reactor

L is the length of the reactor

For the fixed bed reactor with particle Reynold's number larger than 10, experimental works of Levenspiel and Bischoff [15] showed that

$$D_a/vd \approx 0.5 \qquad \text{(V-23)}$$

Combining Equations (V-22) and (V-23) yields

$$d/L < 0.02 \qquad \text{(V-24)}$$

Since in this study the characteristic length d, the length of unit compartment, is selected as 1 in., and L becomes much larger than 5 ft., Equation (V-24) is satisfied. Under this condition, the compartment-in-series model employed satisfactorily represents the equivalent characteristics of the dispersed plug flow model for a fixed bed reactor.

2.2 Performance Equations

Material balances for each component around n-th compartment are given as follows:

$$F_i^n = F_i^{n-1} + V_c^n r_{CO} \qquad i = 1, 2, \ldots 6 \qquad \text{(V-25)}$$

where r_{CO} is the reaction rate of carbon monoxide and is negative for i =1.2, positive for i = 3,4, zero for i = 5,6; F_1^n, F_2^n, F_3^n, F_4^n, F_5^n, and F_6^n are the molar flow rates of carbon monoxide, steam, hydrogen, carbon dioxide, methane, and nitrogen at the exit of the n-th compartment, respectively; and V_c^n is the catalyst volume per unit compartment.

The energy balance around the adiabatic n-th compartment may also be expressed as:

$$-(T^{n-1}-T_o)\sum_{i=1}^{6} F_i^{n-1} C_{p_{im}} + (T^n-T_o)\sum_{i=1}^{6} F_i^n C_{p_{im}} = -\Delta H_{To} V_c^n r_{CO} \qquad \text{(V-26)}$$

where

T_o is the standard temperature taken as 77°F

$$C_{p_{im}} = \int_{T_o}^{T} C_{pi}\, dT/(T-T_o), \Delta H_{To} = -17698 \text{ B.t.u./lb.mole}$$

The pressure effect on heat capacities is almost negligible even at 1000 psig except that of steam. For the calculation of pressure drop , Ergun's equation is applied [10]:

$$\Delta p = \frac{150(1-\varepsilon)\left(\frac{\mu}{d_p G}\right) + 1.75}{\left(\frac{\varepsilon^3}{1-\varepsilon}\right)\left(\frac{d_p}{C_L}\right)\left(\frac{\rho g_c}{G^2}\right)(144)} \qquad \text{(V-27)}$$

where

Δp is the pressure drop across the unit compartment[lb_c/sq.in.]

ρ and μ are the density[lb./cu.ft.] and viscosity [lb./ft.hr.] of gas, respectively

G is mass velocity of gas [lb./$ft.^2$ hr.]

d_p is the diameter of the catalyst pellet [ft.]

C_L is the height of the unit compartment [ft.]

ε is the void fraction of catalyst bed.0.4 is used.

3. Optimization

3.1 Process Description

The block diagram of the system for optimization is shown in Figure V-5. Since the temperature of the raw gas from gasifier is usually much higher than the operating temperature for shift conversion, cooling by waste heat boiler is necessary before it goes into the reactor. The gas, after cooled to a proper temperature, is then introduced to the reactor in which the mole ratio of carbon monoxide to hydrogen is adjusted to about 1/3. Therefore, for any fixed inlet gas composition, there is always a required conversion of carbon monoxide. Before the gas enters the reactor, a certain amount of steam is added to this stream. The additional steam also brings the steam to gas ratio high enough so that carbon deposition will not take place. Determination of the proper steam to gas ratio is not a simple problem, however, because it requires the knowledge of many factors including the reaction kinetics of carbon with gases. Furthermore, the amount of steam introduced would greatly affect not only the steam cost but also reaction rate, equilibrium conversion, etc., and the optimum operating conditions.

The required conversion of carbon monoxide can be achieved in the reactor by one throughput. However, because of the cost of steam and the heavy duty required in the product gas cooler, it will be more advantageous to by-pass a portion of the feed, and mix it with the product gas that has been converted in excess in the reactor. The conversion in the reactor is adjusted to achieve the required conversion upon mixing. It is observed that in order to meet the required conversion by this scheme, the conversion in the reactor has to closely approach the equilibrium

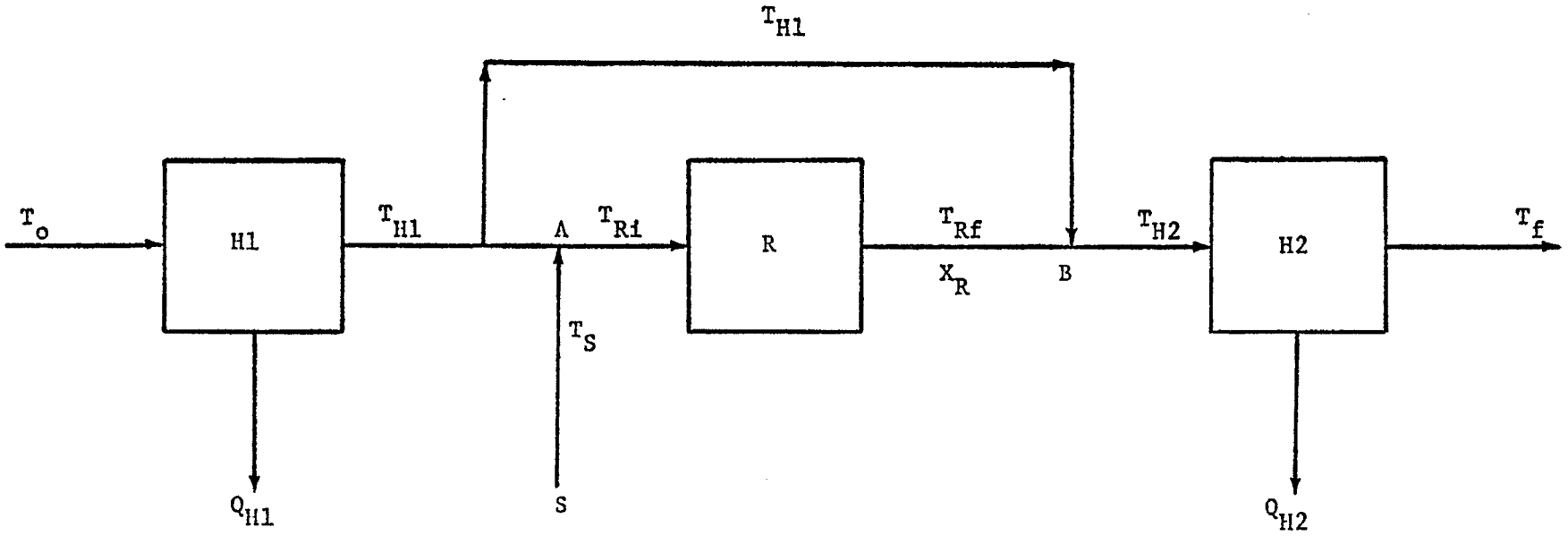

H1: Waste Heat Boiler
H2: Product Gas Cooler
R: Reactor
S: Steam

Q_{H1}: Heat Removed in H1
Q_{H2}: Heat Removed in H2
X_R: Conversion of CO
T: Temperature of Stream

FIGURE V- 5 Schematic Diagram for the Optimization of Water-Gas Shift Conversion System

conversion. The temperature of the product gas after the shift conversion is approximately 900°F, or lower if this product is mixed with the by-passed gas. Again, the outlet gas is to be cooled before purification. The outlet temperature of product gas cooler is decided as an optimal value in connection with the performance of a purifier.

3.2 Heat Exchanger

The temperature of effluent gas from the gasifier ranges from 1000°F to 1700°F depending upon the type of gasifier employed. In the waste heat boiler, the outlet temperature must be decided by an optimum search based on the entire process including the reactor and the product gas cooler. On the other hand, in the product gas cooler, the optimum inlet temperature must be under a constraint of a fixed outlet temperature.

Since both heat exchangers are similar, the same procedure is applied in actual calculation. The cooling water flows tube side in a counter-current direction to the gas stream, and is converted to a high pressure saturated steam which will be supplied to the reactor. Here, 50% of the cooling water is assumed vaporized, and the remaining 50% of the saturated water is recycled to the feed water.

The allowable pressure drop in the shell side is 3 psi, and no phase change takes place under present conditions. Rather than performing a complete optimization for the heat exchangers, a simplified procedure is adapted. This involves determination of optimum heat transfer coefficient of heat exchangers.

The heat balance considering 50% vaporization of water in the tube side is:

$$Q = W_s C_p (T_2 - T_1) \quad \text{for shell side} \qquad \text{(V-28)}$$

$$= W_T [C_p' (t_2 - t_1) + 0.5\lambda] \quad \text{for tube side} \qquad \text{(V-29)}$$

where

W, C_p, T_1, t_2, T_2, t_1 are the mass flow rate [lb./hr.], heat capacity [Btu/lb.°F], and outlet and inlet temperatures [°F] respectively

λ is the latent heat of water.

The heat transfer coefficient of shell side is calculated from:

$$\left(\frac{h_o D_o}{k_g}\right) = 0.36 \left(\frac{D_o G_S}{\mu}\right)^{0.55} \left(\frac{C_p \mu}{k_g}\right)^{1/3} \qquad \text{(V-30)}$$

where D_o is equivalent diameter for heat transfer tube [ft.]

k_g is the thermal conductivity of gas [Btu/ft.hr.°F]

G_S is the mass velocity [lb./ft^{2}hr.]

C_p is the heat capacity [Btu/lb.°F]

μ is the viscosity of gas [lb./hr.ft.]

For the estimation of pressure drop in the shell side, the following equation is available [12]:

$$\Delta p = \frac{f_s G_S^2 D_S L_H}{5.22 \times 10^{10} D_o s B} \qquad \text{(V-31)}$$

$$f_s = 0.01185 \left[\frac{D_o G_S}{\mu}\right]^{-0.1876} \qquad \text{(V-32)}$$

where

D_S is the inside diameter of the shell [ft.]

L_H is the length of the heat exchanger [ft.]

B is the baffle spacing [ft.]

s is the specific gravity

Δp is the pressure drop of the heat exchanger [psi]

Clearly, the increasing mass velocity has a favorable effect on the heat transfer coefficient but will cause larger pressure drop. The maximum

heat transfer coefficient will, therefore, be obtained by applying the highest velocity within the allowable pressure drop of 3 psi.

The tube side heat transfer coefficient for the case of no phase change may be computed by:

$$\left(\frac{h_i D_i}{k_w}\right) = 0.027 \left(\frac{D_i G_i}{\mu_w}\right)^{0.8} \left(\frac{C_p' \mu_w}{k_w}\right)^{1/3} \left(\frac{\mu_w}{\mu_o}\right)^{0.14} \qquad \text{(V-33)}$$

where

D_i is the inside diameter of the tube [ft.]

G_i is the mass velocity of water [lb./ft^2.hr.]

Actually , however, the vaporization is taking place inside the tube with much higher value of heat transfer coefficient. In such a case, it is not easy to calculate the heat transfer coefficient. In this study, therefore, the situation is simplified by separating the heat exchanger fictitiously into two zones: heating zone and vaporizing zone.

The vaporization temperature T_m, corresponding to the boundary of the two zones in the tube, can be calculated by a heat balance:

$$T_m = T_1 + W_T C_p' (t_2 - t_1)/(W_s C_p) \qquad \text{(V-34)}$$

The log-mean temperature difference in the heating zone is:

$$\Delta T^1_{l.m} = \frac{(T_m - t_2) - (T_1 - t_1)}{\ln \frac{T_m - t_2}{T_1 - t_1}} \qquad \text{(V-35)}$$

Similarly in the vaporization zone,

$$\Delta T^2_{l.m} = \frac{(T_2 - t_2) - (T_m - t_2)}{\ln \frac{T_2 - t_2}{T_m - T_2}} \qquad \text{(V-36)}$$

The overall heat transfer coefficient for each zone can be obtained by:

$$\frac{1}{U} = \frac{1}{h_i} + \frac{1}{h_o} + R_d \qquad \text{(V-37)}$$

where R_d is a dirt factor.

The heat transfer area for the heating zone becomes

$$A_h = W_T C_p' (t_2-t_1)/(U_h \Delta T^1_{lm}) \quad \text{(V-38)}$$

and for the vaporization zone:

$$A_v = 0.5 \lambda W_T/(U_v \Delta T^2_{lm}) \quad \text{(V-39)}$$

Thus the total area is

$$A_T = A_h + A_v \quad \text{(V-40)}$$

The average overall heat transfer coefficient U_T may be obtained,

$$U_T = Q/A_T \Delta T^\circ_{lm} \quad \text{(V-41)}$$

where

$$\Delta T^\circ_{lm} = [(T_2-t_2)-(T_1-t_1)]/\ln[(T_2-t_2)/(T_1-t_1)] \quad \text{(V-42)}$$

The calculation of heat exchanger costs is shown in the procedure described in Section 1.5, Chapter II. Figure V-6 shows the cost variation of heat exchangers with changing temperature of inlet or outlet for Case II. Similar tendencies are indicated in other cases.

3.3 Adiabatic Reactor System

i. Reactor

As stated before, the water-gas shift reaction is moderately exothermic. Because of this, the adiabatic reactor is an economically attractive system, particularly when the concentration of carbon monoxide in the feed gas is low.

The adiabatic operation may be expressed more clearly on the conversion-temperature plot. Figure V-7 shows the equilibrium curves for different values of steam to gas ratio based on the feed composition of Case II. On the same figure the adiabatic operating lines are shown. These lines represent the energy balance relationship starting from the given inlet temperatures. The intersection

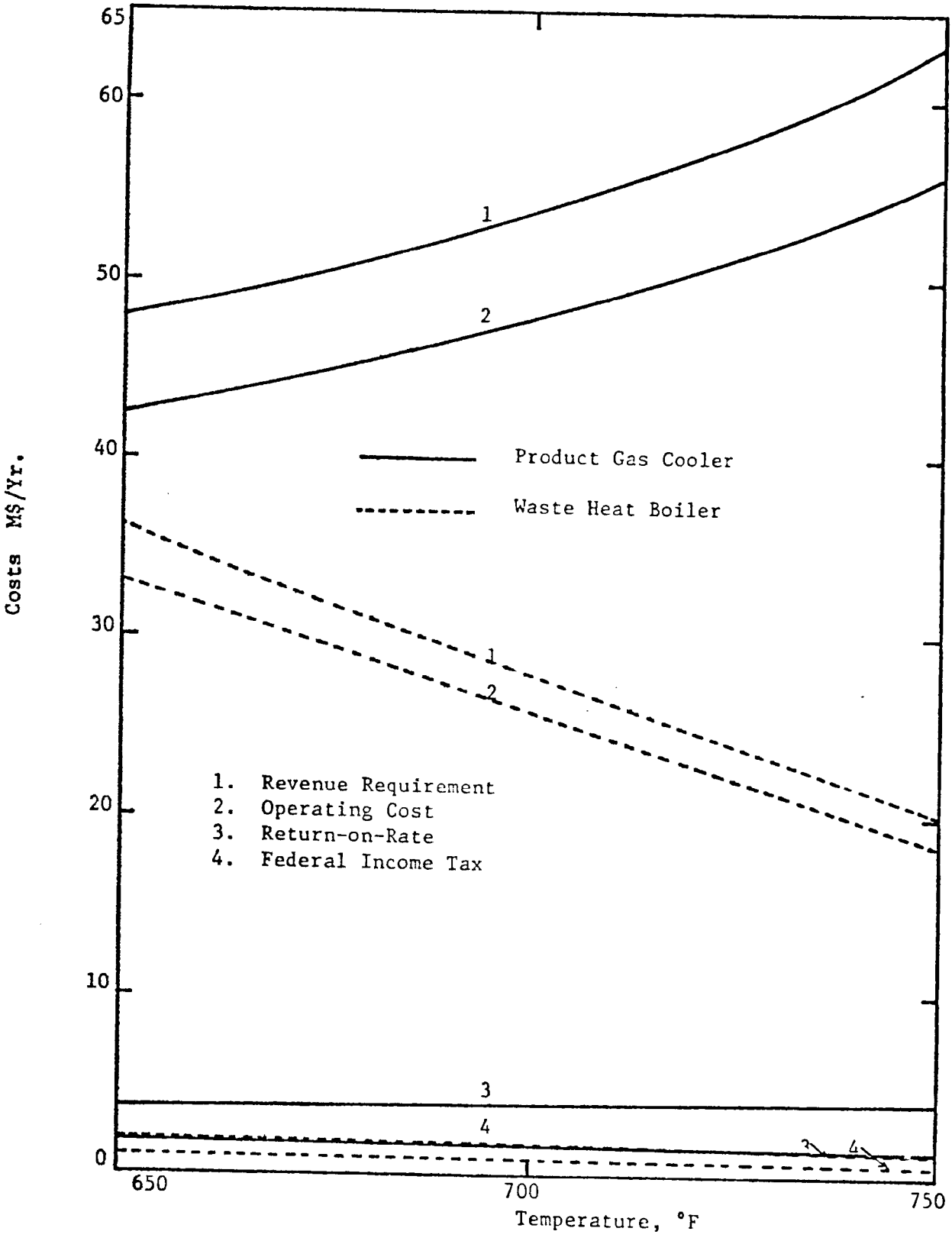

FIGURE V-6 Cost of Waste Heat Boiler Versus Outlet Temperature and Cost of Product Gas Cooler Versus Inlet Temperature in Case II

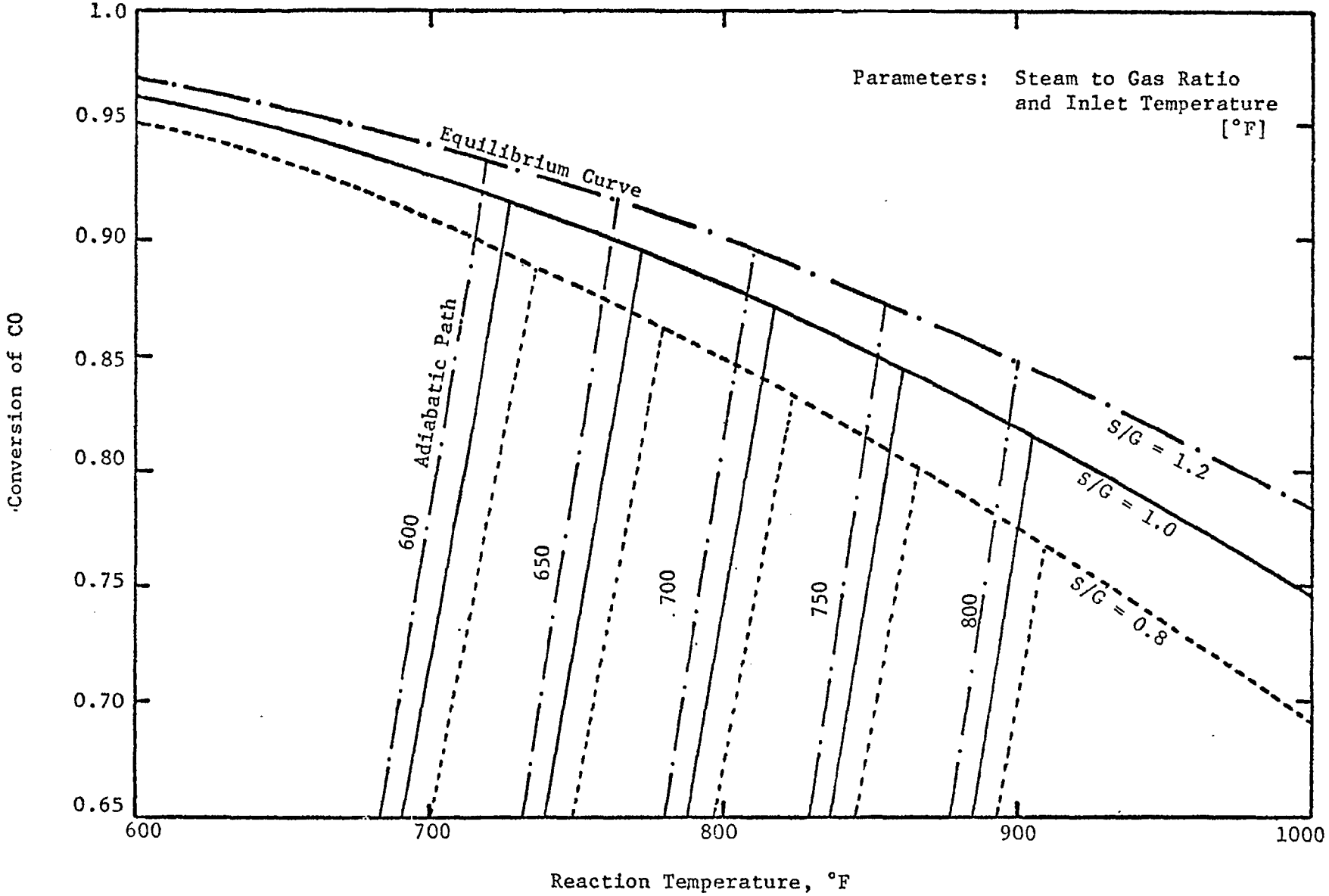

FIGURE V-7 Adiabatic Equilibrium Conversion with Different Values of Steam to Gas Ratio for Case I1

of adiabatic path with equilibrium curve is adiabatic-equilibrium point which indicates the maximum attainable conversion and temperature in an adiabatic operation. The inlet temperature to the reactor is one of the decision variables, but has a range of 600°F to 800°F. The maximum allowable operating temperature is selected as 900°F, because it has been shown experimentally that undesirable phenomena such as catalyst sintering, carbon deposition and other side reactions might take place above this temperature.

The operating pressure depends on that of the gasifier, since it was assumed that no substantial change in pressure between the gasifier and shift converter occurs. Since three cases, namely Case II, Case III and Case S-1, have been studied in this adiabatic system, two distinct operating pressures, 1000 psig and 380 psig are treated. The allowable pressure drip through the reactor is selected at 10 psi.

(a) Optimization Procedure

The optimization of the shift convertor is to find the reaction conditions at which the total annual cost is minimized. However, since the entire system to be optimized includes heat exchangers, the optimum conditions cannot be decided from the reactor study alone. In other words, the reactor is regarded as one stage while the entire process constitutes a multistage process. Therefore, at each stage the optimal decisions are obtained for every admissible value of state variables.

As described, three different feeds are treated, each of which has specific values of temperature, pressure, flow rate and composition, requiring a certain extent of conversion to be achieved. The decision variables for the optimization of the reactor portion are the inlet temperature, the conversion (or by-pass fraction), and the diameter of the reactor. In this system, the temperature of gas is taken as the state variable and the remaining

quantities the decision variables. The reactor optimization will then follow the procedure of searching for the optimum conversion and diameter for every admissible value of inlet temperature.

It can be proven that, for a given volume, a smaller diameter reactor weighs less than a larger diameter reactor because of the thickness of the reactor wall. Therefore, once the volume of the reactor is determined from the conversion, the smallest diameter will be chosen as the optimum diameter which offers the allowable pressure drop through the reactor. This reduces the number of decision variables and simplifies the calculation.

In the optimization, the adiabatic equilibrium conversion is first calculated and the corresponding temperature is determined for each of the assumed inlet temperatures with given feed composition. Since the reactor is assumed to be of plug flow type, an initial trail value of diameter is estimated approximately from the required conversion, average temperature and pressure. In searching for the optimum conversion, it appeared best to start from the point near the equilibrium conversion, because the steam cost in this case is always the dominant factor over the other factors. Nevertheless the selection of proper conversion is important and requires special care, since near the equilibrium point the reaction rate is nearly zero and the size of the reactor approaches infinity. Thus, the annual cost for the reactor is calculated at each point along the adiabatic line by taking a small interval of conversion. In this procedure, any search method may be used, and the size of interval can be changed accordingly. However, in the present study, a constant interval of 0.05 is used, progressing step by step until the cose is increased. Meanwhile, at each conversion the correct diameter of the reactor satisfying the pressure drop limitation is calculated by an iteration starting from the first approximated value.

The determination of conversion in the reactor automatically fixes the by-pass fraction of the feed gas. Once the optimum conversion and the correct value of the diameter are obtained for a single reactor, the optimum number of parallel reactors can be readily decided, based on the optimum space velocity obtained. Figure V-8 shows the determination of the optimum conversion for Case II and Figure V-9 indicates the effect of the number of reactors on costs for Case III.

The computer flow diagram for detailed optimization procedure is shown in the Appendix B.

(b) Results

Case II

In Case II where the concentration of CO is quite low, the rate of reaction is rather slow, showing the suitability of the adiabatic reactor.

The profiles of temperature, concentration and reaction rate along the reactor under optimum conditions are shown in Figures V-10, V-11 and V-12, respectively. The costs versus inlet temperature are shown in Figures V-13 and V-14. As can be seen from the figures, the annual total cost does not change appreciably with inlet temperature, while the equipment cost does. Thus, for the reactor portion the optimum inlet temperature is $700^{\circ}F$ and the optimum conversion of CO is 0.855.

Case S-1

Figures V-15 through V-17 show the profiles of temperature, concentration and reaction rate for this case. Since the concentration of Co in the feed gas is higher than that in Case II, the reaction rate has the prominent profile exhibiting maximum rates in the reactions.

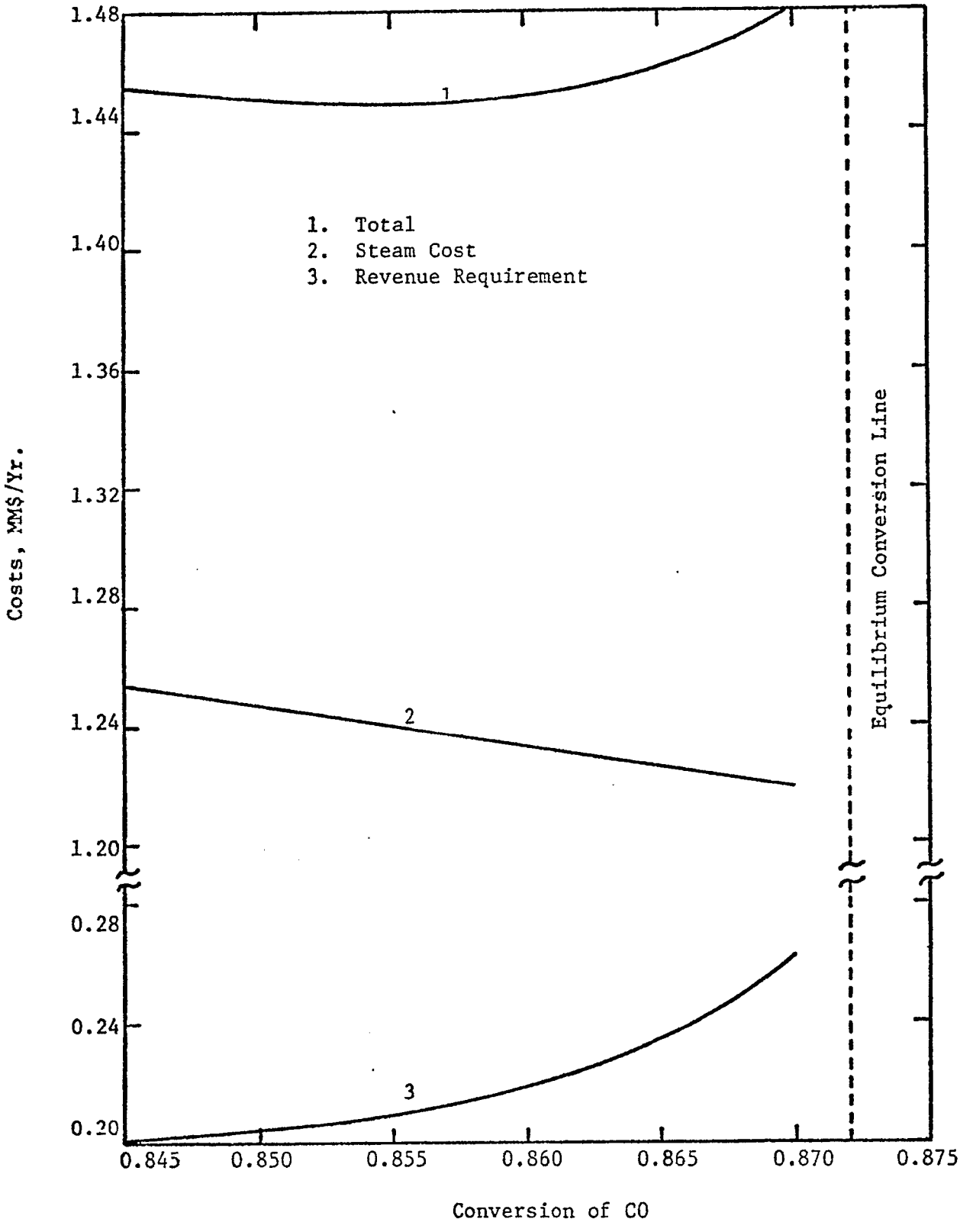

FIGURE V- 8 Costs Versus Conversion of CO Indicating Optimum Conversion 0.855 for CaseII at 700°F Inlet Temperature

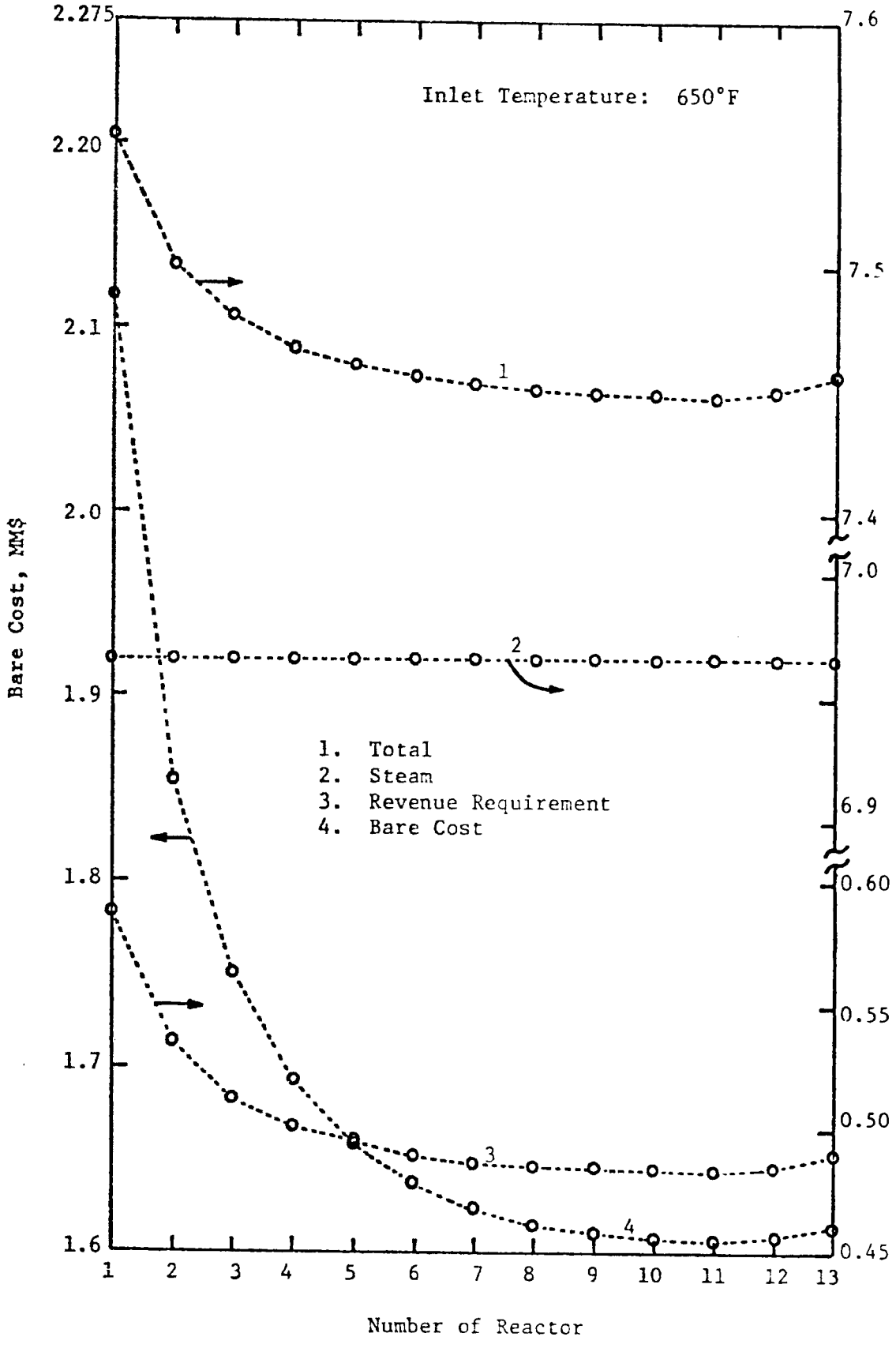

FIGURE V- 9 Costs Versus Number of Reactors Indicating 11 is the Optimum Number for Case II

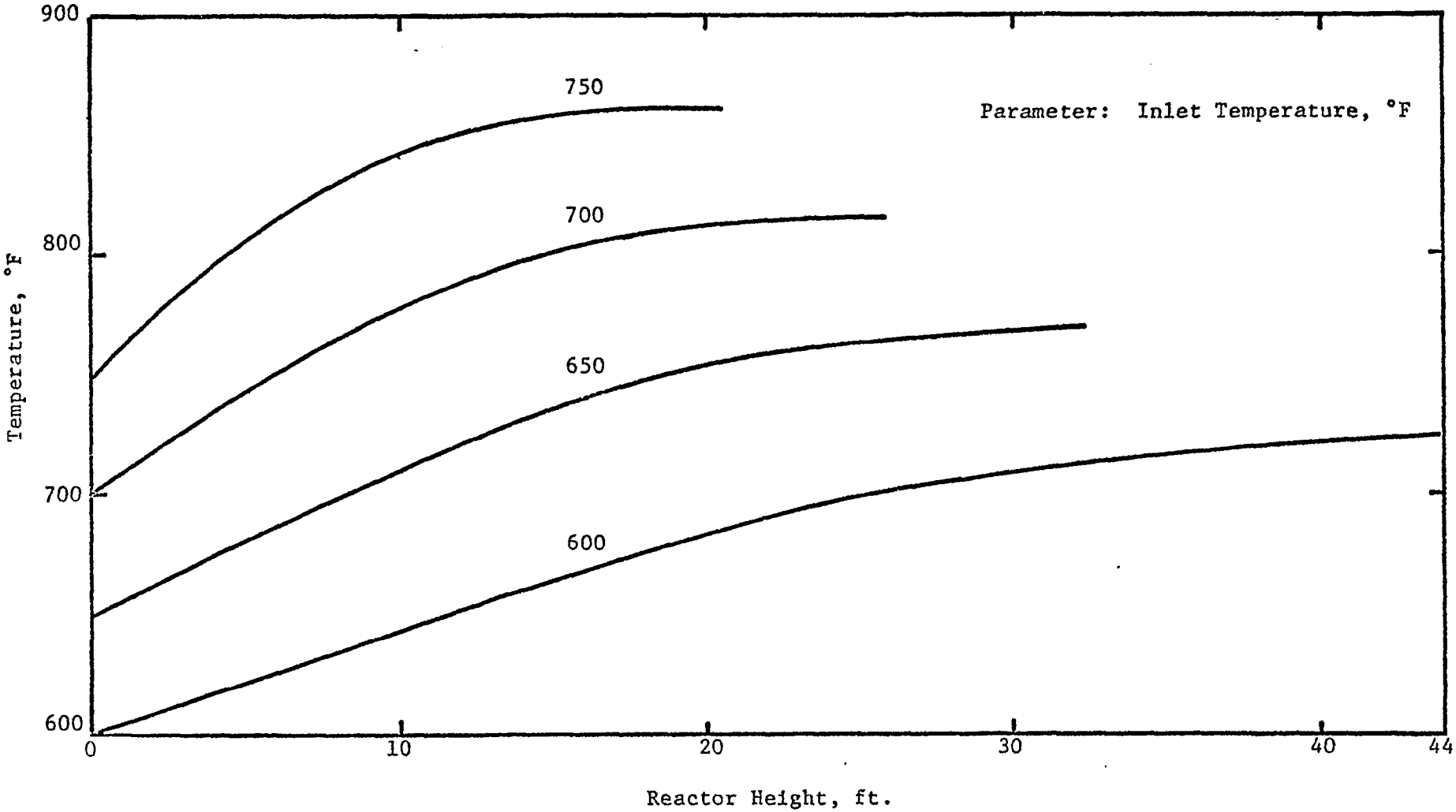

FIGURE V-10 Temperature Profile for Case II

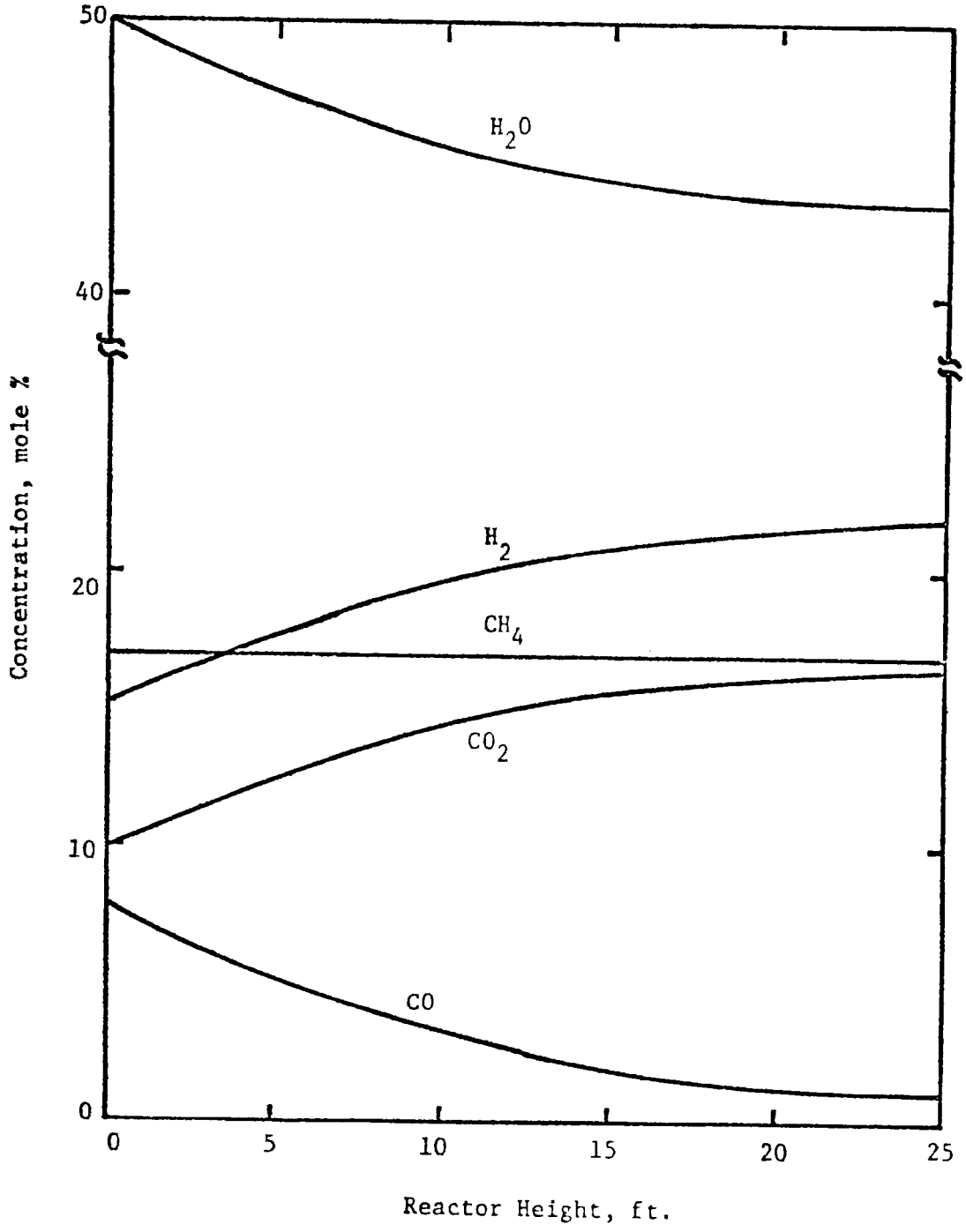

FIGURE V- 11 Concentration Profile for Case II with the Inlet Temperature of 700°F

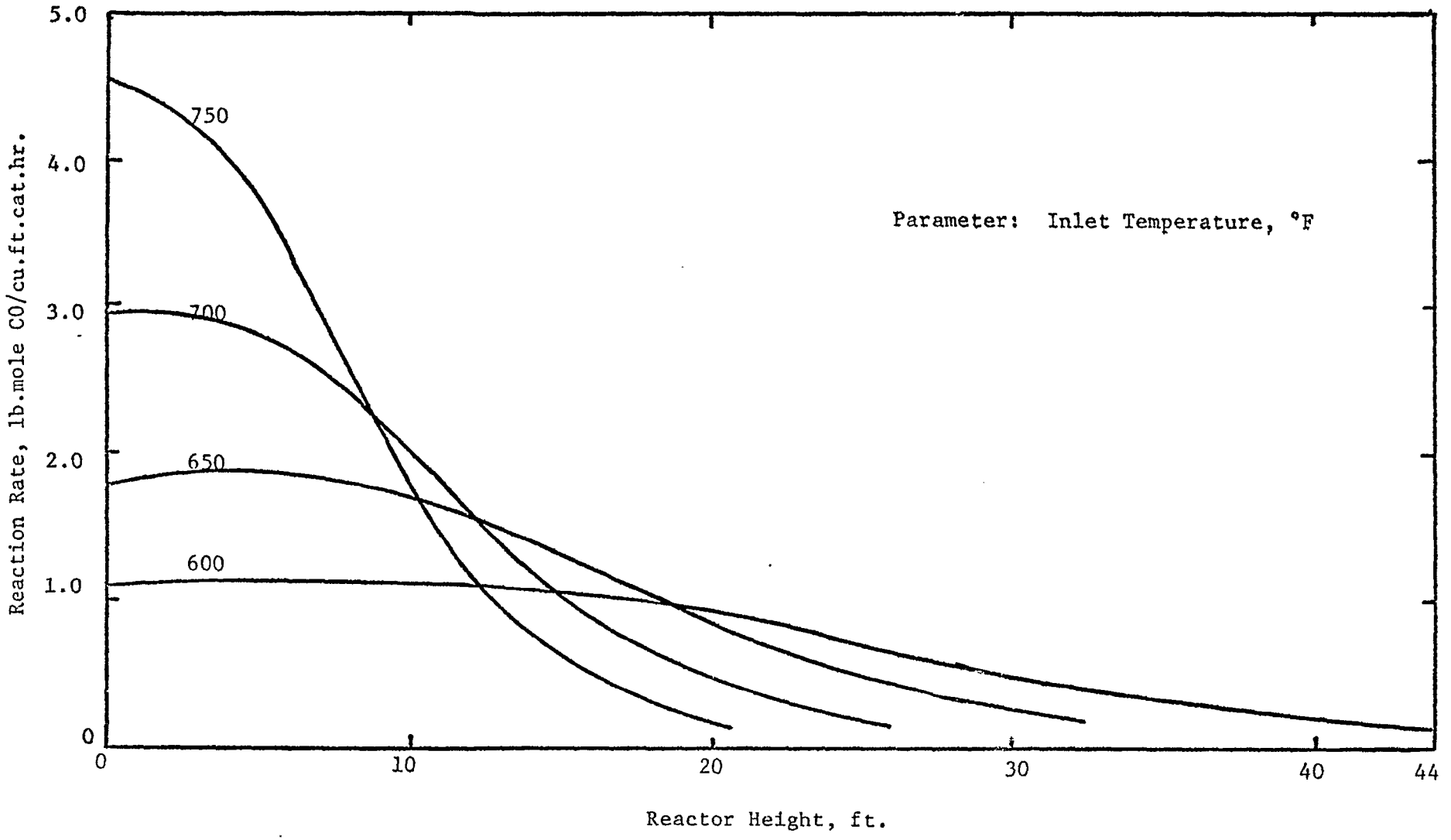

FIGURE V- 12 Reaction Rate Profile for Case II

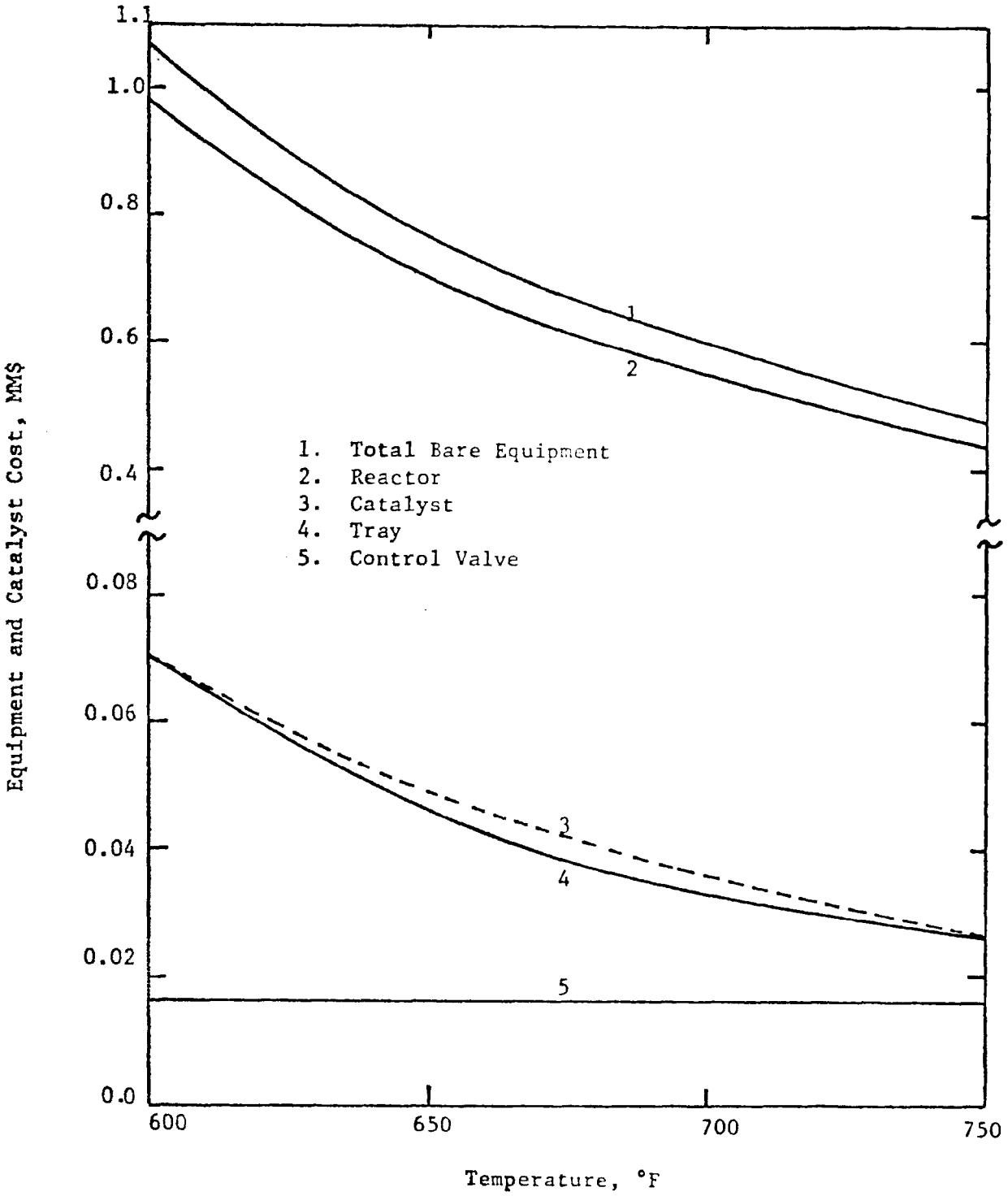

FIGURE V- 13 Cost of Equipment and Catalyst Versus Inlet Temperature of Reactor for Case II

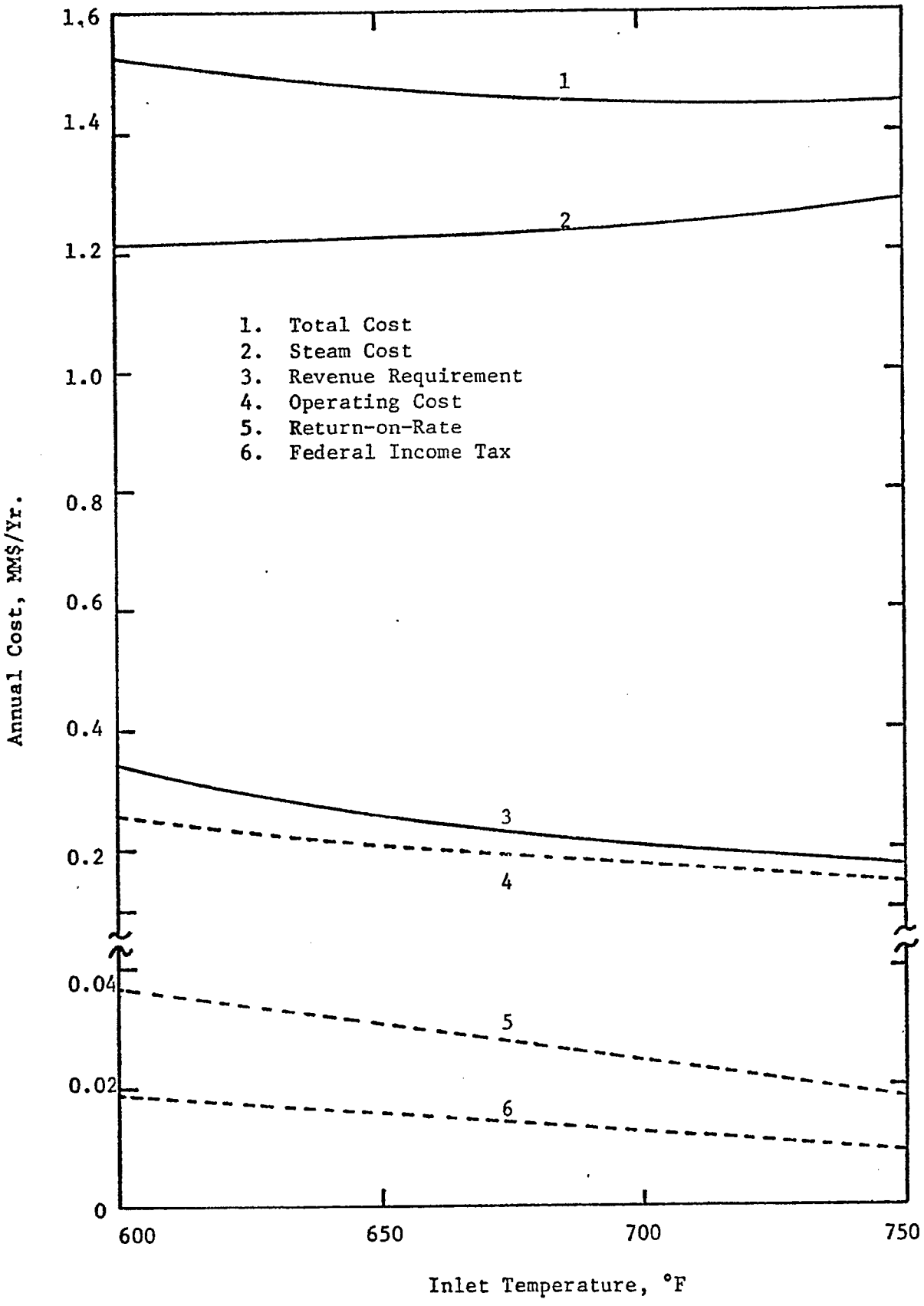

FIGURE V-14 Annual Cost Versus Inlet Temperature of Reactor for Case II

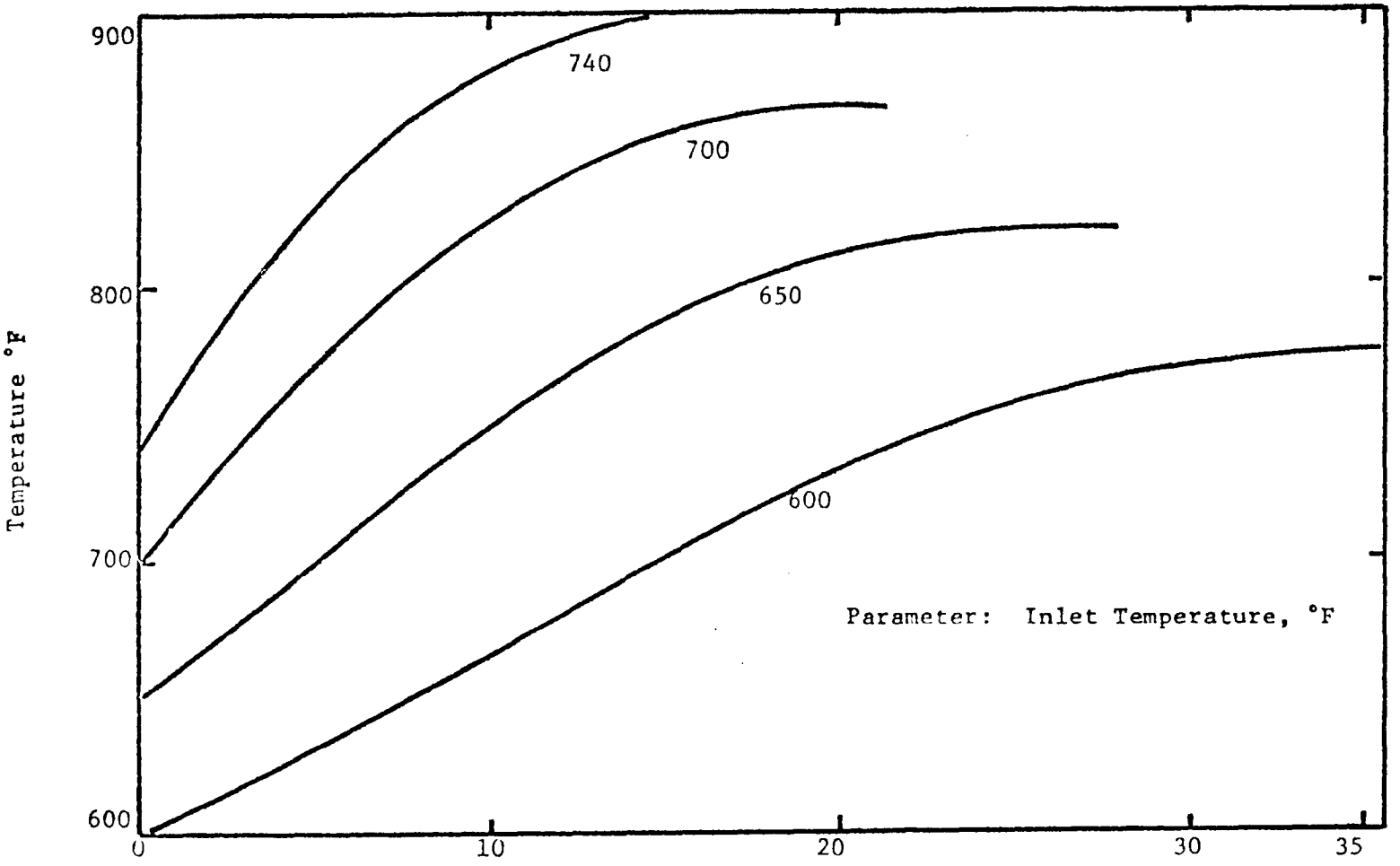

FIGURE V-15 Temperature Profile for Case S-1

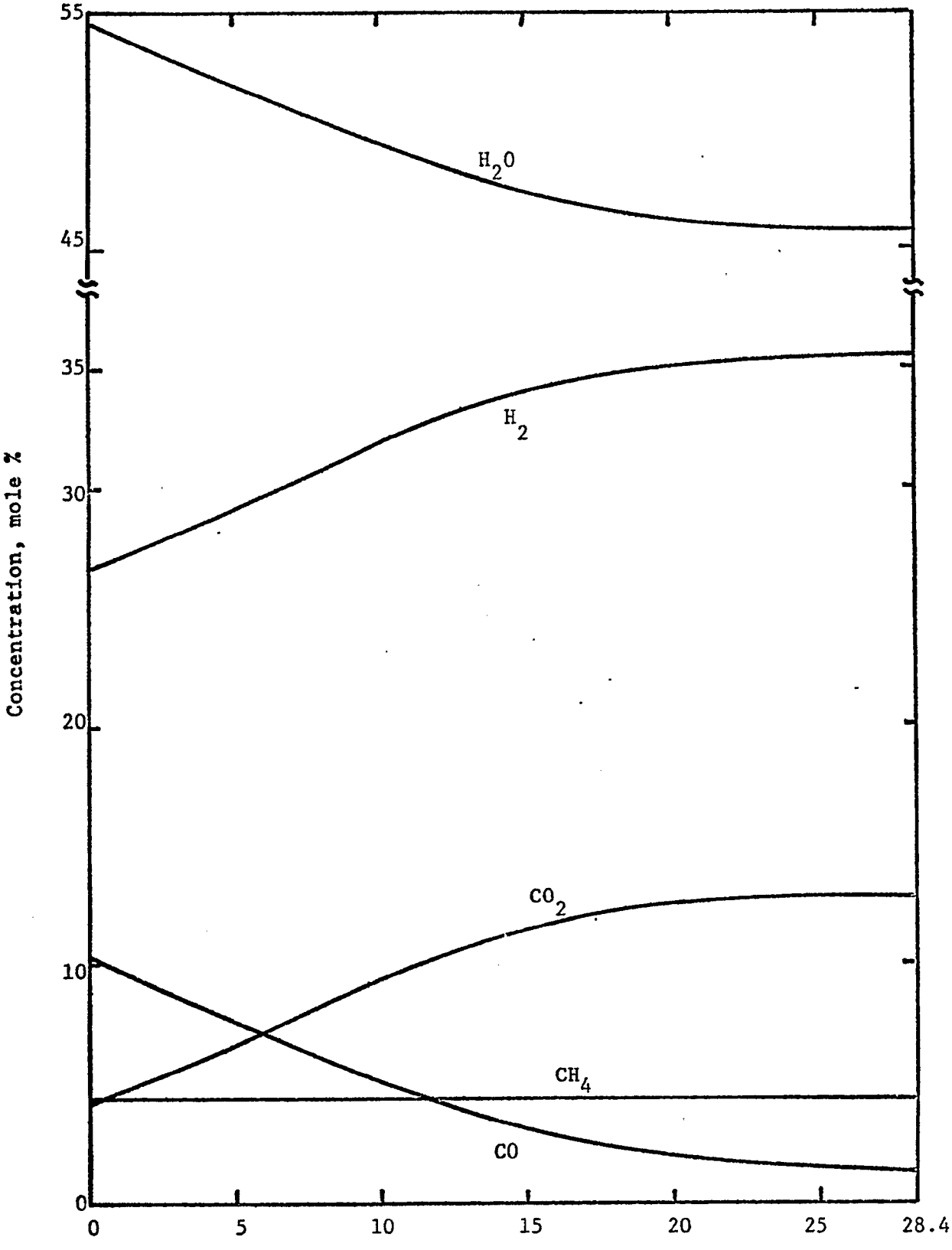

FIGURE V-16 Concentration Profile for Case S-1 with the Inlet Temperature of 650°F

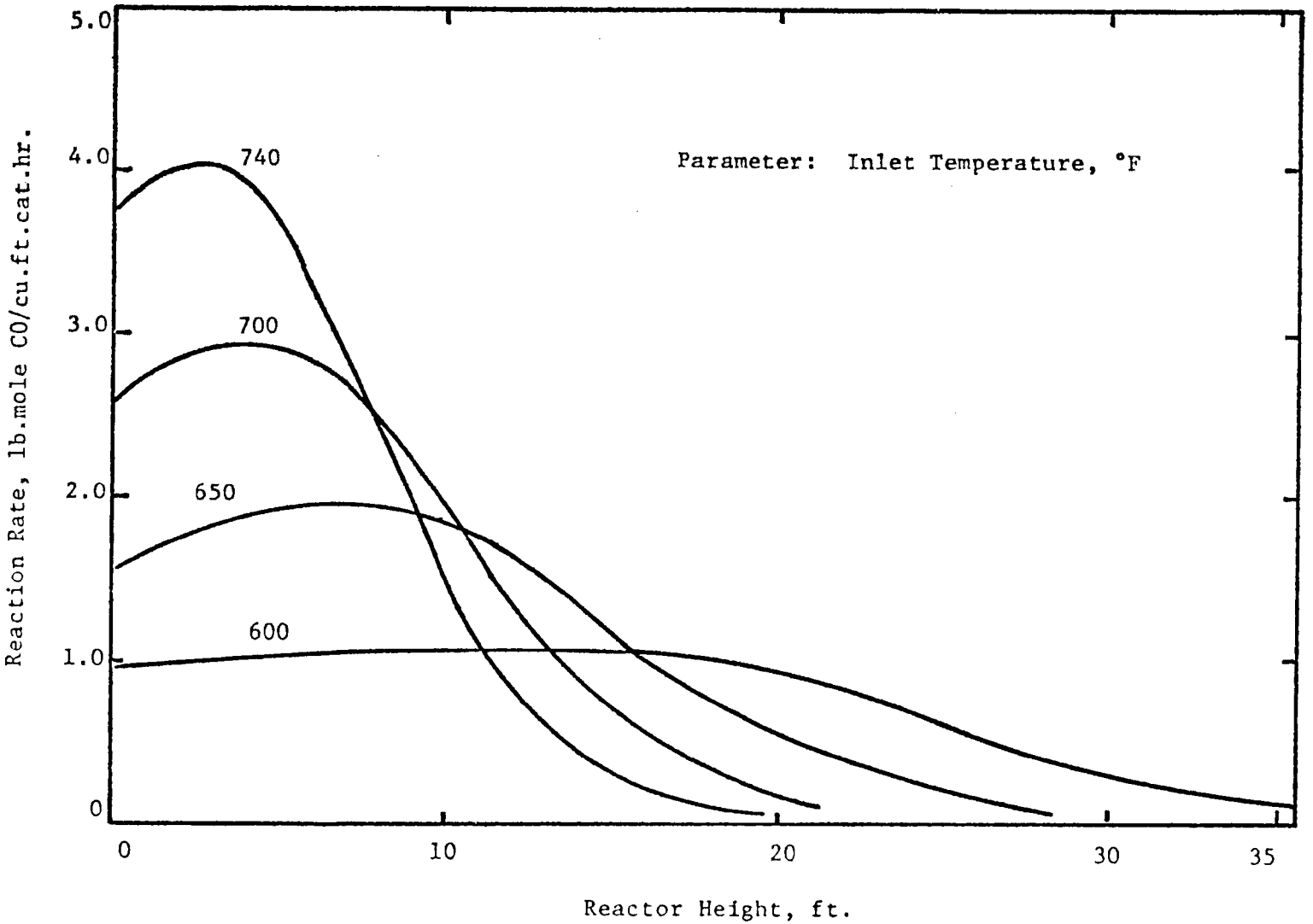

FIGURE V-17 Reaction Rate Profile for Case S-1

Figures V-18 and V-19 show the cost variation with inlet temperature. The relatively low cost is due to the original high concentration of hydrogen in the feed gas. The effect of temperature on cost for this case shows a similar tendency to that shown in Case II. The optimum inlet temperature and conversion of CO in the reactor are 650°F and 0.868, respectively.

Case III

The results of the study for Case III are plotted in Figures V-20 to V-22. It is seen that the changes of temperature, concentration and reaction rate are more drastic compared to the former two cases. This is of course due to the high concentration of CO in the feed gas.

In the present case, the maximum allowable inlet temperature is 650°F. This implies that in order to carry out the reaction in an adiabatic reactor, cooling devices are required for operations at higher temperatures.

The various costs are plotted in Figures V-23 and V-24 showing rather appreciable changes with inlet temperature. Thus the optimum inlet temperature is 650°F and for this case the optimum conversion of CO is 0.883.

ii. Reactor and Heat Exchangers

The optimization of the entire water-gas shift system including the three stages of the waste heat boiler, reactor and product gas cooler is performed next. The block diagram for this system is already shown in Figure V-5. Since each stage is previously optimized for every admissible inlet and outlet temperature, the results can be combined to locate the optimum temperatures for the overall system. To accomplish this, it is first necessary to decide the steam temperature, T_s. From Figure V-5 it is evident that the increasing value of T_{H1} favors the cost of H1 but affects that of H2 adversely if T_{Rf} is fixed. These variations are shown in Figure V-25

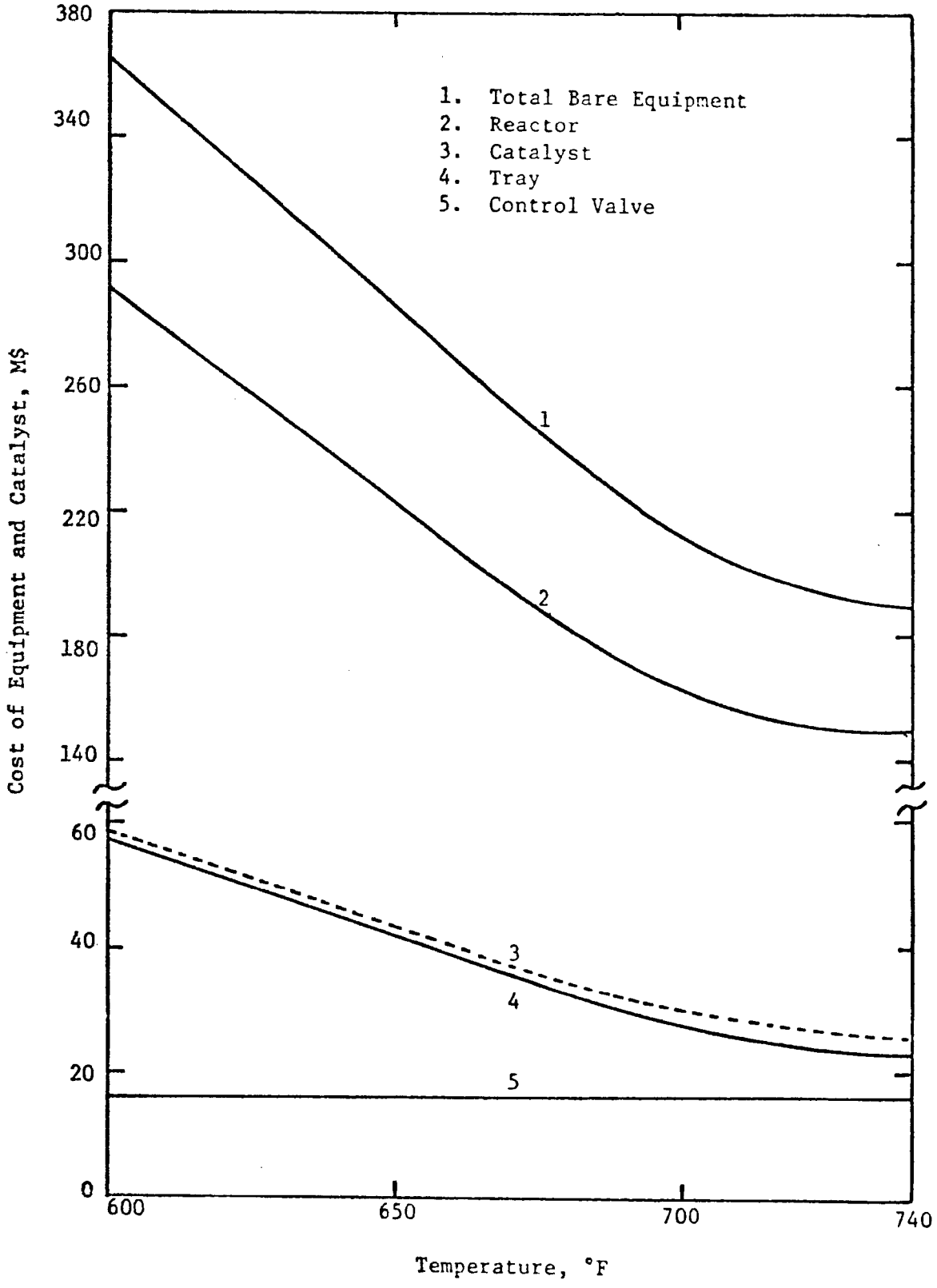

FIGURE V- 18 Costs of Equipment and Catalyst Versus Inlet Temperature of Reactor for Case S-1

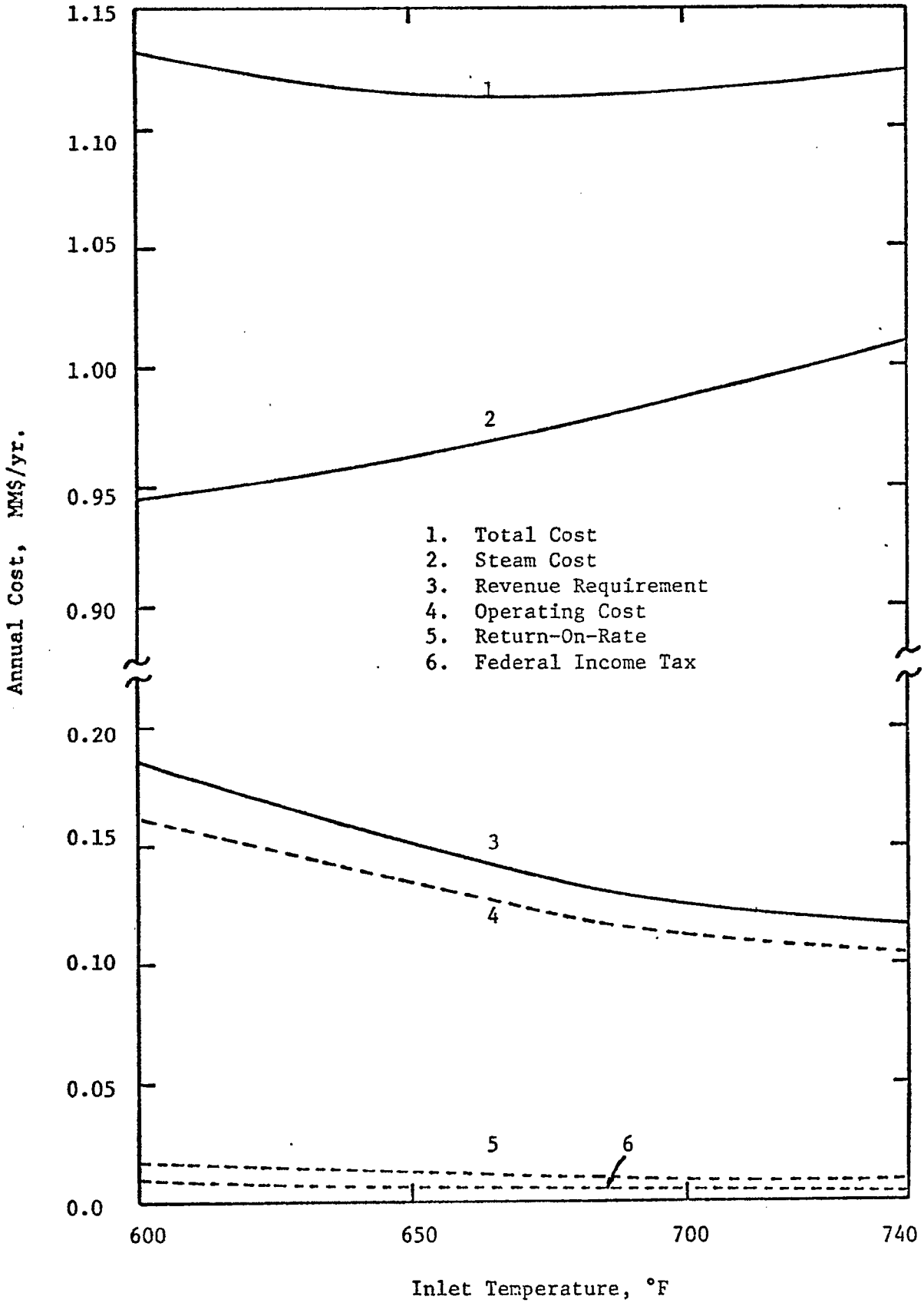

Figure V-19 Annual Cost Versus Inlet Temperature of Reactor for Case S-1

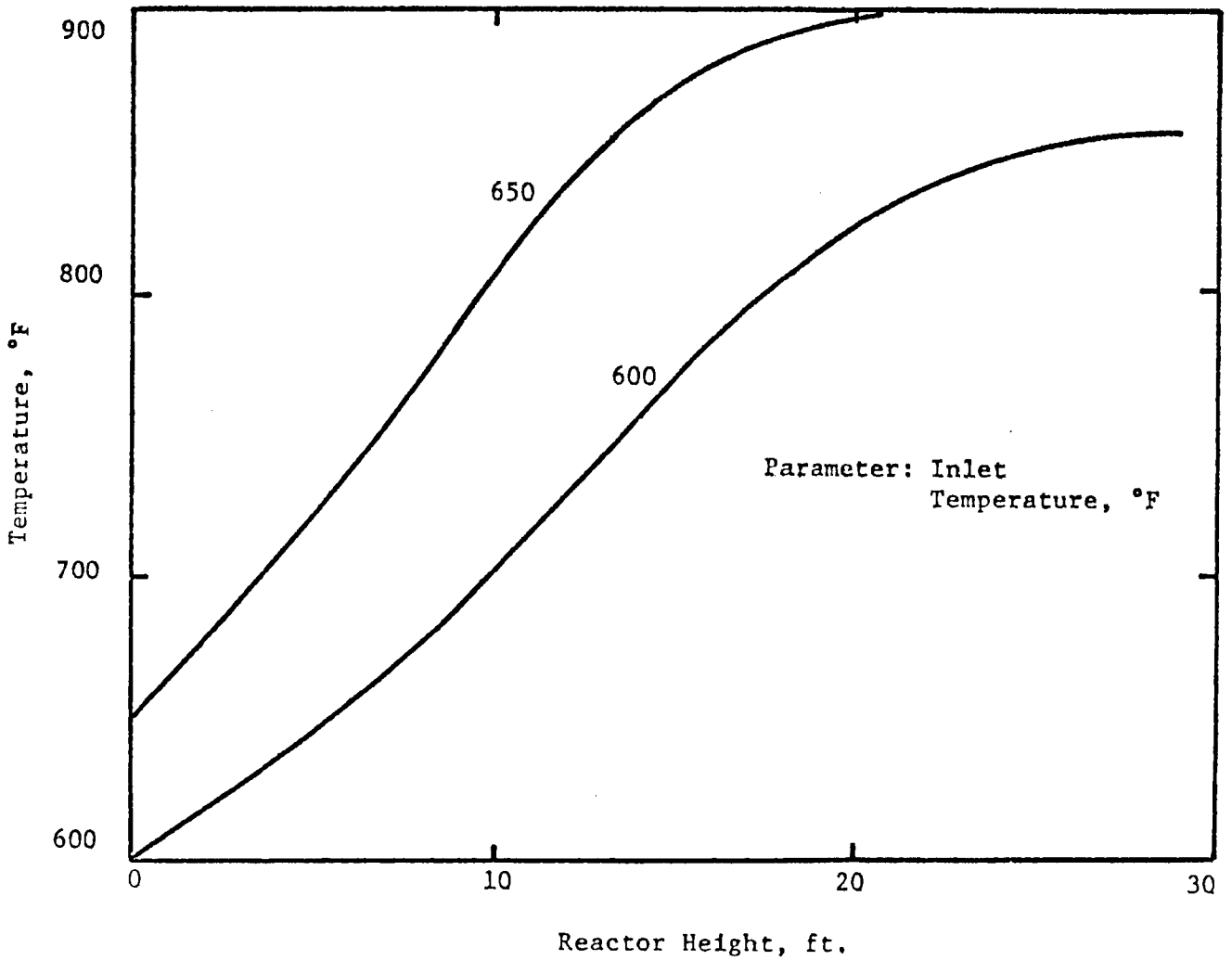

FIGURE V- 20 Temperature Profile for Case III

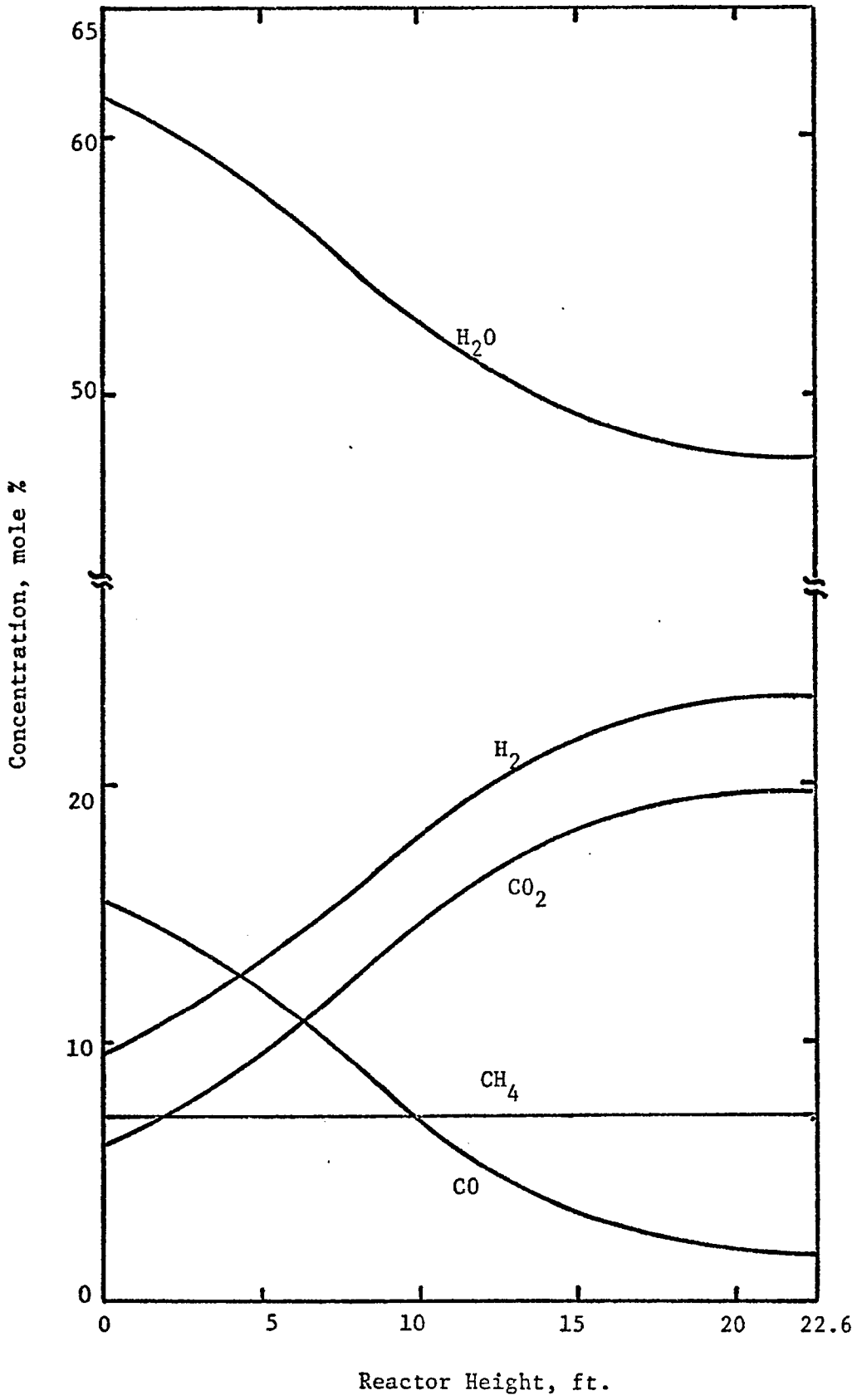

FIGURE V- 21 Concentration Profile for Case III with the Inlet Temperature of 650°F

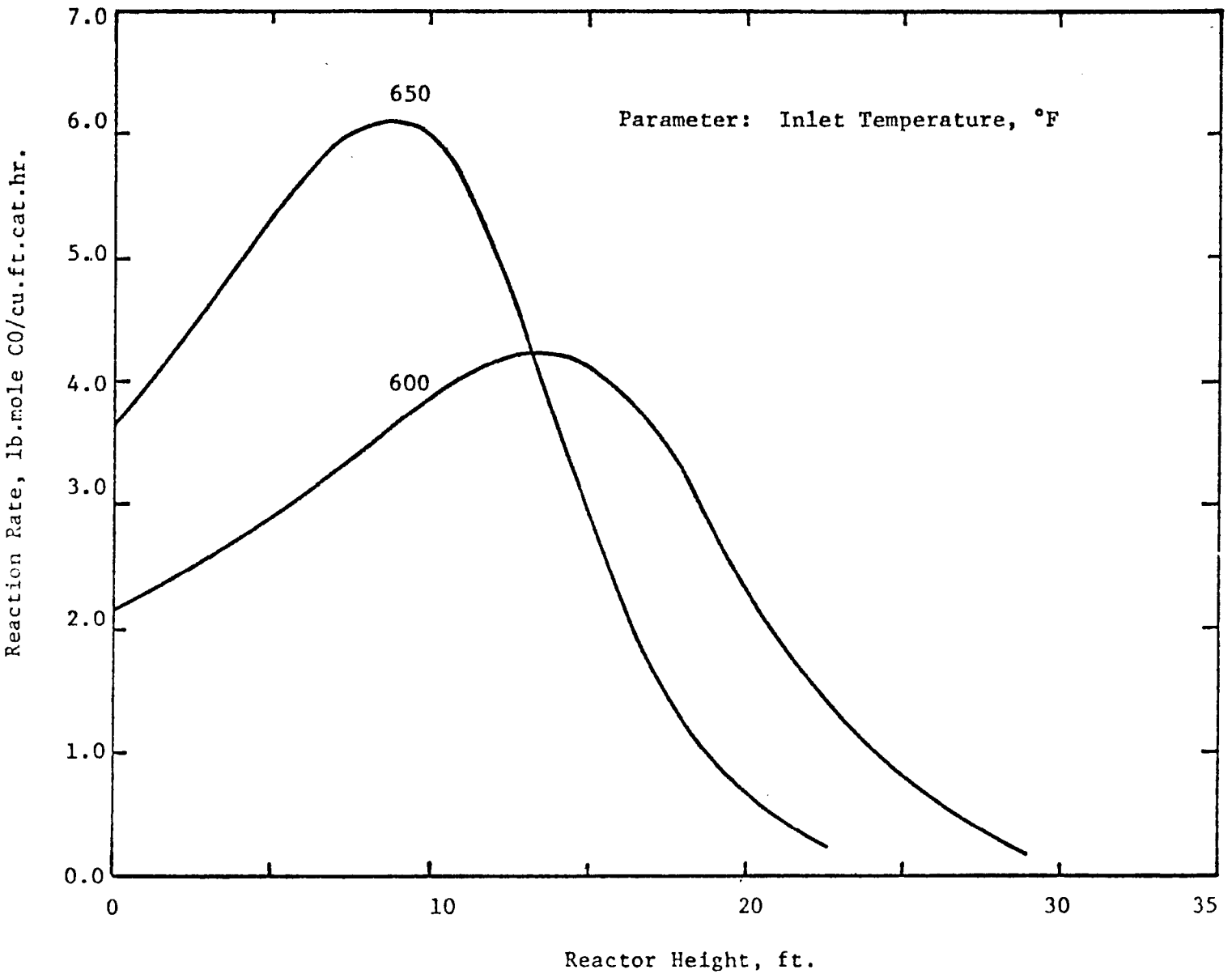

FIGURE V-22 Reaction Rate Profile for Case III

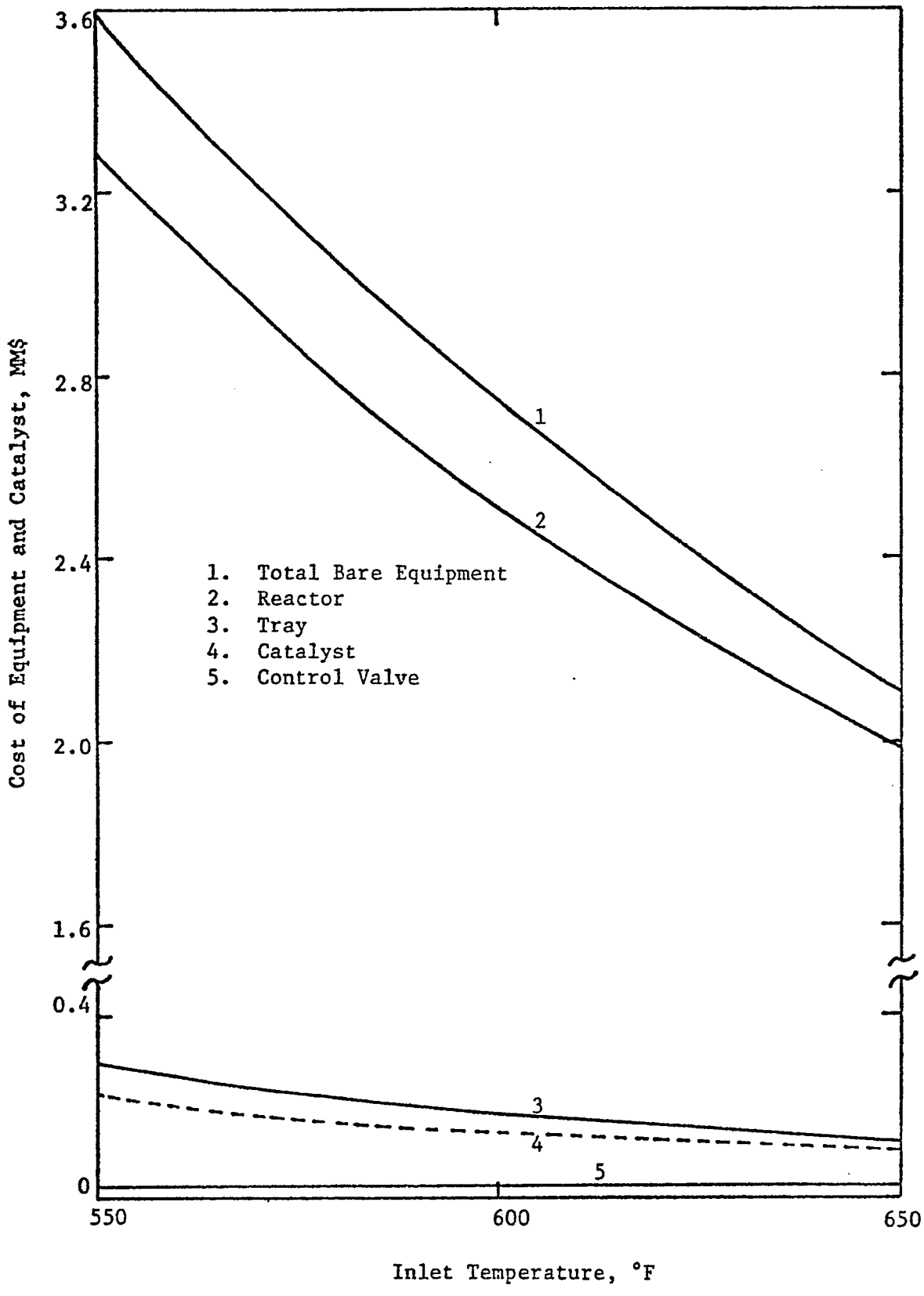

FIGURE V- 23 Costs of Equipment and Catalyst Versus Inlet Temperature of Reactor for Case III

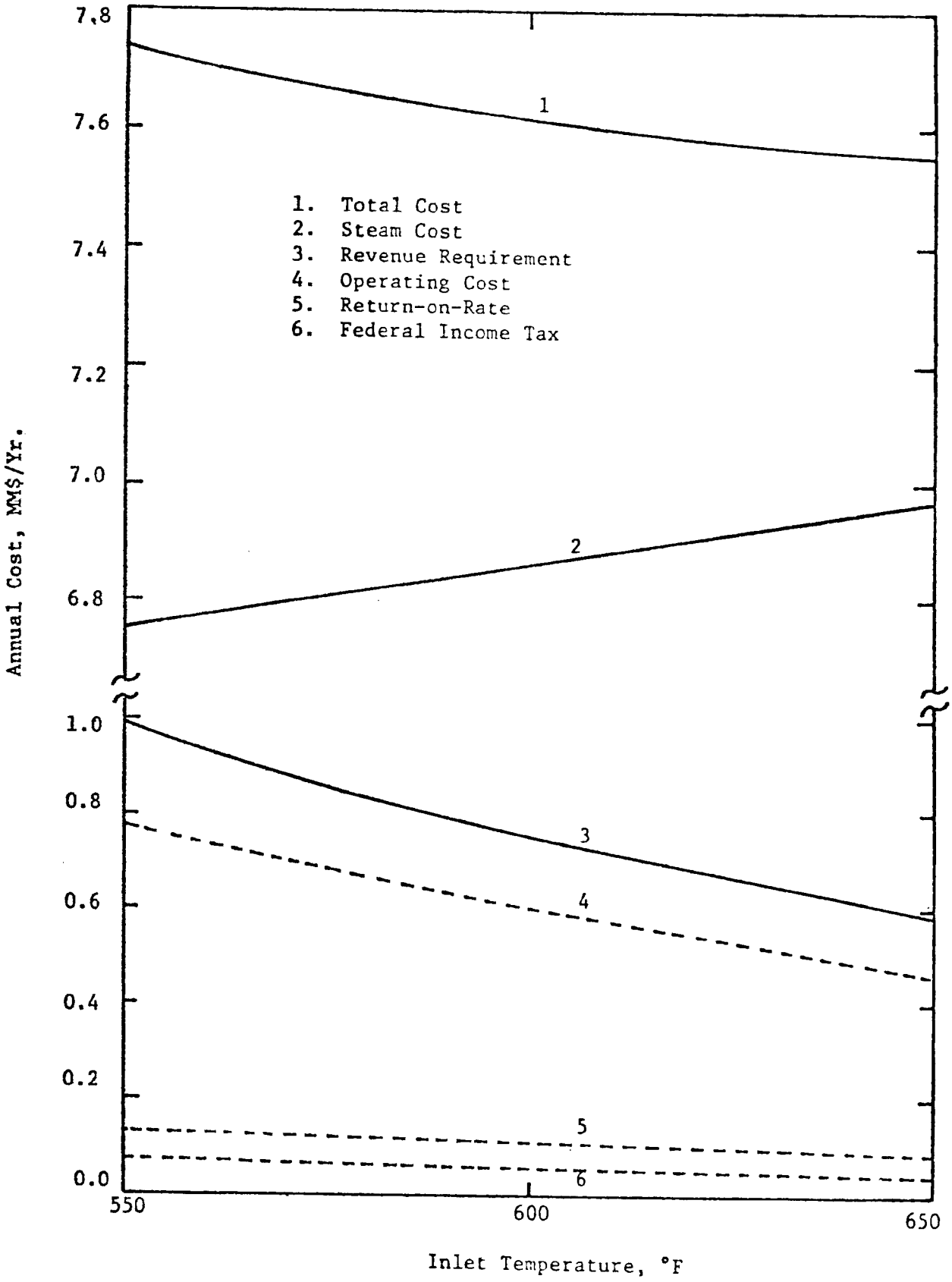

FIGURE V- 24 Annual Cost Versus Inlet Temperature of Reactor for Case III

indicating that the highest possible T_{H1}, and consequently the lowest possible T_S, should be selected for a more economical operation. In this study, T_S is selected as the saturated temperature at the operating pressure. Once the temperature of steam is fixed, the remaining procedure is straightforward. For every value of T_{Ri}, the value of T_{H1} is calculated by material and energy balances around point A. Since the corresponding value of T_{Rf} is already obtained by an optimum X_R in the reactor, the similar material and energy balances around point B yields the value of T_{H2}. Hence, all the necessary inlet and outlet temperatures for estimating the overall costs are obtained.

The results for the three cases are shown in Figures V-26, V-27 and V-28 exhibiting rather low sensitivity to the reactor inlet temperature except for Case III. The optimum operating conditions and corresponding costs are listed in Tables V-2 to V-7.

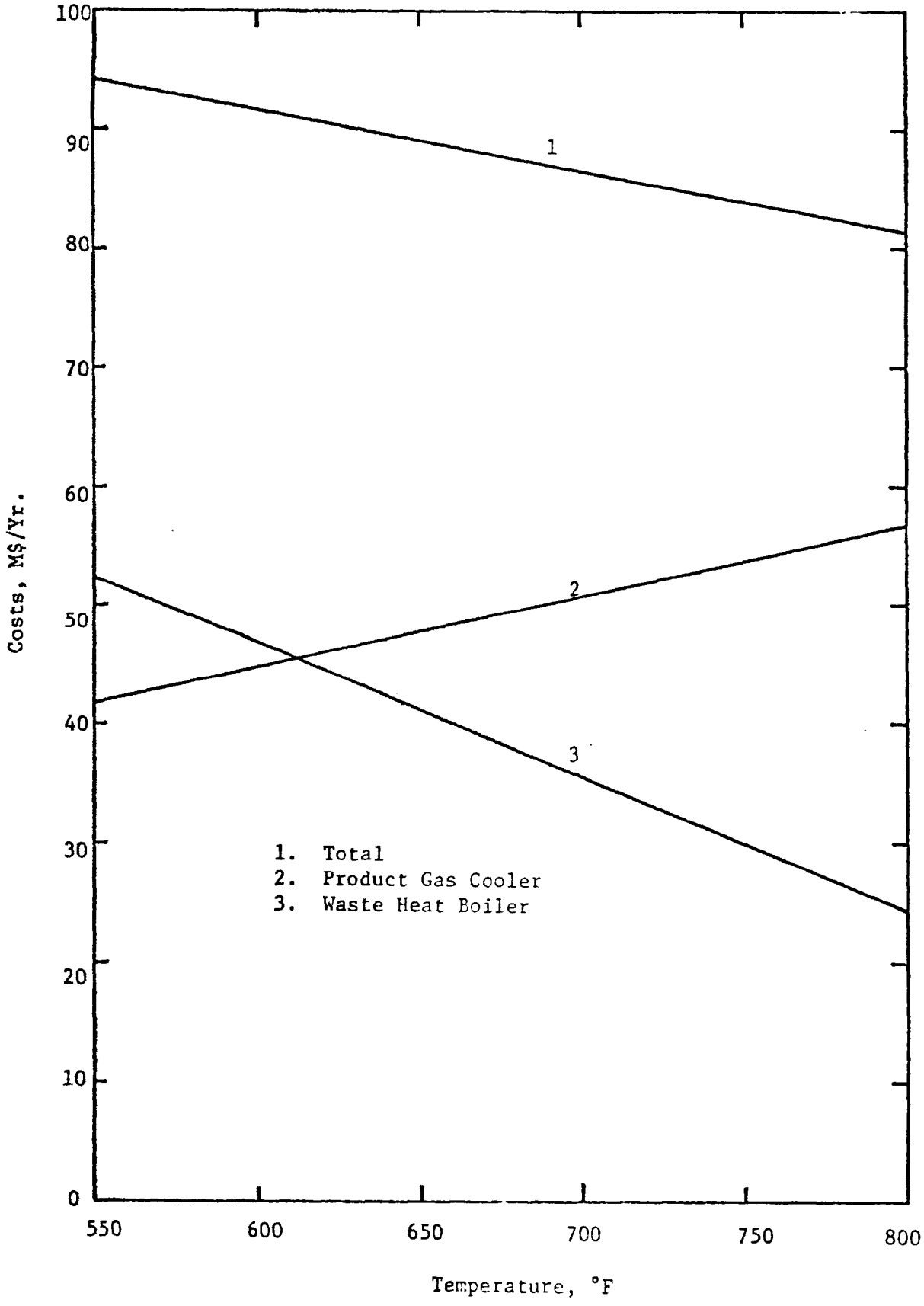

FIGURE V- 25 Annual Cost of Product Gas Cooler and Waste Heat Boiler in Terms of TH_1

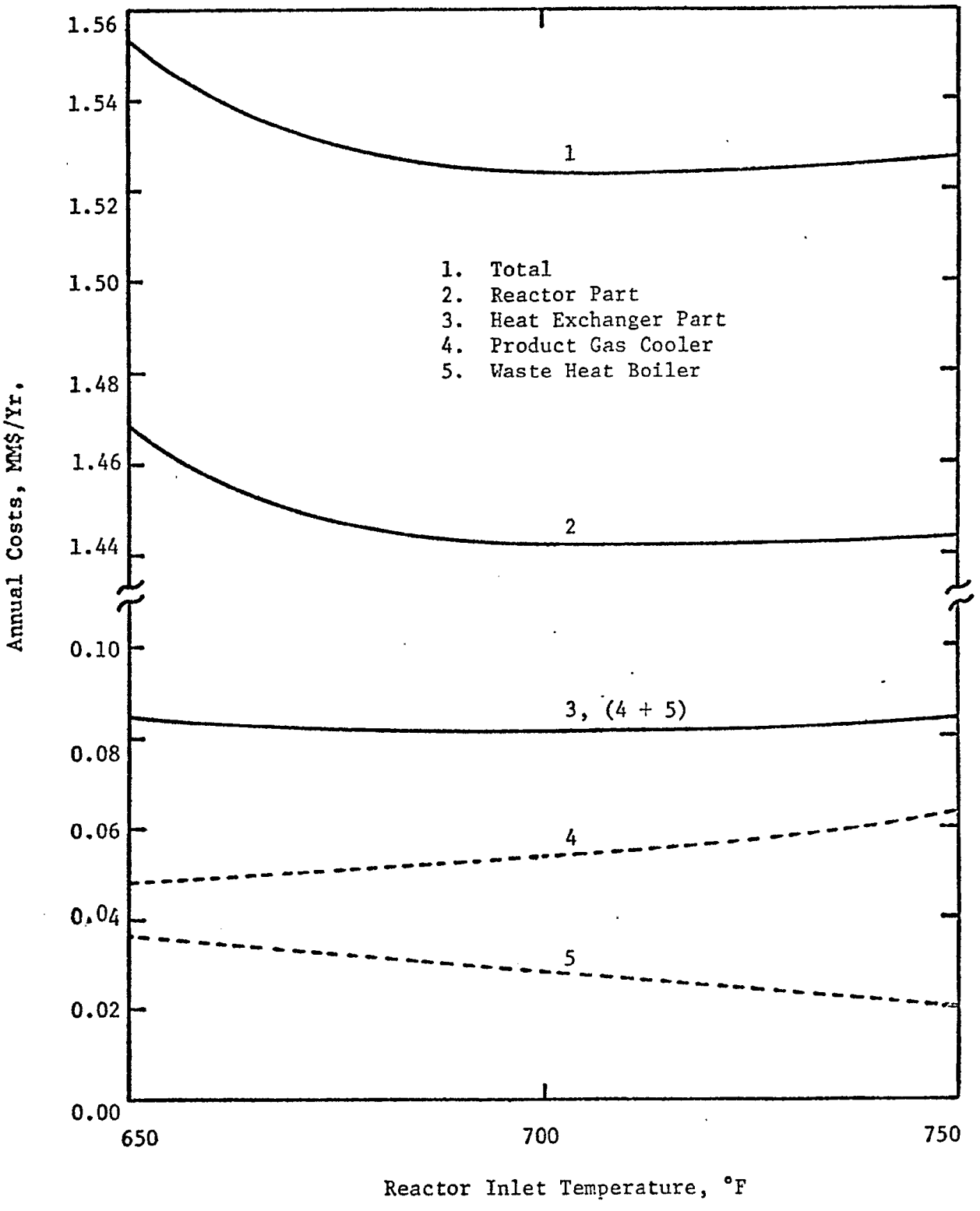

FIGURE V- 26 Total Cost in Terms of Inlet Temperature of Reactor Indicating 700°F is Optimum for Case II

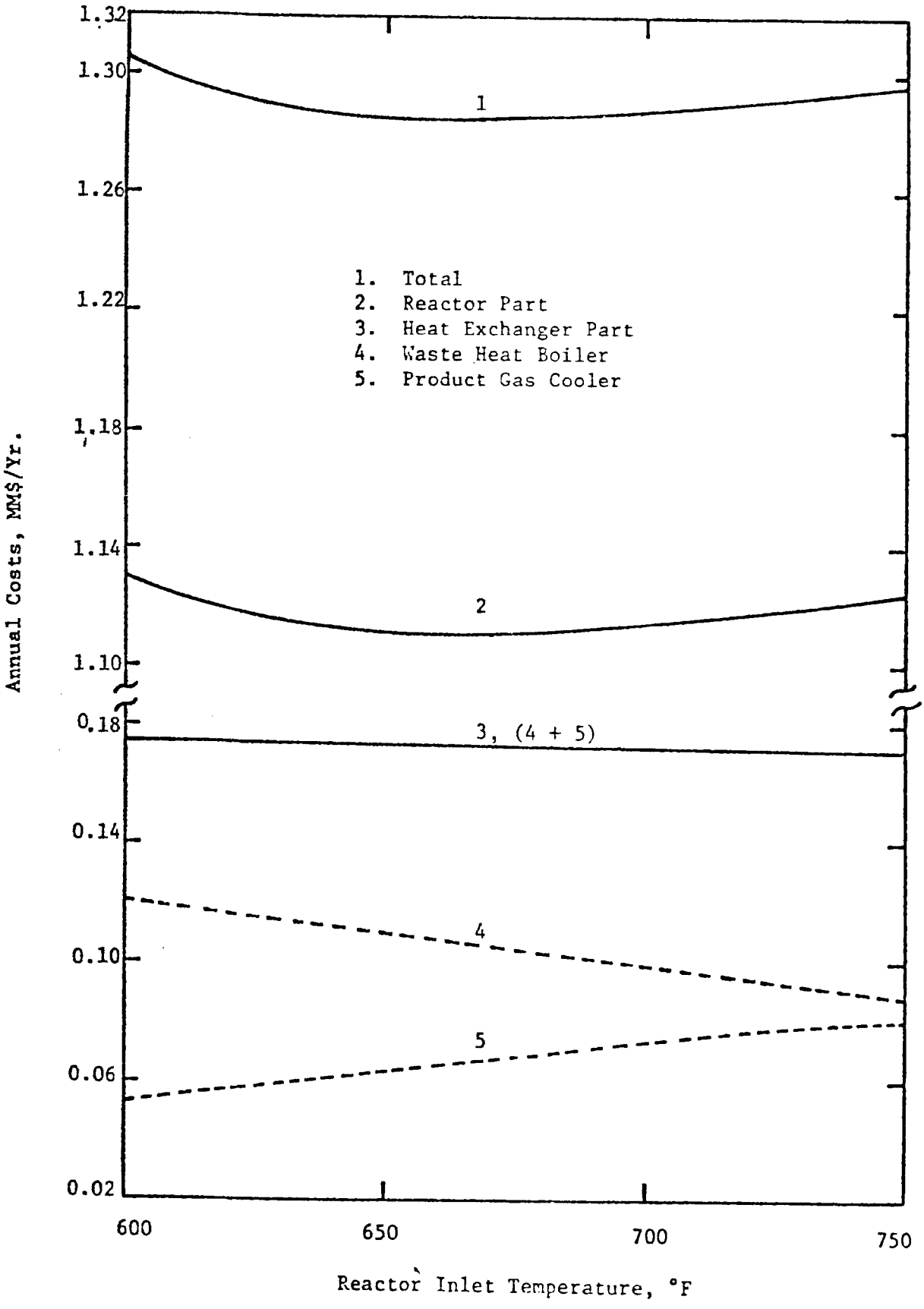

FIGURE V- 27 Total Cost in Terms of Inlet Temperature of Reactor Indicating 650°F is Optimum for Case S-1

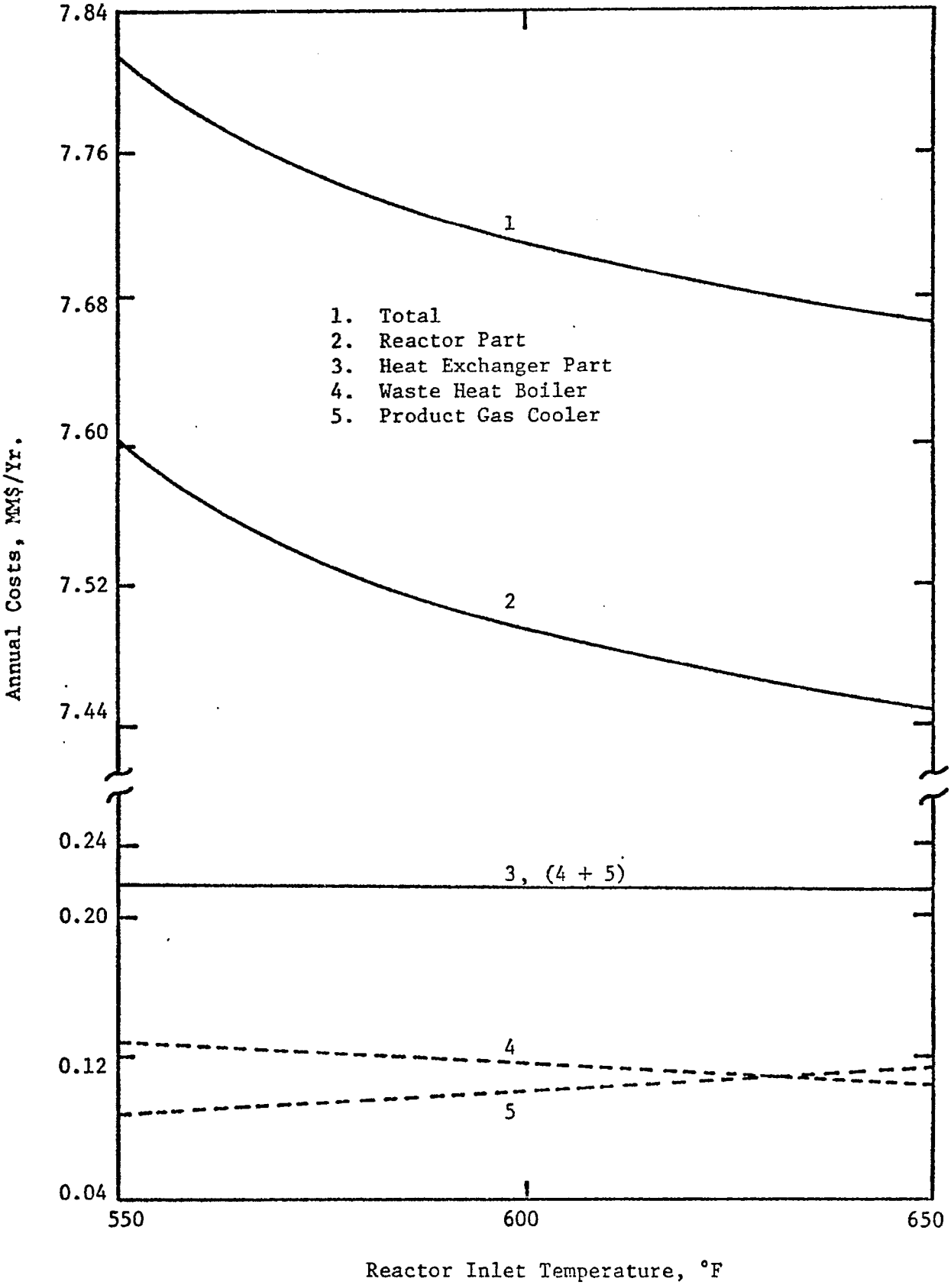

FIGURE V- 28 Total Cost in Terms of Inlet Temperature of Reactor Indicating 650°F is Optimum for Case III

TABLE V-2 OPTIMUM OPERATING CONDITIONS FOR CASE II[@]

1. Reactor	
Inlet Temperature, °F	700
Outlet Temperature, °F	815
Conversion of CO	0.855
Fraction of Gas By-Passed	0.649
Space Velocity,* hr^{-1}	4380
Temperature of Steam Supplied, °F	556
Number of Parallel Reactors	3
Diameter, ft.	7.0
Height, ft.	25.9
Thickness, in.	3.73
Catalyst Amount/unit, cu.ft.	600

*Based on dry gas at 60°F, 1 atm.

@Steam to gas ratio selected: 1.0 [mole/mole] (See Section 4.11)

TABLE V-2 OPTIMUM OPERATING CONDITIONS FOR CASE II(CONT.)

2. Heat Exchangers	Waste Heat Boiler	Product Gas Cooler
Inlet Temperature of Gas, °F	1000	788
Outlet Temperature of Gas, °F	765	704
Number of Heat Exchangers	6	5
Flow Rate of Gas/unit, M lb./hr.	247.4	347.4
Flow Rate of Water/unit, M lb./hr.	58.5	30.6
Temperature of Steam Produced, °F	556	556
Heat Load/unit, MM Btu/hr.	32.3	16.9
Heat Transfer Area/unit, sq. ft.	850	733
Heat Transfer Coefficient, Btu/(hr. sq. ft.°F)	88.1	79.3

TABLE V-3 OPTIMUM OPERATING CONDITIONS FOR CASE S-1[@]

1. Reactor	
Inlet Temperature, °F	650
Outlet Temperature, °F	821
Conversion of CO	0.868
Fraction of Gas By-Passed	0.866
Space Velocity[*], hr^{-1}	2190
Temperature of Steam Supplied, °F	440
Number of Parallel Reactors	2
Diameter, ft.	9.0
Height, ft.	28.2
Thickness, in.	1.74
Catalyst Amount/unit, cu.ft.	1080

[*] Based on dry gas at 60°F, 1 atm.

[@] Steam to gas ratio selected: 1.2 (See Section 4.11)

TABLE V-3 OPTIMUM OPERATING CONDITIONS FOR CASE S-1(CONT.)

2. Heat Exchangers	Waste Heat Boiler 1	Waste Heat Boiler 2	Product Gas Cooler
Inlet Temperature of Gas, °F	1600	990	799
Outlet Temperature of Gas, °F	990	793	460
Number of Heat Exchangers	12	10	13
Flow Rate of Gas/unit, M lb./hr.	147.8	147.8	151.5
Flow Rate of Water/unit,M lb./hr.	101.3	37.4	53.6
Temperature of Steam Produced, °F	456	440	250
Heat Load/unit, MM Btu/hr.	56.5	21.9	30.5
Heat Transfer Area/unit, sq.ft.	615.4	431.1	874.8
Heat Transfer Coefficient, Btu/(hr.sq.ft.°F)	101.2	93.0	84.0

TABLE V-4 OPTIMUM OPERATING CONDITIONS FOR CASE III[@]

1. Reactor	
Inlet Temperature, °F	650
Outlet Temperature, °F	899
Conversion of CO	0.883
Fraction of Gas By-Passed	0.309
Space Velocity*, hr^{-1}	3890
Temperature of Steam Supplied, °F	551
Number of Parallel Reactors	11
Diameter, ft.	6.7
Height, ft.	22.7
Thickness, in.	3.42
Catalyst Amount/unit, cu.ft.	480

*Based on dry gas at 60°F, 1 atm.

@Steam to gas ratio selected: 1.6 (See Appendix A)

TABLE V-4 OPTIMUM OPERATING CONDITIONS FOR CASE III(CONT.)

2. Heat Exchangers	Waste Heat Boiler	Product Gas Cooler
Inlet Temperature of Gas, °F	1700	878
Outlet Temperature of Gas, °F	771	570
Number of Heat Exchangers	10	17
Flow Rate of Gas/unit, M lb./hr.	192.7	196.1
Flow Rate of Water/unit, M lb./hr.	151,9	62.2
Temperature of Steam Produced, °F	551	551
Heat Load/unit, MM Btu/hr.	84.1	34.4
Heat Transfer Area/unit, sq. ft.	1262	1884
Heat Transfer Coefficient, Btu/(hr. sq.ft. °F)	91.4	66.9

TABLE V-5 EQUIPMENT AND OPERATIONAL COSTS IN ADIABATIC SYSTEM FOR CASE II

	Waste Heat Boiler	Reactor	Product Gas Cooler	Total
Reactor Cost, M $	--	496.8	--	496.8
Catalyst Cost, M $	--	36.3	--	36.3
Tray Cost, M $	--	33.8	--	33.8
Control Valve Cost, M $	--	20.0	--	20.0
Heat Exchanger Cost, M $	41.2	--	34.2	75.4
Pump Cost, M $	24.8	--	15.2	40.0
Cooling Water Cost, M$/yr	20.7	--	9.0	29.7
Working Capital, M$/yr	4.7	20.7	2.4	27.8
Operating Cost, M$/yr	49.2	167.8	24.4	241.4
Return On Rate, M$/yr	2.8	22.6	2.0	27.4
Federal Income Tax, M$/yr	1.4	11.4	1.0	13.8
Revenue Requirement, M$/yr	53.4	201.8	27.4	282.6
Steam Cost, M$/yr	--	1240.2	--	1240.2
Total Annual Cost, M$/yr	53.4	1442.0	27.4	1522.8

TABLE V-6 EQUIPMENT AND OPERATIONAL COSTS IN ADIABATIC SYSTEM FOR CASE S-1

	Waste Heat Boiler 1	Waste Heat Boiler 2	Reactor	Product Gas Cooler	Total
Reactor Cost, M $	--	--	217.6	--	217.6
Catalyst Cost, M $	--	--	43.1	--	43.1
Tray Cost, M $	--	--	40.1	--	40.1
Control Valve Cost, M $	--	--	16.0	--	16.0
Heat Exchanger Cost, M $	50.7	37.5	--	64.6	152.8
Pump Cost, M $	41.8	20.2	--	9.6	71.6
Cooling Water Cost, M$/yr	70.6	21.7	--	41.1	133.4
Working Capital, M$/yr	10.2	3.6	16.9	5.1	35.8
Operating Cost, M$/yr	110.4	36.9	133.8	52.9	334.0
Return On Rate, M$/yr	4.2	2.4	11.8	3.1	21.5
Federal Income Tax, M$/yr	2.2	1.2	6.0	1.6	11.0
Revenue Requirement, M$/yr	116.8	40.5	151.6	57.6	366.5
Steam Cost, M$/yr	--	--	960.8	--	960.8
Total Annual Cost, M$/yr	116.8	40.5	1112.4	57.6	1327.3

TABLE V-7 EQUIPMENT AND OPERATIONAL COST IN ADIABATIC SYSTEM FOR CASE III

	Waste Heat Boiler	Reactor	Product Gas Cooler	Total
Reactor Cost, M $	--	1415.8	--	1415.8
Catalyst Cost, M $	--	106.1	--	106.1
Tray Cost, M $	--	94.8	--	94.8
Control Valve Cost, M $	--	52.0	--	52.0
Heat Exchanger Cost, M $	68.5	--	115.6	184.1
Pump Cost, M $	63.0	--	70.7	133.7
Cooling Water Cost, M$/yr	89.6	--	62.5	152.1
Working Capital, M$/yr	17.2	51.2	13.7	82.1
Operating Cost, M$/yr	186.8	387.0	144.1	717.9
Return On Rate, M$/yr	6.2	64.0	8.0	78.2
Federal Income Tax, M$/yr	3.3	32.1	4.1	39.5
Revenue Requirement, M$/yr	196.3	483.1	156.2	835.6
Steam Cost, M$/yr	--	6965.5	--	6965.5
Total Annual Cost, M$/yr	196.3	7448.6	156.2	7801.1

3.4 Cold-Quenching Reactor System

1. Reactor

In the previous section, the operation of water-gas shift conversion under adiabatic condition is studied. The Adiabatic system provides a simple and economical process when the concentration of carbon monoxide in the feed gas stream is low. However, when the CO concentration is high, the rate of heat evolution is so high that the removal of heat from the system becomes necessary in order to keep the reaction temperature within the desirable range. Hence, from the point of temperature control, a more flexible cold-quenching system must be employed.

The cold-quenching in water-gas shift conversion is achieved by injecting a suitable amount of cold water and vaporizing it in the quenching zone of the reactor. Since steam behaves as a reactant and is required in excess, the water-quenching accomplishes the dual effects of temperature reduction and steam supply.

In this study, again three cases are selected: Case II and Case III for methanation, and Case S-2 for hydrogen production. Case S-1 is not considered here because the required conversion of CO is so small that the total cost will not be changed significantly by the different operational schemes.

As shown in Figure V-29, the raw gas from the coal gasifier is cooled to a desired temperature by the waste-heat boiler before entering the shift converter. In the same manner as in the adiabatic system, a part of the gas stream is by-passed and the remainder is introduced into the reactor after being mixed with a required amount of steam. The reaction progresses under an adiabatic condition in the first reaction

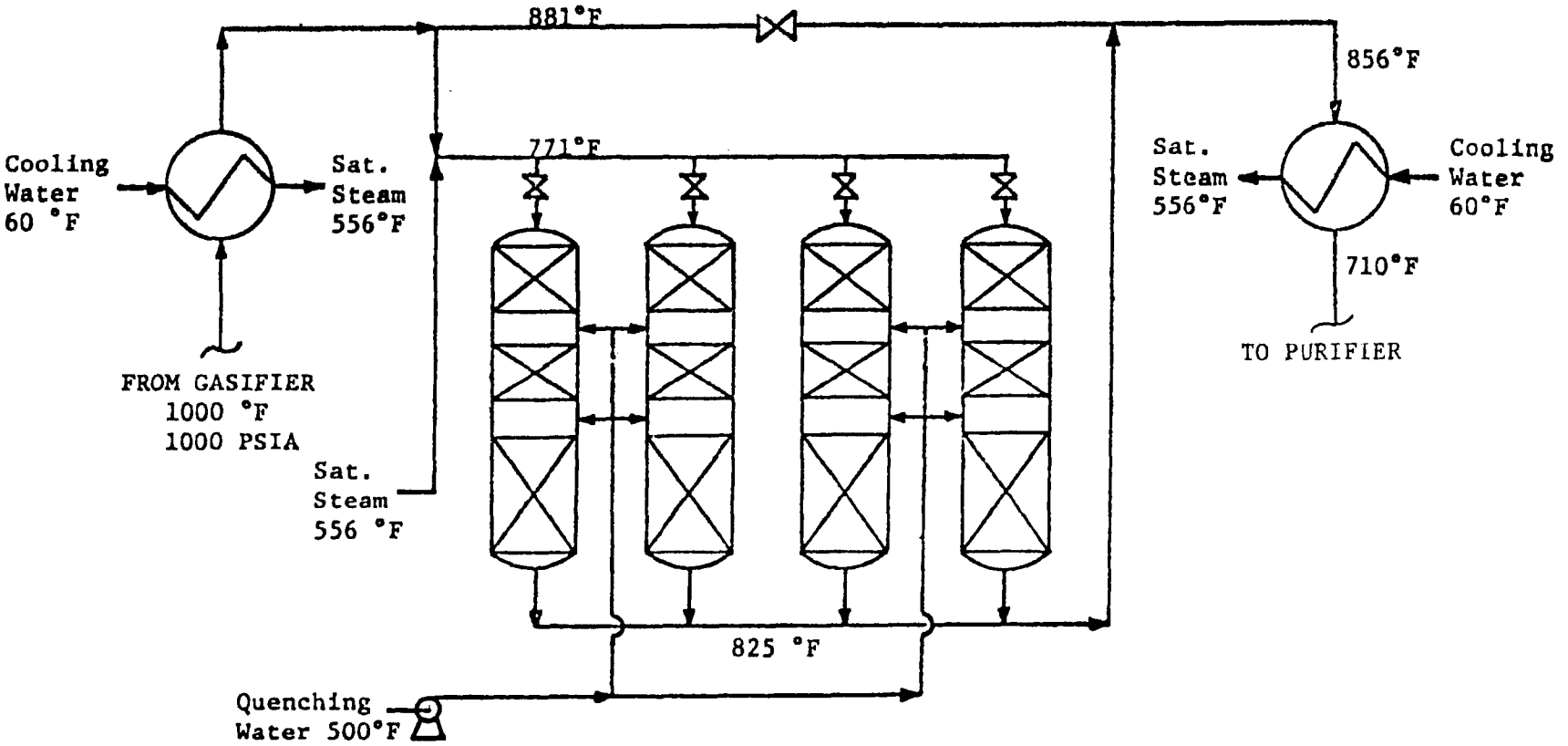

Figure V-29 Flow Diagram For CaseII In Cold Quenching Water-Gas Shift Conversion System

zone. When the reaction has achieved a certain extent of conversion, the quenching is performed in the quenching zone by pressurized low temperature cooling water which is completely vaporized and mixed with the reacting gas stream before entering the next reaction zone. Care must be exercised in the design and operation of the quenching zone to assure complete vaporization of water in the quenching zone. Otherwise, the unvaporized water will drastically contaminate the catalyst in the subsequent reaction zone. After quenching, the low temperature gas continues to react in the second reaction zone. The alternate quenching and reaction continues until the desired conversion is achieved.

Thus, the gas stream which has accomplished an optimum value of total conversion leaves the final reaction zone, and meets again with the by-passed gas stream. This gas mixture constitutes a suitable composition for methanation. The cooling in the product gas cooler which follows the reactor is the same as that in the adiabatic system.

In the case of hydrogen production, there is no by-passing required. All of the feed gas is passed through the reactor, because the required conversion to produce process hydrogen is already very close to equilibrium conversion, making the situation simpler than above cases.

(a) Optimization Technique

Since the cold-quenching system consists of a series of adiabatic beds, the typical optimization technique for multi-stage process, the dynamic programming, is used. In this study, a three-stage system is selected based on the results of simulation. The backward dynamic program algorithm is expressed by the well-known Bellman's principle of optimality [3] as: "Whatever the initial state and decisions are, the remaining decisions must constitute an optimal policy with regard to the state resulting from the first decision." Extensive studies have been made by numerous workers on the dynamic programming technique for various systems. Among these the analysis of Aris [1] is most frequently cited.

In contrast to the backward dynamic program algorithm, a forward dynamic program algorithm [4] has been proposed as: "Whatever the ensuing state and decisions are, the preceding decisions must constitute an optimal policy with regard to the state existing before the last decision." This technique is known to have a suitable applicability to a certain nonautonomous optimal control problem.

The selection of a backward or forward algorithm will depend on the type of problem as well as the given boundary conditions.

In Figure V-30a, the present system of water-gas shift conversion is shown. As described earlier, the initial state, (X^I, X^I), and final state, (X^E, T^F) are fixed. but all other values at intermediate stages must be determined by optimization. Since the procedure of connecting the reactor with the heat exchangers was shown in the section

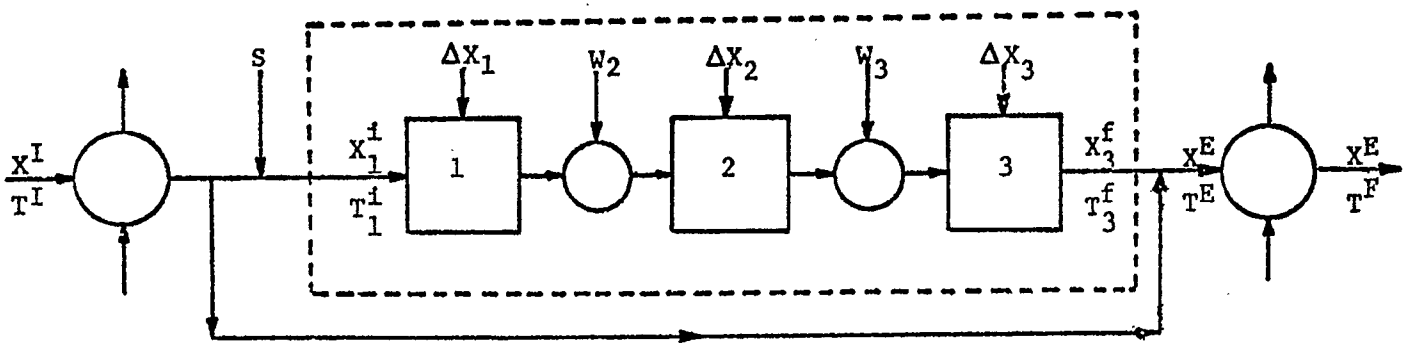

Figure V-30 a

X: Conversion of CO
T: Temperature
S: Steam
W: Quenching Water

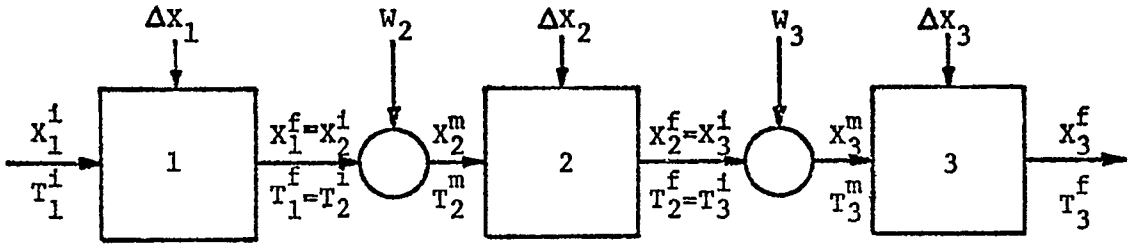

Figure V-30 b

Figure V-30 Block Diagram Of Cold Quenching Water-Gas Shift Conversion System Considered For Optimization

on the adiabatic system, only the optimization of the reactor will be considered here. In addition, from the relationship between the X_3^f and the amount of gas by-passed, it is possible to confine our system of optimization to the region surrounded by the dotted line in Figure V-30a. Figure V-30b shows the modified system to be optimized with given X_1^i. Each stage except stage 1 consists of one quenching zone and one reaction zone with two state variables, X, T, and two decision variables, W and ΔX. For example, if we use backward algorithm in stage 3, for any given value of (X_3^i, T_3^i), we can find the optimal decisions W_3 and ΔX_3 such that the total cost is minimized. In stage 1 although there is no quenching water W, the principle of computational procedure is still the same.

Generally, a backward approach has been used more frequently, and is also applicable to the present problem. However, in this study the forward concept is used, because the problem is of initial condition type and the equilibrium constraint existing at the end of each stage is helpful for taking the admissible ranges of state variables.

The general recurrance formula in N-stage process is

$$F_N(\bar{Y}_N) = \underset{\bar{\theta}_N}{\text{Min}} \left[G_N(\bar{Y}_N, \bar{\theta}_N) + F_{N-1}(\bar{Y}_N) \right] \qquad \text{(V-43)}$$

where $\bar{Y}_N$ and $\bar{\theta}_N$ are the state and decision vectors at N-th stage,

G_N and F_N are the objective and maximum objective function, respectively. Then the following functional equation can be written for each stage.

First stage,

$$F_1(X_1^f,T_1^f) = \underset{\{\Delta X_1\}}{\text{Min}} \left[G_1(X_1^f,T_1^f,\Delta X_1)\right] \qquad \text{(V-44)}$$

Second stage,

$$F_2(X_2^f,T_2^f) = \underset{\{\Delta X_2,W_2\}}{\text{Min}} \left[G_2(X_2^f,T_2^f,\Delta X_2,W_2)+ F_1(X_1^f,T_1^f)\right] \qquad \text{(V-45)}$$

Third stage,

$$F_3(X_3^f,T_3^f) = \underset{\{\Delta X_3,W_3\}}{\text{Min}} \left[G_3(X_3^f,T_3^f,\Delta X_3,W_3) + F_2(X_2^f,T_2^f)\right] \qquad \text{(V-46)}$$

Based on the above equations and using the material and energy balance relations, the optimization was performed from the first stage. Although the system is different and involves a multi-dimensionality problem, the basic principle for optimization at each stage is quite similar to that of the adiabatic case. The amount of quenching water is adjusted within the capacity of the quenching zone, and the intervals of variables are properly selected, based on the sensitibity of objective function and the computing time in each case. A linear interpolation approximation is applied to connect the stages.

The computational procedure is as follows:

1. At the exit of the first stage, the admissible ranges of X_1^f and T_1^f are found. In doing this, the restricted range of operating temperature, $550°F \leq T \leq 900°F$, and the equilibrium temperature-conversion relationship are considered. Then within the range, the net-wise two-dimensional lattice points of (X_1^f, T_1^f) are formulated.

2. The corresponding T_1^i for each of the lattice point is calculated using material and energy balance relationship in the stage. The size of reactor is evaluated, and consequently G_1 is obtained to list up.

3. Similarly, at the exit of the second stage, the admissible values of (X_2^f, T_2^f) are found.

4. In the second stage, (X_2^i, T_2^i) for different values of $(\Delta X_2, W_2)$ are calculated, and the evaluated G_2's are listed.

5. Interpolation is performed between (X_1^f, T_1^f) and (X_2^i, T_2^i), and the obtained minimum value of $G_1 + G_2$ are listed for every value of (X_2^f, T_2^f).

6. By the similar computation at the third stage, all the values of (X_3^i, T_3^i) and G_3 are also obtained from the admissible values of (X_3^f, T_3^f) and $(\Delta X_3, W_3)$.

7. Interpolation is performed between (X_2^f, T_2^f) and (X_3^i, T_3^i). Hence the total objective function $G_1 + G_2 + G_3$ is obtained for every value of (X_3^f, T_3^f), from which we can find the optimum result. Table V-8 shows one example of the optimization calculation.

ii. Reactor and Heat Exchangers

Again the reactor part and heat exchanger part can be combined by the similar procedure shown in adiabatic system.

Table V-8 Optimization Calculation

1 - Stage

X_1^f	T_1^f	T_1^i	$G_1 \times 10^{-5}$
0.685	900	807.2	1.1918
0.685	880	786.4	1.2215
0.725	880	780.9	1.2885
0.725	860	760.1	1.3332
0.735	880	779.5	1.3034
0.735	860	758.7	1.3577
0.735	840	737.9	1.4098
0.745	880	778.1	1.3183
0.745	860	757.3	1.3727
0.745	840	736.5	1.4248

X: Fraction of CO converted
T: Temperature, °F
G: Cost, $/year

2 - Stage

X_2^f	T_2^f	X_2^i	T_2^i	$G_2 \times 10^{-5}$	$(G_1 + G_2) \times 10^{-5}$
0.765	820	0.685	893.8	0.7964	1.9975
0.765	840	0.725	878.8	0.7443	2.0355
0.775	820	0.735	879.3	0.7518	2.0571
0.775	840	0.735	859.0	0.7518	2.1121
0.785	840	0.745	879.8	0.7592	2.0781
0.785	860	0.745	859.5	0.7592	2.1332

3 - Stage

X_3^f	T_3^f	X_3^i	T_3^i	$G_3 \times 10^{-5}$	$E_{ST} \times 10^{-5}$	$(G_1 + G_2 + G_3) \times 10^{-5}$
0.845	820	0.765	852.3	1.0317	10.6908	13.7346
0.855	800	0.775	832.5	1.0763	10.5658	13.7199
0.865	800	0.785	833.0	1.1828	10.4436	13.7238

iii. Results

Case II

Figure V-31 shows the reaction path under an optimum condition on a conversion-temperature plane, employing the cold quenching system at the first, second and third stages, respectively. The profiles of temperature, concentration and reaction rate are shown in Figures V-32, V-33, and V-34, respectively. In contrast to the adiabatic case, it is seen from these figures that the higher reaction temperatures and rates are obtained, thereby reducing the size of the catalyst bed. The optimum operating conditions, equipment sizes and costs are listed in Tables V-9 and V-10.

Case III

The optimum reaction paths, and profiles of temperature, concentration and reaction rate are shown in Figures V-35 to V-38. Again the differences and advantages over the adiabatic system are evident in this case. In Tables V-11 and V-12 the optimum operating conditions, optimum sizes of equipment, and the corresponding costs are listed.

Case S-2

Similarly, the various paths and profiles for this case are shown in Figures V-39 to V-42 and the corresponding optimum operating conditions and costs are listed in Tables V-13 and V-14.

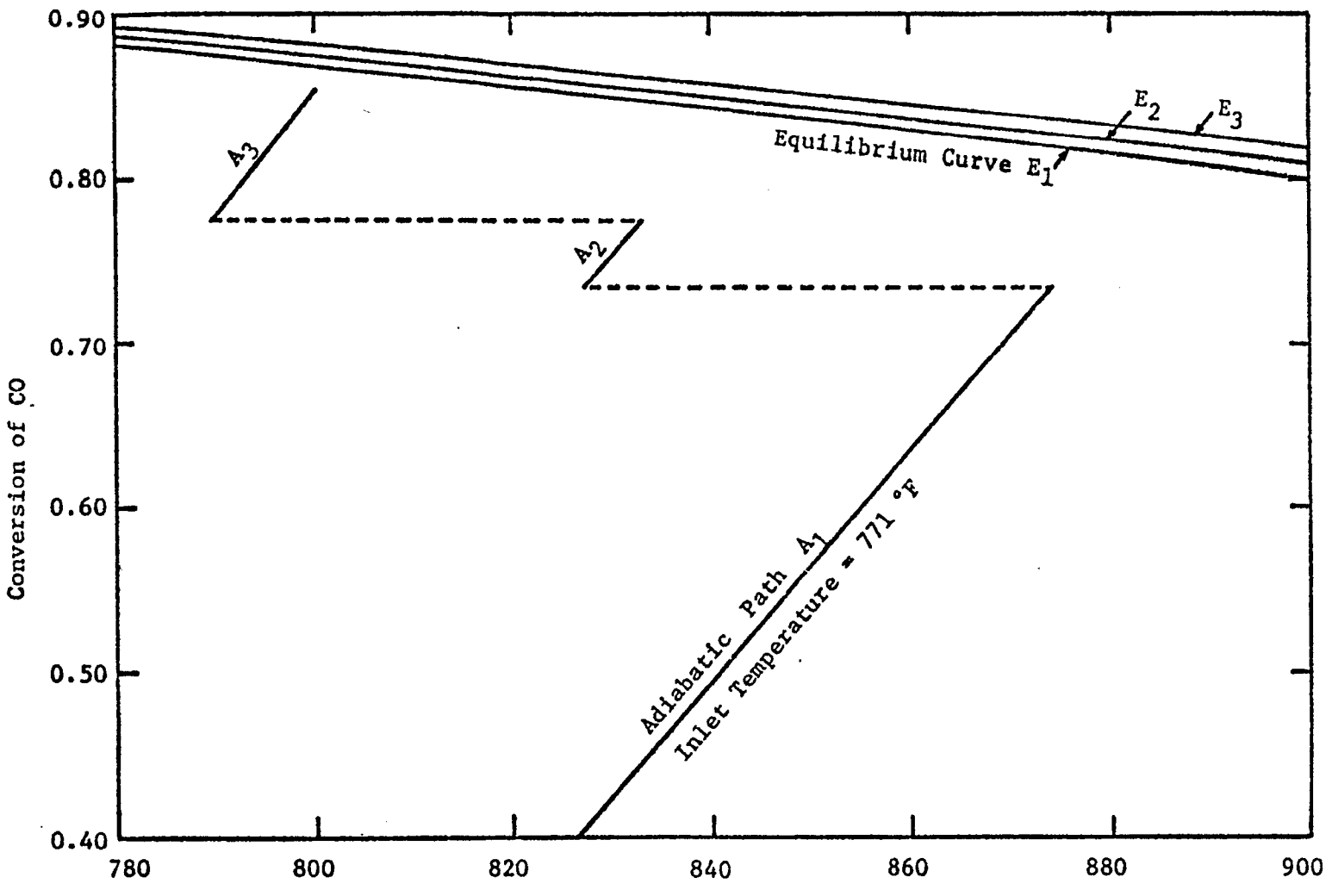

Figure V-31 Reaction Path In Cold Quenching System For Case II

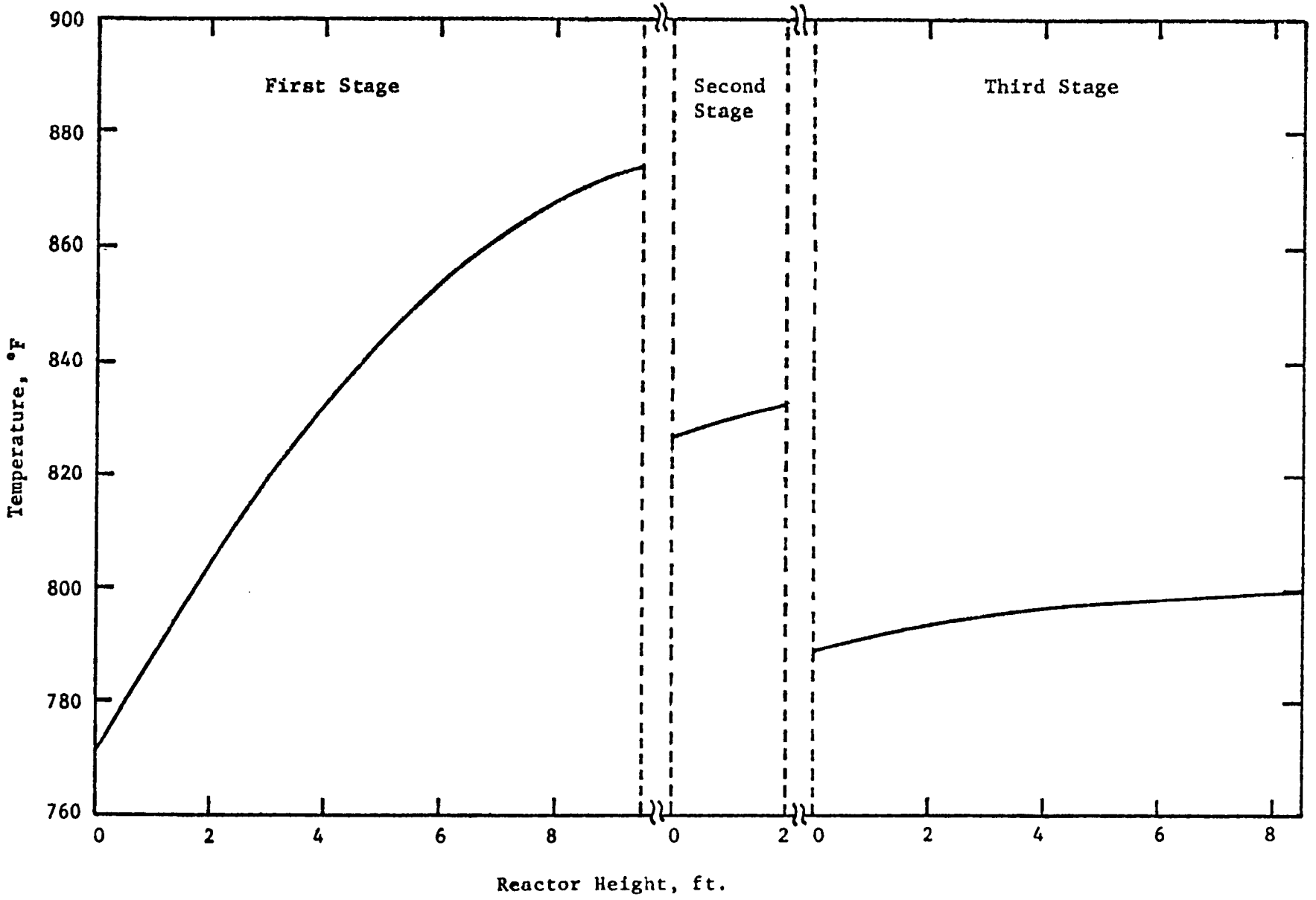

Figure V-32 Temperature Profile In Cold Quenching System For Case II

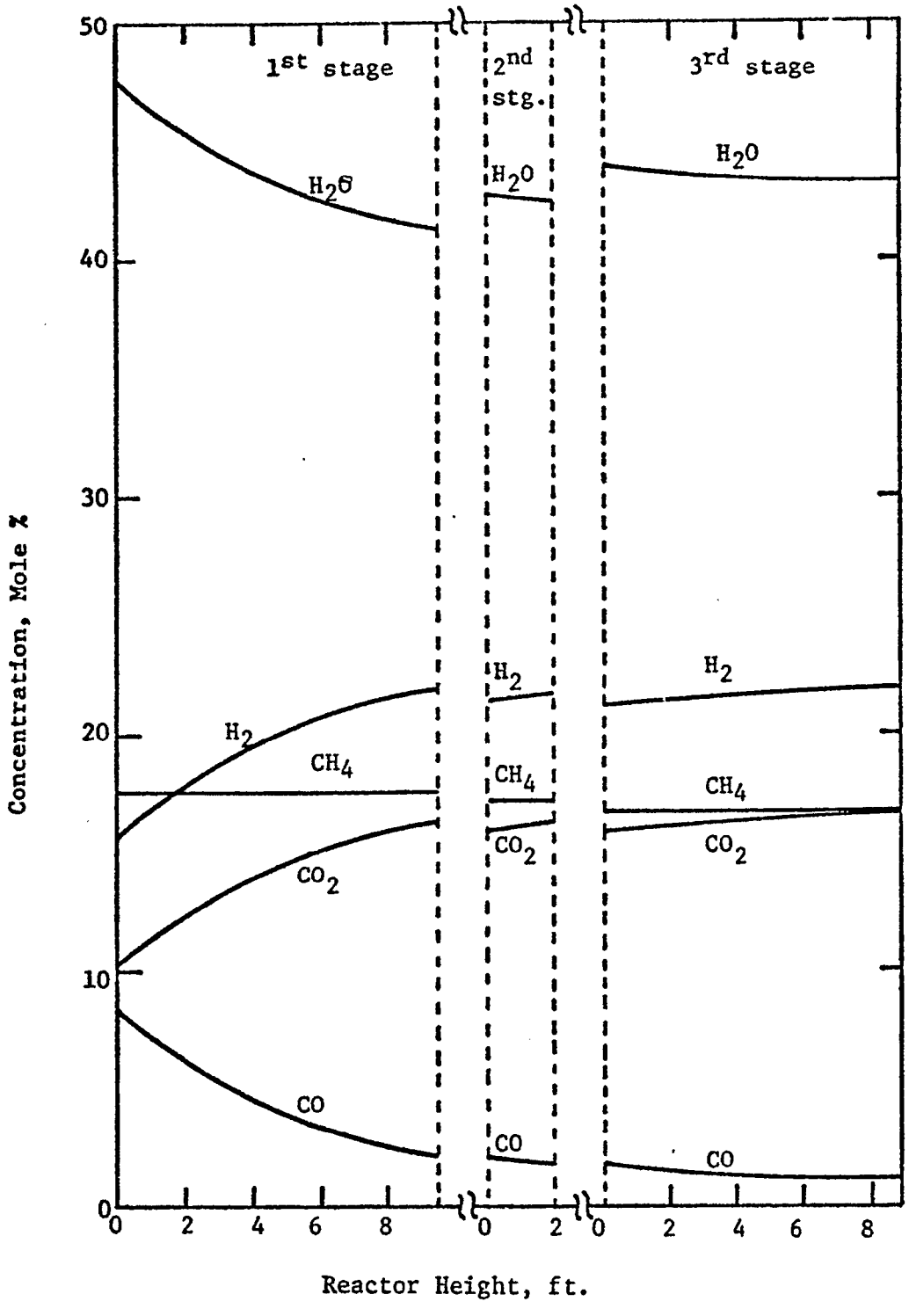

Figure V-33 Concentration Profile In Cold Quenching System For Case II

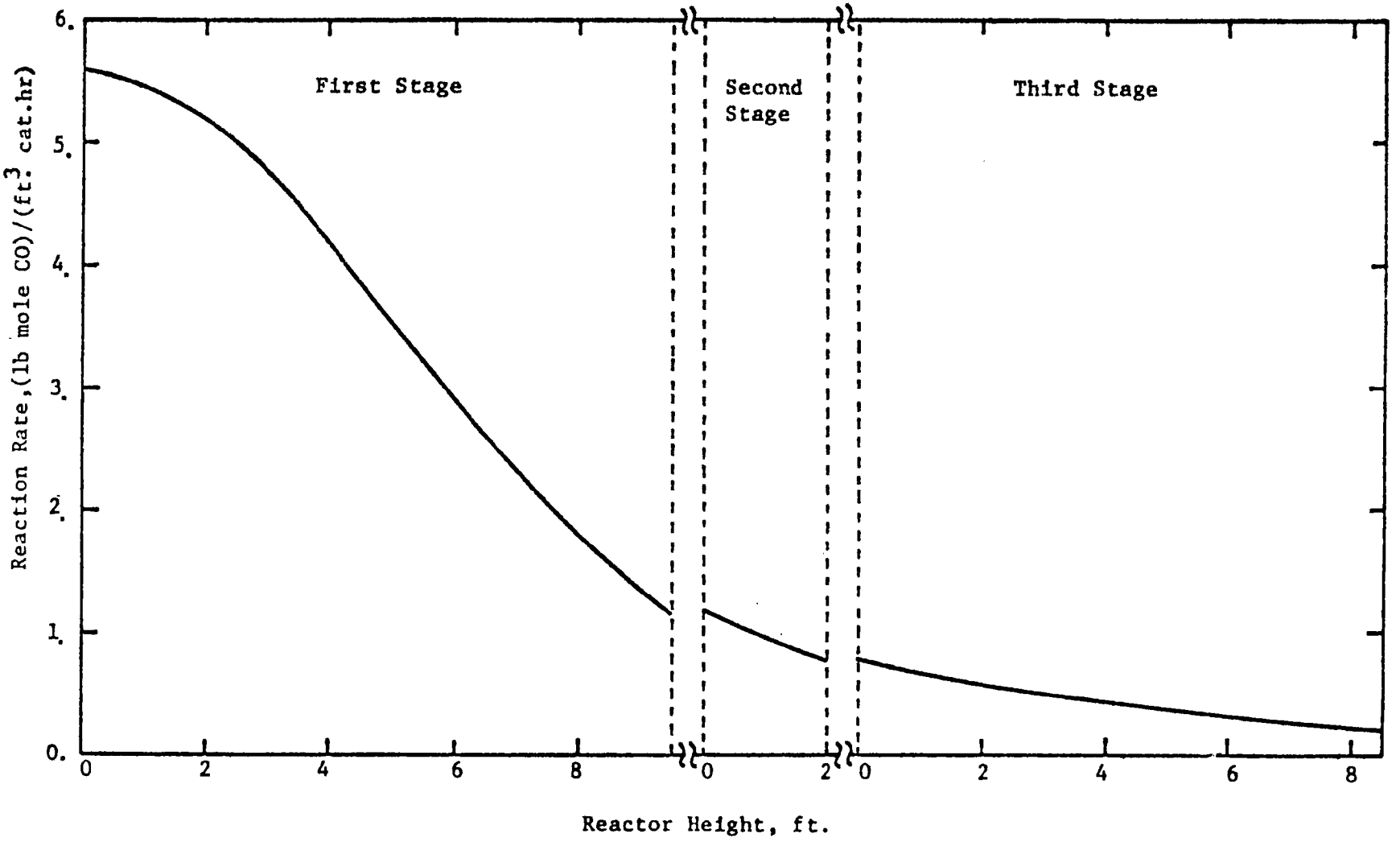

Figure V-34 Reaction Rate Profile In Cold Quenching System For Case II

Table V-9 Optimum Operating Conditions for Case II

1. Reactor

	1st Stage	2nd Stage	3rd Stage
Inlet Temperature, °F	771	827	812
Outlet Temperature, °F	872	833	825
Conversion of CO Achieved	0.735	0.775	0.855
Height of Catalyst Bed, ft	9.5	2.0	9.0
Amount of Quenching Water, lb/hr	--	18,000	18,000
Temperature of Quenching Water, °F			500
Volume Fraction of Gas By-passed			0.649
Space Velocity*, hr^{-1}			5490
Temperature of Steam Supplied, °F			556
Number of Parallel Reactors			4
Diameter, ft.			6.1
Height, ft.			26.5
Thickness, in.			3.3
Amount of Catalyst/unit, cu. ft.			358
Amount of Packing/unit, cu. ft.			58

*Based on dry gas at 60°F, 1 atm.

2. Heat Exchangers

	Waste Heat Boiler	Product Gas Cooler
Inlet Temperature of Gas, °F	1000	856
Outlet Temperature of Gas, °F	881	710
Number of Heat Exchangers	4	6
Flow Rate of Gas/unit, Mlb/hr	371.1	290.7
Flow Rate of Water unit Mlb/hr	44.9	42.7
Temperature of Steam Produced, °F	556	556
Heat Load/unit, MM BTU/hr	24.77	23.52
Heat Transfer Area/unit, sq.ft.	517	873
Heat Transfer Coefficient, BTU/(hr.ft^2°F)	98	82

Table V-10 Equipment and Operational Costs for Case II

	Waste Heat Boiler	Reactor	Product Gas Cooler	Total
Reactor Cost (M $)	--	497.9	--	497.9
Catalyst Cost (M $)	--	28.6	--	28.6
Tray Cost (M $)	--	19.4	--	19.4
Control Valve Cost (M $)	--	24.0	--	24.0
Heat Exchanger Cost (M $)	24.8	--	41.8	66.6
Pump Cost (M $)	14.6	2.9	21.4	38.9
Cooling Water Cost (M $/yr)	10.6	7.1	15.1	32.8
Working Capital (M $/yr)	2.5	29.2	3.7	35.4
Operating Cost (M $/yr)	26.0	270.0	38.0	334.0
Return on Rate (M $/yr)	1.7	22.6	2.6	26.9
Federal Income Tax (M $/yr)	0.8	11.5	1.3	13.6
Revenue Requirement (M $/yr)	28.5	304.1	41.9	374.5
Steam Cost (M $/yr)	--	1056.6	--	1056.6
Total Annual Cost (M $/yr)	28.5	1360.7	41.9	1431.1

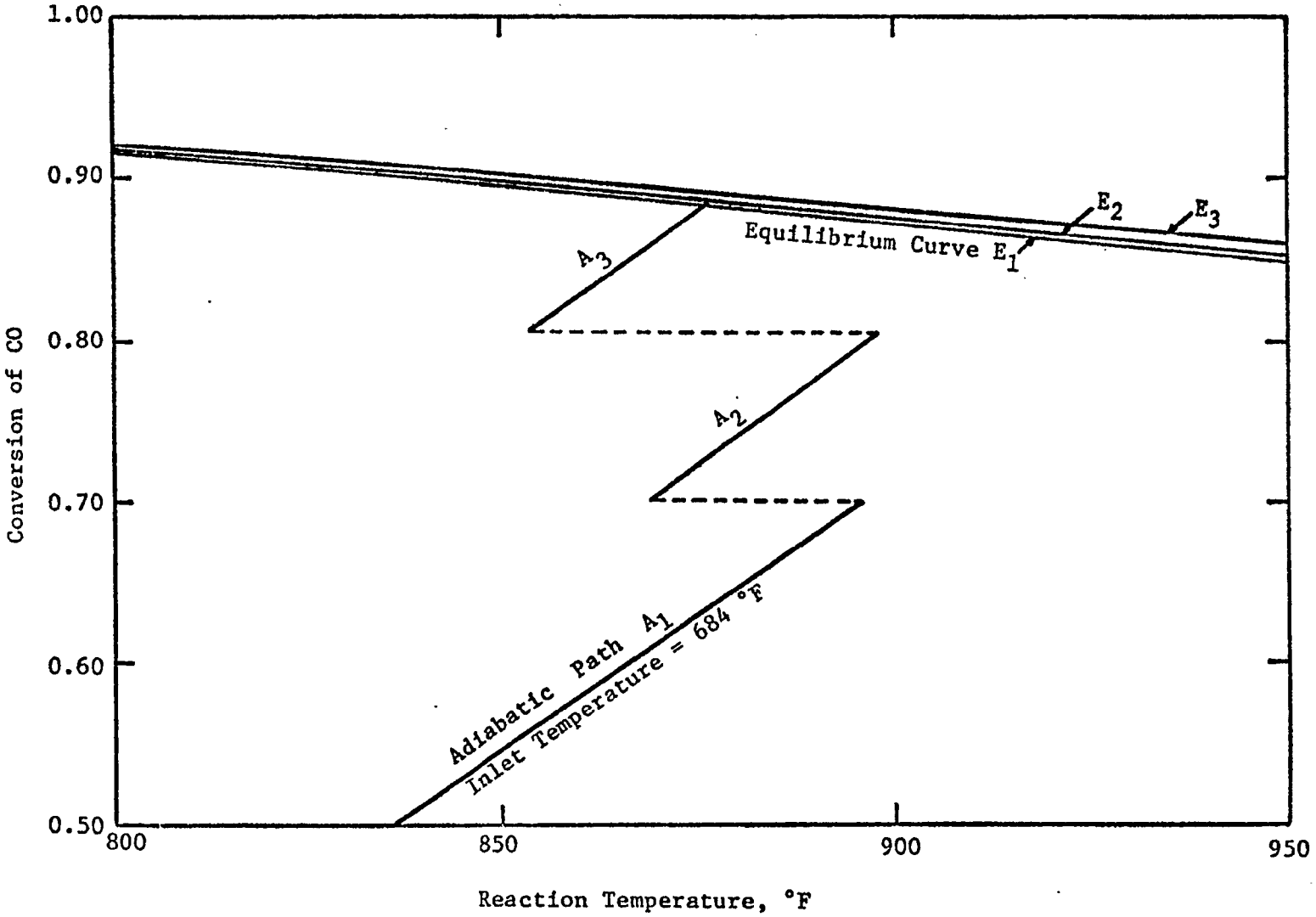

Figure V-35 Reaction Path In Cold Quenching System For Case III

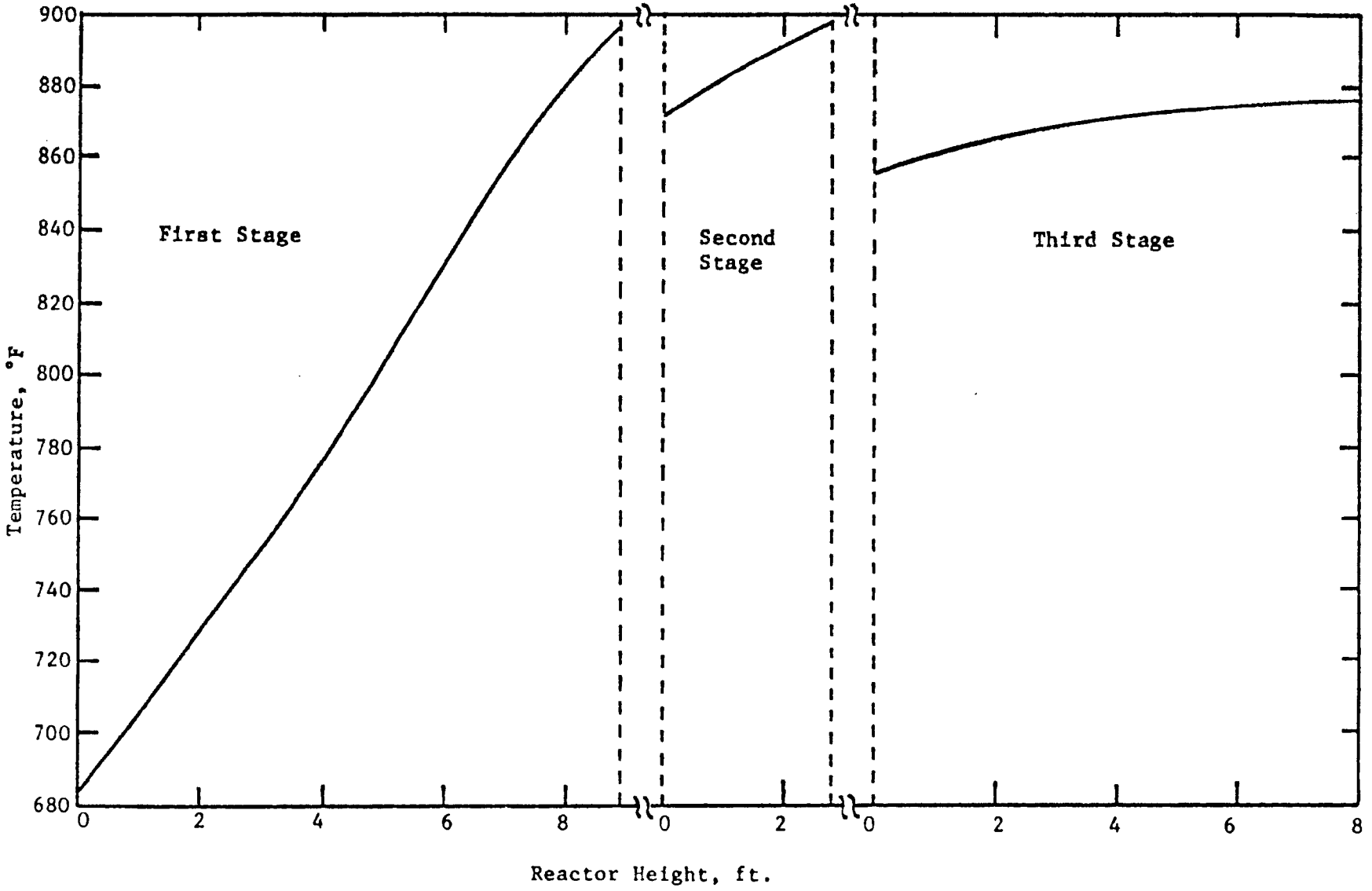

Figure V-36 Temperature Profile In Cold Quenching System For Case III

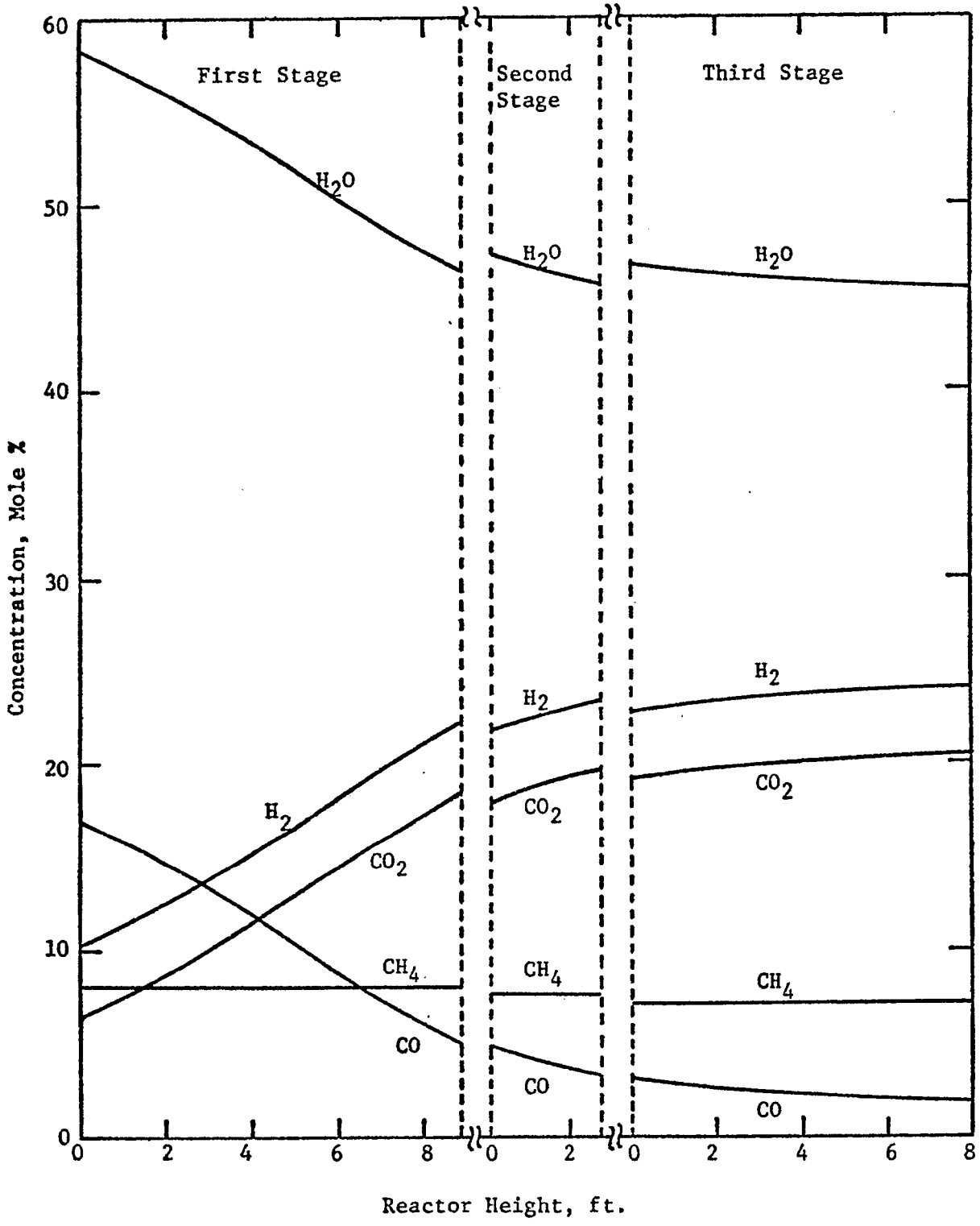

Figure V-37 Concentration Profile In Cold Quenching System For Case III

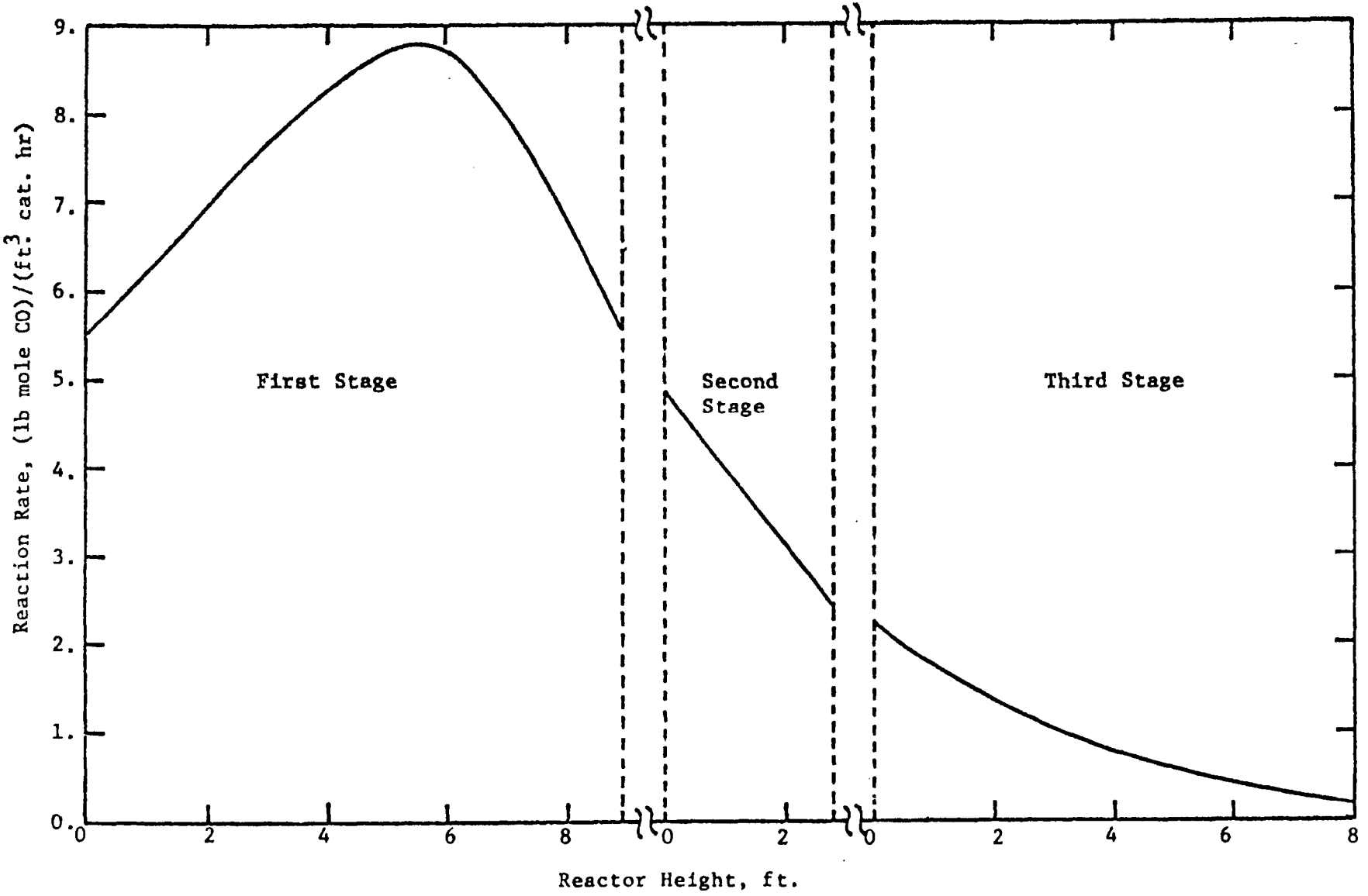

Figure V-38 Reaction Rate Profile In Cold Quenching System For Case III

Table V-11 Optimum Operating Conditions for Case III

1. Reactor

	1st Stage	2nd Stage	3rd Stage
Inlet Temperature, °F	684	869	853
Outlet Temperature, °F	895	898	876
Conversion of CO Achieved	0.701	0.803	0.883
Height of Catalyst Bed, ft	8.9	2.7	8.0
Amount of Quenching Water, lb/hr	--	32,400	57,600
Temperature of Quenching Water, °F			500
Volume Fraction of Gas By-passed			0.309
Space Velocity*, hr^{-1}			4480
Temperature of Steam Supplied, °F			551
Number of Parallel Reactors			13
Diameter, ft			6.2
Height, ft			28.6
Thickness, in			3.2
Amount of Catalyst/unit, cu ft			353
Amount of Packing/unit, cu ft			91

*Based on dry gas at 60°F, 1 atm

2. Heat Exchangers

	Waste Heat Boiler	Product Gas Cooler
Inlet Temperature of Gas, °F	1700	867
Outlet Temperature of Gas, °F	823	570
Number of Heat Exchangers	9	15
Flow Rate of Gas/unit, M lb/hr	214.1	217.9
Flow Rate of Water/unit, M lb/hr	159.3	59.8
Temperature of Steam Produced, °F	551	551
Heat Load/unit, MM BTU/hr	88.26	33.14
Heat Transfer Area/unit, sq. ft.	1218	1809
Heat Transfer Coefficient, BTU/(hr ft^2 °F)	104	68

Table V-12 Equipment and Operational Costs for Case III

	Waste Heat Boiler	Reactor	Product Gas Cooler	Total
Reactor Cost (M $)	--	1693.5	--	1693.5
Catalyst Cost (M $)	--	91.6	--	91.6
Tray Cost (M $)	--	64.5	--	64.5
Control Valve Cost (M $)	--	60.0	--	60.0
Heat Exchanger Cost (M $)	63.3	--	105.3	168.6
Pump Cost (M $)	58.0	4.2	61.2	123.4
Cooling Water Cost (M $/yr)	84.6	17.7	52.9	155.2
Working Capital (M $/yr)	16.2	64.6	11.8	92.6
Operating Cost (M $/yr)	176.0	533.5	123.2	832.7
Return on Rate (M $/yr)	5.7	73.1	7.1	85.9
Federal Income Tax (M $/yr)	3.1	36.8	3.7	43.6
Revenue Requirement (M $/yr)	184.8	643.4	134.0	962.2
Steam Cost (M $/yr)	--	6004.8	--	6004.8
Total Annual Cost (M $/yr)	184.8	6648.2	134.0	6967.0

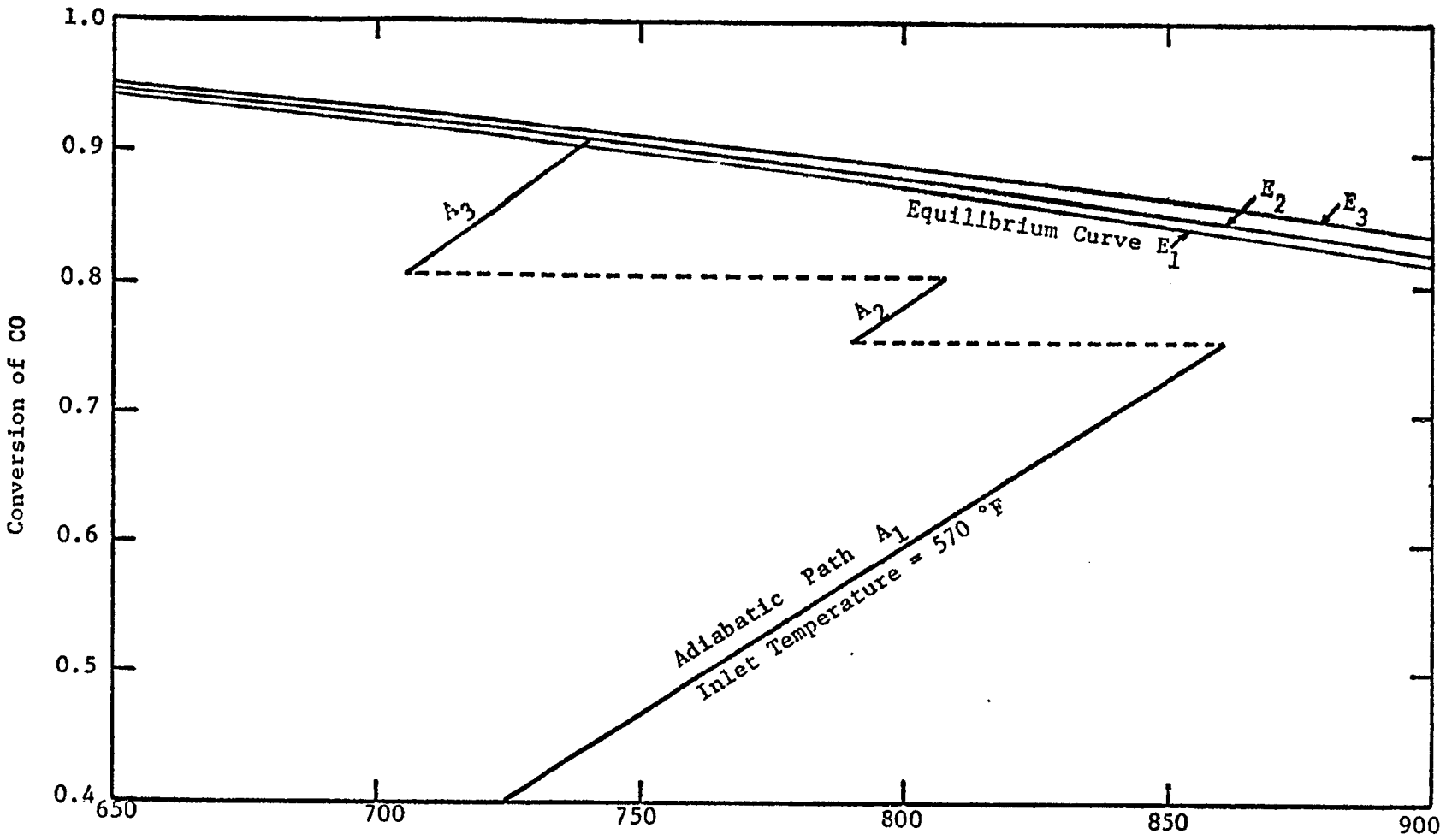

Figure V-39 Reaction Path In Cold Quenching System For Case S-2

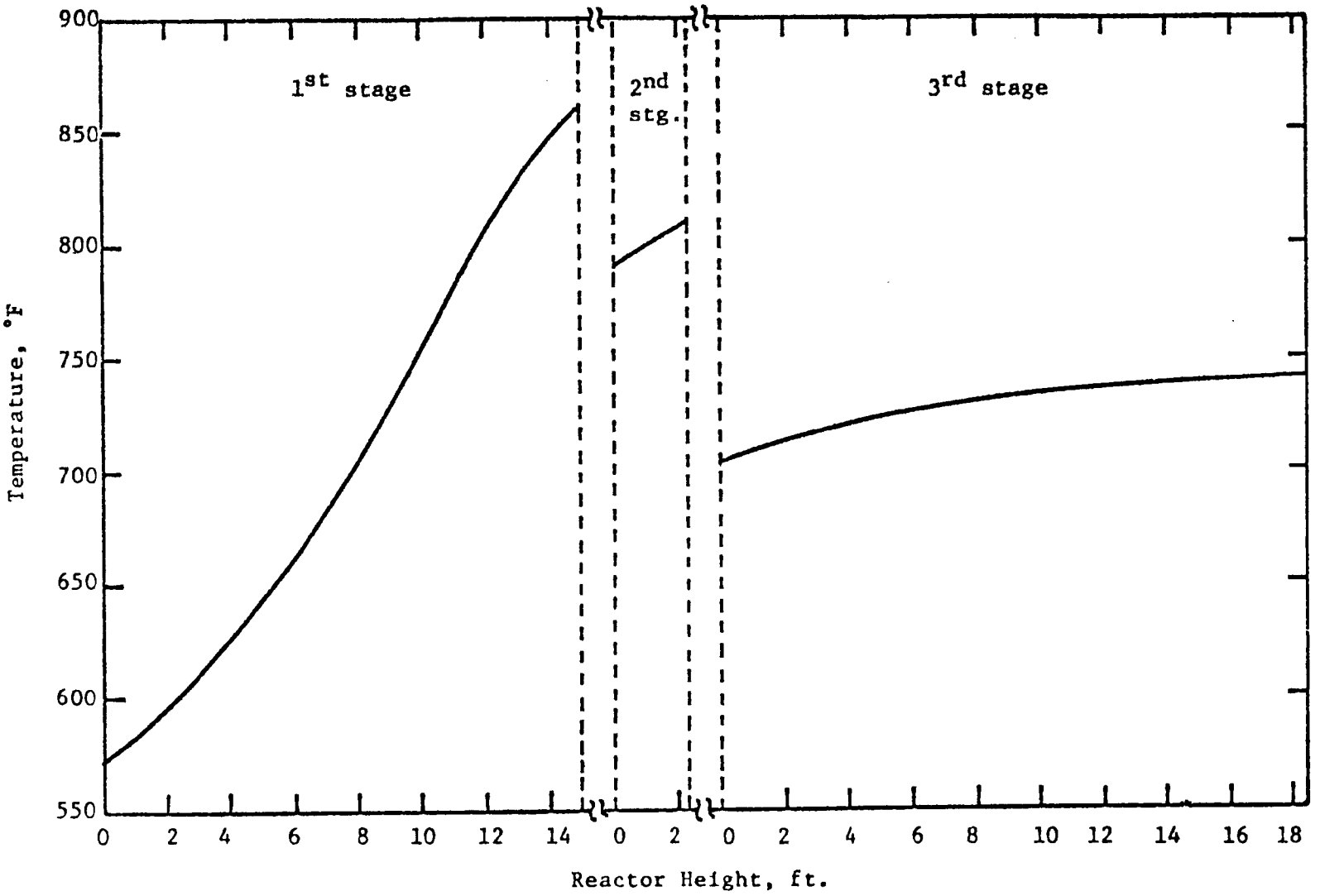

Figure V-40 Temperature Profile In Cold Quenching System For Case S-2

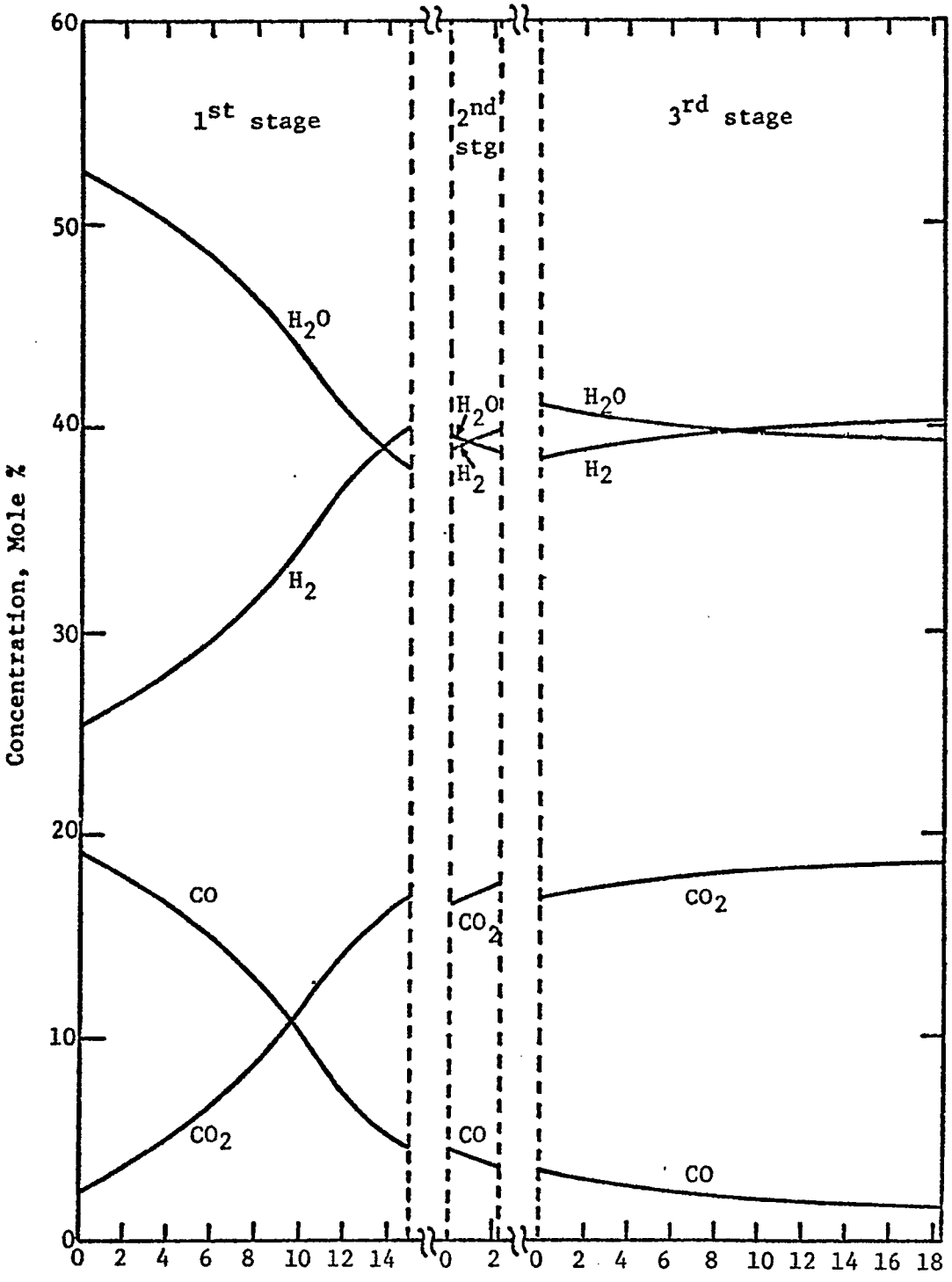

Figure V-41 Concentration Profile In Cold Quenching System For Case S-2

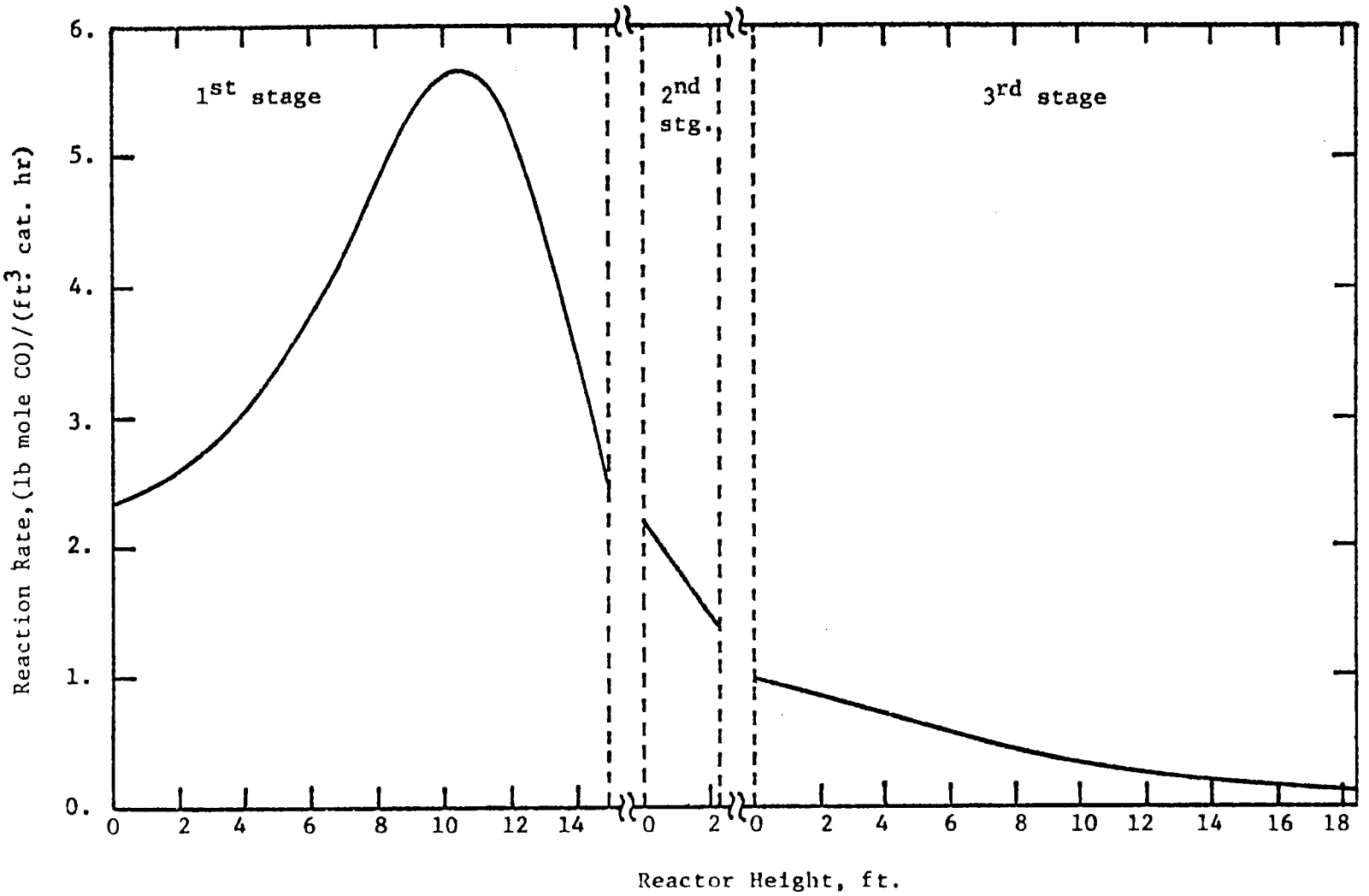

Figure V-42 Reaction Rate Profile In Cold Quenching System For Case S-2

Table V-13 Optimum Operating Conditions of Reactor for Case S-2@

	1st Stage	2nd Stage	3rd Stage
Inlet Temperature, °F	570	790	705
Outlet Temperature, °F	861	808	740
Conversion of CO Achieved	0.757	0.807	0.907
Height of Catalyst Bed, ft	14.9	2.3	18.4
Amount of Quenching Water, lb/hr	--	36,000	54,000
Temperature of Quenching Water, °F			100
Space Velocity*, hr^{-1}			2020
Temperature of Steam Supplied, °F			570
Number of Parallel Reactors			10
Diameter, ft			6.3
Height, ft			44.6
Thickness, in			3.7
Amount of Catalyst/unit, cu ft			670
Amount of packing/unit, cu ft			93

*Based on dry gas at 60°F, 1 atm
@steam to gas ratio: 1.12 (mole/mole)(See Section 4.11)

Table V-14 Equipment and Operational Costs for Case S-2

	Waste Heat Exchanger	Reactor	Product Gas Coolers	Total
Reactor Cost (M $)	--	2263.8	--	2263.8
Catalyst Cost (M $)	--	134.1	--	134.1
Tray Cost (M $)	--	116.1	--	116.1
Control Valve Cost (M $)	--	48.0	--	48.0
Heat Exchanger Cost (M $)	130.3	--	152.4	282.7
Pump Cost (M $)	10.5	7.3	11.9	29.7
Cooling Water Cost (M $/yr)	14.4	17.7	46.3	78.4
Working Capital (M $/yr)	4.4	81.0	7.4	92.8
Operating Cost (M $/yr)	41.5	646.4	73.8	761.7
Return on Rate (M $/yr)	5.6	97.3	6.7	109.6
Federal Income Tax (M $/yr)	2.8	48.9	3.4	55.1
Revenue Requirement (M $/yr)	49.9	792.6	83.9	926.4
Steam Cost (M $/yr)	--	3185.8	--	3185.8
Total Annual Cost (M $/yr)	49.9	3978.4	83.9	4112.2

4. Discussion

4.1 Effect of Steam to Gas Ratio on the Performance of Adiabatic Water-Gas Shift Converter

As was seen, the amount of steam introduced in terms of the steam to gas ratio plays an important role in the water-gas shift conversion process. However, in this study, the steam to gas ratio has been selected by a simple approach because of the difficulties involved. To see how this factor affects the performance of the reactor and optimization, different values of steam to gas ratio are employed for conditions of Case II. Since the heat exchangers occupy a minor portion of the total cost, only the reactor portion is calculated.

Figure V-43 shows the reaction rate profiles along the reactor height with the steam to gas ratios at 0.8, 1.0 and 1.2. According to this figure, the reaction rate is lower at a larger steam to gas ratio. This is because the rate equation used here is first order with respect to carbon monoxide, the concentration of which is diluted by the larger amount of steam.

The operating conditions and costs are listed in Table V-15 indicating that the major difference in cost comes from the variation in the amount of steam although there is also a considerable change in other costs.

4.2 Effect of Steam Cost Change in Adiabatic System

In this study, the cost of steam is taken as a fixed value at 60 cents per thousand pounds. The effect of steam costs on the optimum conditions is studied by changing its unit cost at 40 cents and 80 cents per thousand pounds. As shown in Table V-16 only a slight change in optimum operating conditions and costs is seen.

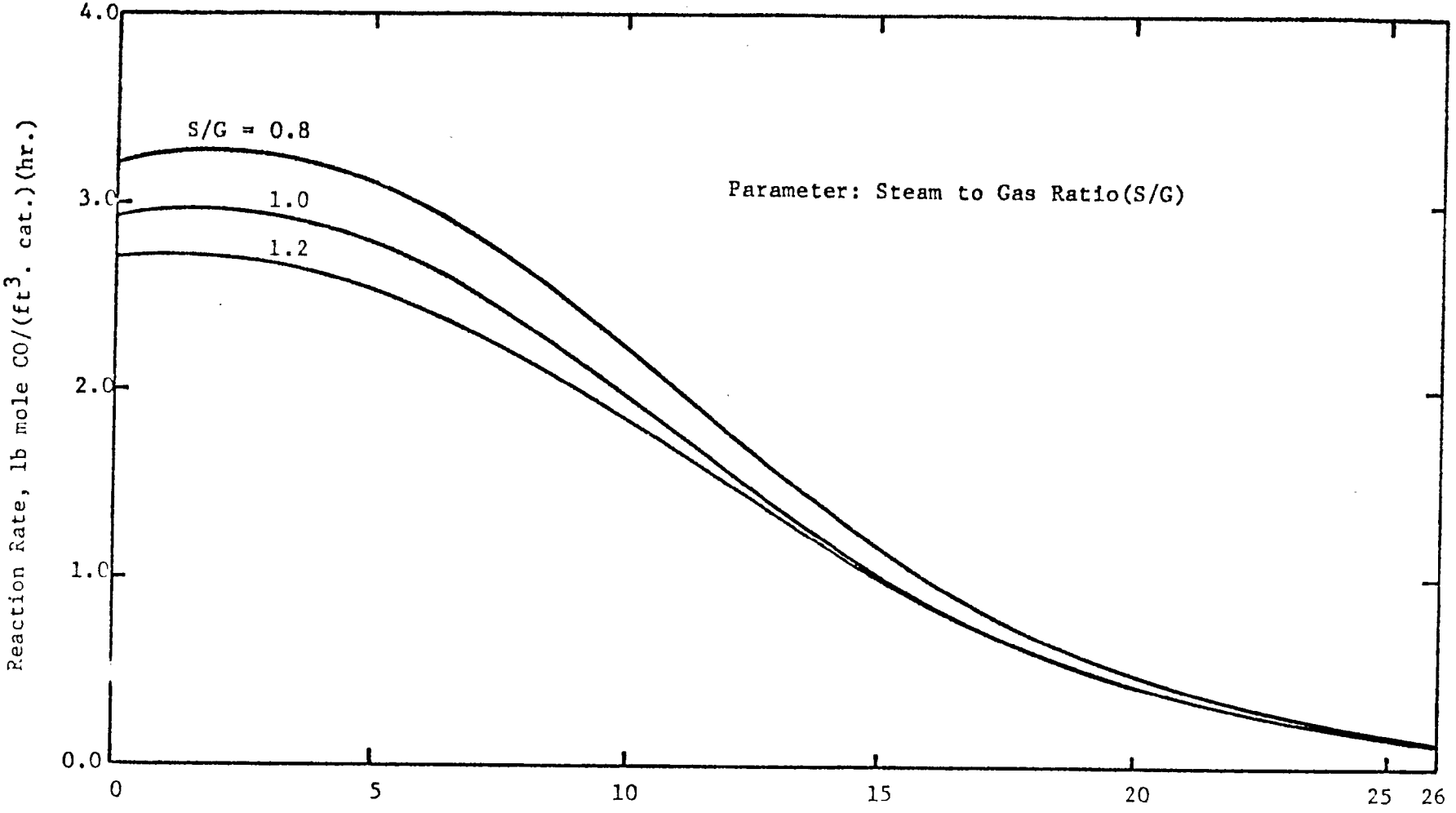

Figure V-43 Reaction Rate Profile for Case II

TABLE V-15 EFFECT OF STEAM TO GAS RATIO FOR CASE II

	S/G=0.8	1.0	1.2
Inlet Temperature (°F)	700	700	700
Conversion of CO	0.815	0.855	0.877
Space Velocity* (hr^{-1})	4290	4380	4640
Number of Reactors	3	3	3
Diameter of Reactor (ft.)	6.7	7.0	7.3
Height of Reactor (ft.)	24.2	25.9	26.3
Thickness (in.)	3.58	3.73	3.86
Reactor Cost (M$)	429.4	496.8	544.5
Catalyst Cost (M$)	31.1	36.3	39.7
Tray Cost (M$)	30.3	33.8	35.1
Control Valve Cost (M$)	20.0	20.0	20.0
Bare Cost (M$)	479.7	550.6	599.6
Revenue Requirement (M$/Yr)	182.4	201.7	215.3
Steam Cost (M$/Yr)	915.8	1240.2	1567.0
Total Annual Cost (M$/Yr)	1098.2	1441.9	1782.3

*Based on dry gas at 60°F, 1 atm.

TABLE V-16 EFFECT OF VARIATION IN STEAM COST FOR CASE II

	40 ¢/Mlb	60 ¢/Mlb	80 ¢/Mlb
Inlet Temperature (°F)	700	700	700
Conversion of CO	0.845	0.855	0.855
Space Velocity* (hr^{-1})	4740	4380	4380
Number of Reactors	3	3	3
Diameter of Reactor (ft.)	7.0	7.0	7.0
Height of Reactor (ft.)	24.2	25.9	25.9
Thickness (in.)	3.67	3.73	3.73
Reactor Cost (M$)	459.1	496.8	496.8
Catalyst Cost (M$)	33.1	36.3	36.3
Tray Cost (M$)	32.1	33.8	33.8
Control Valve Cost (M$)	20.0	20.0	20.0
Bare Cost (M$)	523.1	561.5	561.0
Revenue Requirement (M$/Yr.)	190.8	201.7	201.7
Steam Cost (M$/Yr)	836.6	1240.2	1653.6
Total Annual Cost (M$/Yr)	1027.4	1441.9	1855.3

4.3 Effect of Pressure on the Performance of Adiabatic Reactor

Since not much is known about the reaction kinetics above 400 psig, the validity of rate equation used in this study is uncertain above this pressure. Most commercial plants are operated around 400 psig or less, due to the experimental fact that the activity of iron-chromium-oxide catalyst increases rapidly with pressure, but not much above 400 psig.

Two additional operating pressures of 300 psig and 600 psig are selected to study the effect of pressure on the reactor operation. Figure V-44 shows the profiles of reaction rate while Figure V-45 indicated the variation of equipment costs with inlet temperature under the specified conditions.

The operating conditions and costs are listed in Table V-17 for comparison. These results indicate that at high pressures, although the reaction rate is increased and consequently the volume of the reactor is decreased, the cost of the reactor becomes higher because of the thicker reactor wall. Therefore, there is no general reason to operate the reaction at a high pressure unless other parts of the gasification processes are conducted under high pressure.

4.4 Comparison of the Results Using Different Reaction Rate Expressions in Adiabatic System

In section 1.2, two types of rate equation, the pseudo-first order equation (V-6) and the second order rate equation (V-4) are discussed. Since the design of the reactor depends greatly upon the rate equation, it will be necessary to compare the results obtained using the two rate equations. The operating conditions and the corresponding costs based on the two equations are listed in Table V-18. Because both equations are valid only for low pressure, 300 psig is selected as the operating pressure.

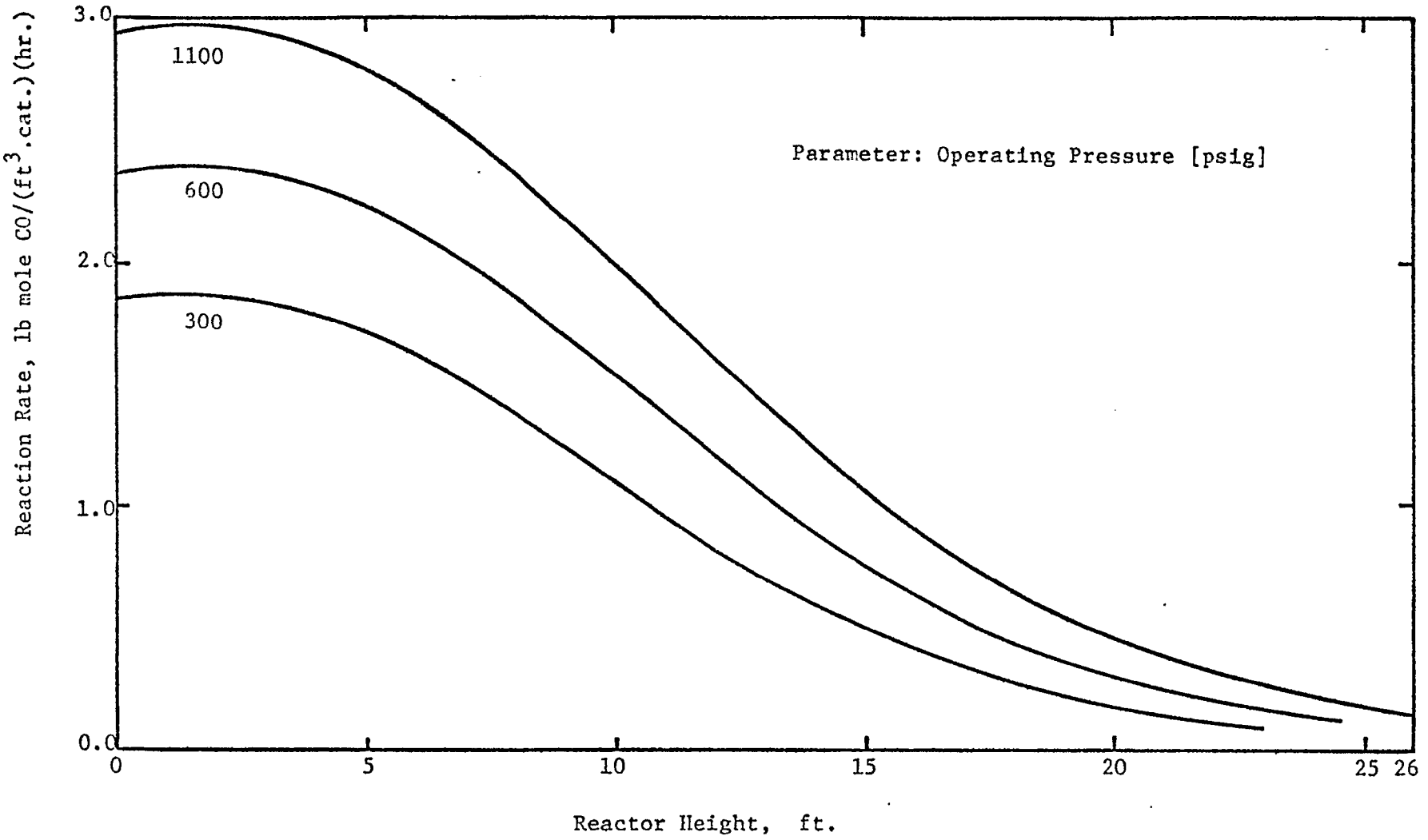

Figure V-44 Effect of Operating Pressure on Reactor Performance for Inlet Temperature 700 °F

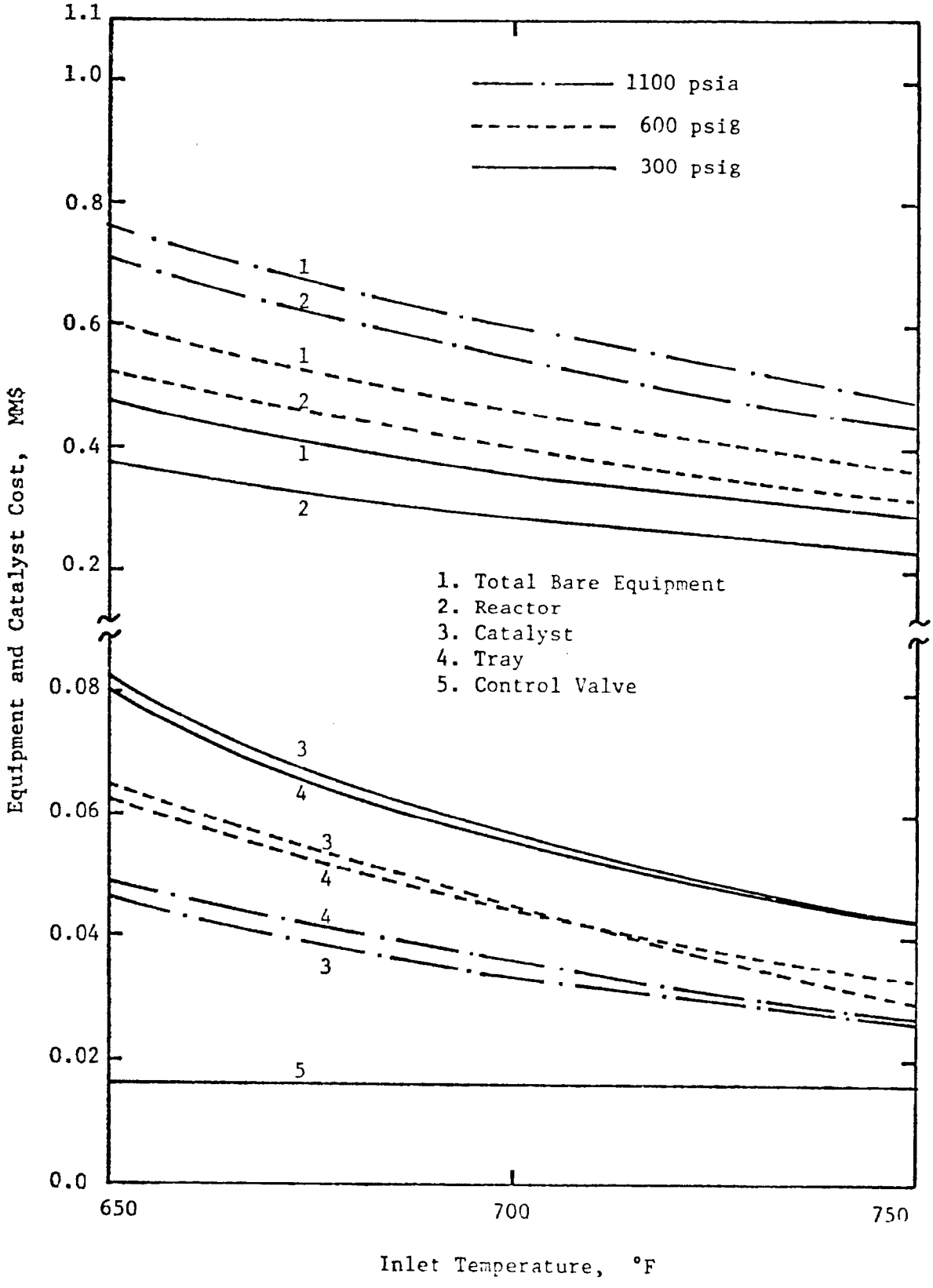

Figure V-45 Cost of Equipment and Catalyst Versus Inlet Temperature of Reactor with Pressure as Parameter for Case II

TABLE V-17 EFFECT OF PRESSURE ON REACTOR OPERATION FOR CASE II

	300 psig	600 psig	1100 psia
Inlet Temperature (°F)	700	700	700
Conversion of CO	0.855	0.855	0.855
Space Velocity* (hr^{-1})	2730	3540	4380
Number of Reactors	3	3	3
Diameter of Reactor (ft.)	9.4	8.0	7.0
Height of Reactor (ft.)	23.0	24.5	25.9
Thickness (in.)	1.54	2.43	3.73
Reactor Cost (M$)	259.8	358.0	496.8
Catalyst Cost (M$)	57.4	44.8	36.3
Tray Cost (M$)	49.2	42.0	33.8
Control Valve Cost (M$)	20.0	20.0	20.0
Bare Cost (M$)	341.0	432.1	561.5
Revenue Requirement (M$/Yr)	177.8	183.8	201.7
Steam Cost (M$/Yr)	1240.2	1240.2	1240.2
Total Annual Cost (M$/Yr)	1418.0	1424.0	1441.9

TABLE V-18 COMPARISON OF THE RESULTS FROM FIRST- AND SECOND- ORDER RATE EQUATION AT 300 PSIG FOR CASE II

	Eq.(2 -6)	Eq.(2 -4)
Inlet Temperature (°F)	700	700
Outlet Temperature (°F)	815.5	814.7
Conversion of CO	0.855	0.849
Space Velocity* (hr^{-1})	2730	2030
Number of Reactors	3	3
Diameter of Reactor (ft.)	9.4	9.9
Height of Reactor (ft.)	23.0	28.1
Thickness (in.)	1.54	1.61
Reactor Cost (M$)	259.8	338.5
Catalyst Cost (M$)	57.4	70.3
Tray Cost (M$)	49.2	73.6
Control Valve Cost (M$)	20.0	20.0
Bare Cost (M$)	341.0	444.1
Revenue Requirement (M$/Yr.)	177.8	219.4
Steam Cost (M$/Yr)	1240.2	1248.9
Total Annual Cost (M$/Yr)	1418.0	1468.3

*Based on dry gas at 60°F, 1 atm.

As can be seen from this table, only small differences exist between the two results indicating that the water-gas shift reaction can be represented by either of the two equations in this range. The second order equation, however, seems to provide more conservative estimate than the first order equation.

4.5 Design and Performance of Quenching Zone

As shown in the results of optimization, the volume of catalyst bed is considerably reduced in comparison to that of the adiabatic system, owing to the higher reaction rate achieved.

In spite of this, the overall size of the reactor is not necessarily smaller because of the quenching zones required. This implies that the efficient design and effective operation of the quenching zone are very important if the quenching system is to be more advantageous over the adiabatic system. The accurate design of the quenching zone will, however, require detailed information on the type of spray equipment, characteristics of packings and the operating behaviors.

Nevertheless, the quenching system is still preferable because the quenching water can substitute the corresponding amount of steam, reducing a substantial amount of operating cost.

4.6 Pressure Drop in Quenching Zone

Since the quenching zone is usually packed with rings and saddles, more pressure drop is expected in this region. Either of the following equations may be used for the estimation of pressure drop [19,25];

$$\Delta P/Z = 0.012\ C_f G^2/6g_c \rho \qquad \text{(V-47)}$$

or

$$\Delta P/Z = k' V^n \qquad \text{(V-48)}$$

where $\Delta P/Z$ is the pressure drop per unit height of packing, lb/(in.^{2} ft.)

G, V are the mass velocity based on empty tower, lb/(ft.^{2} hr.)

and the linear velocity, ft/sec, of gas, respectively. C_f, k', and n are the constants related to the characteristics of packings and the flow behavior of fluid.

ρ, g_c are the density of gas, lb/ft^3, and the gravitational acceleration conversion factor, $ft.lb_m/(lb_f \cdot hr^2)$, respectively. If the values, G = 7000 and ρ = 1.5 are used, then we obtain $\Delta p/Z$ = 0.005 psi/ft by Eq. (V-47) and 0.03 psi/ft by Eq. (V-48). Therefore, the pressure drop through quenching zone in this study can be neglected, unless the packing height is much larger than anticipated.

4.7 Effect of Quenching

The reaction rate profiles shown in Figures V-34 and V-38 are similar to those of the adiabatic system except for their peak values obtained at the first stage. The values of maximum rates are higher in quenching system than in adiabatic system because of the elevated inlet temperatures. As is known, an exothermic temperature reaction achieves the best performance when the initial temperature is as high as possible, but the final temperature is as low as possible. The temperature profile also affects the determination of the amount of quenching water in the second and third stages with the latter requiring more than the former. The extent of quenching appears prominent in the third stage which occupies a larger part of the total reactor. It is also shown, however, that near the optimum point the determination of total amount of quenching water, $(W_1 + W_2)$, is more important than that of each amount, W_1, W_2, within the fixed total amount.

4.8 Performance in Individual Stage

From Figures V-31, V-35, and V-39, it is noticed that as the concentration of CO in the feed gas becomes higher, the exit temperature of

each stage deviated from the equilibrium temperature more in the first stage, but less in the last stage. The optimum fractions of total conversion achieved in each stage fall in the following ranges: 80 ~ 85% in the first stage, 5 ~ 10% in the second stage, and 10% in the third stage. However, over 80% of the total reactor size is distributed between the first and third stages, and only about 10% of the volume is occupied by the second stage, indicating the importance of the performance of both end stages.

4.9 Effect of Sulfur Content in Gas

The sulfur content in gas is another important factor, greatly affecting the performance of the water-gas shift reaction. If the amount of sulfur exceeds the allowable value, the catalyst activity deteriorates considerably requiring periodical regeneration. However, since the allowable sulfur content varies considerably depending on the type of catalyst used, the determination must be based on the experimental data obtained for each specific catalyst.

The study of Bohlbro [6] indicates that the kinetics of water-gas shift reaction may be modified by the presence of H_2S in the feed gas. According to his experimental results, if the content of H_2S is less than 100 ppm (part per million) only physical absorption on the surface of catalyst takes place; but at above 1000 ppm the kinetics will be altered because of the transformation of iron oxide into iron sulfide.

On the other hand, Girlder [8] described that the sulfur content above 150 ppm reduces the activity of catalyst greatly; but below 50 ppm sulfur does not have any significant effect on the activity of their catalyst. Mars [16] also discussed the effect of sulfur content on the activity of the catalyst showing that a better removal of sulfur compounds from the feed gas considerably increases the performance of the reactor.

The sulfur content in raw gas from gasifier varies widely depending on the process, some of which could have as much as 0.9% H_2S. This study is, however, made based on the assumption that the sulfur content is low enough to be tolerated by the catalyst without causing substantial deactivation.

In general, unless the sulfur content in the feed gas is very high, it is possible to select a proper type of catalyst that will withstand the sulfur poisoning for a substantial length of time. On the other hand, if the catalyst gets deactivated, it is also possible to modify the space velocity in the reactor for the corresponding reduction in catalyst activity. The recent study of Ting and Wan [24] shows another approach for handling sulfur-containing gases. Here the rate constant is modified by a sulfur correction factor, the values of which are obtained in terms of operating pressure up to 30 atm for the gases containing H_2S as high as 0.24%.

4.10 Sensitivity Analysis

The current optimization involves a number of specific system parameters. But the information on these parameters are not necessarily accurate. Such an uncertainty of parameters is incurred by various internal and external factors and may affect the performance of optimization considerably under certain conditions.

The sensitivity study here is intended to bring about a better system performance by analysing the effect of variation in parameters on objective function. The sensitivity of a given parameter, S_e, may be represented as[27]

$$S_e = [(J-\bar{J})/\bar{J}]/[(w-\bar{w})/\bar{w}] \qquad \text{(V-49)}$$

where

J and $\bar{J}$ are the objective function for a given value of parameter and that at the optimum condition, respectively.

w and $\bar{w}$ are the parameter subject to variation and that at a specific value considered, respectively.

Referring to the results listed in Table V-19, it is seen that the objective function is most sensitive to the parameters involved in the kinetic expression. As is also expected, the dimension and character of catalyst pellet play an important role in the reactor performance.

TABLE V-19 PARAMETER SENSITIVITY ON OBJECTIVE FUNCTION OF ADIABATIC WATER-GAS SHIFT REACTION

Parameters	Sensitivity	
	Case II	Case III
U_h	-0.3522×10^{-2}	-0.1218×10^{-2}
U_v	-0.8555×10^{-2}	-0.1977×10^{-2}
k_o	-0.3540×10^{-1}	-0.1902×10^{-1}
E	1.452	0.7046
d_p	0.7971×10^{-1}	0.4530×10^{-1}
S_p	-0.3340×10^{-1}	-0.1847×10^{-1}
ρ_p	-0.3457×10^{-1}	-0.1892×10^{-1}
D_{e_p}	-0.3311×10^{-1}	-0.1832×10^{-1}
ρ	-0.1181×10^{-2}	-0.1305×10^{-4}
μ	-0.7195×10^{-3}	-0.8584×10^{-5}

4.11 Selection of Steam to Gas Ratio

In the water-gas shift conversion process, the steam to gas ratio is selected primarily for the prevention of carbon deposition. However, the determination of proper ratio is difficult because of the lack of information on the quantitative factors affecting the carbon deposition. They are probably related to the concentration of each component, conversion of carbon monoxide, operating temperature and pressure, etc. The information from Girdler [29][8] indicates that the steam to gas ratio normally ranges from 1.0 to 3.0 depending on the conditions and that the most important factor is the concentration of carbon monoxide.

In this study therefore, a rather arbitrary and simple approach is taken for the determination of the steam to gas ratio. The simplification is made by adding all the carbon deposition reactions (2), (3), (4), (5) shown in Section 1.1, resulting $3\ CO + H_2 + CH_4 = 4C + 3H_2O$. According to this reaction, if the concentrations of CO, H_2, CH_4 are high , the carbon deposition reaction will be more likely to occur. Therefore, the amount of steam should be increased as the concentration of CO, H_2, CH_4 are increased. Thus, the steam to gas ratio may be considered roughly proportional to the sum of the concentrations, $\sum a_i C_i \equiv 3\ C_{CO} + C_{H_2} + C_{CH_4}$. If we follow this approach, the value of $\sum a_i C_i$ based on the mole fraction of each component for Case II, Case S-1, and Case III are 1.1, 1.35, and 1.65, respectively. Since in Girdler's experimental results [29] a steam

to gas ratio of 1.2 is used for the CO concentration approximately equivalent to Case S-1, the value of $\sum a_i C_i$ is adjusted to 1.2. By multiplying the proportionality factor (1.2/1.35), the values of $\sum a_i C_i$ for Case II and Case III are obtained as 1.0 and 1.5, respectively. For Case III however, a slightly higher value is used considering its higher conversion of CO than Case II or Case S-1. Since Case S-2 is for pure hydrogen production, a very high CO conversion must be achieved for this purpose. In this study the steam to gas ratio for Case S-2 is taken from the value used already by I.G.T. [13].

5. Conclusion

5.1 In the operation of a water-gas shift reactor, steam cost occupies the major portion of the total cost. The reduction of the amount of steam is therefore most important in making the process more economical.

5.2 The total annual cost is not affected to a great degree by the variation in the reactor inlet temperature between 650°F to 750°F when the concentration of CO in the feed gas is low or moderate. For the gas of high CO concentration, however, the sensitivity due to the inlet temperature variation is increased.

5.3 The optimum conversion is very close to the equilibrium conversion in most cases, which is mainly due to the role of steam cost in the objective function.

5.4 Although the kinetics information of water-gas shift reaction may not be accurate for high pressures, the operation beyond 400 psig is seemingly of no particular advantage.

5.5 The concentration of CH_4 and CO in the feed gas is the primary factor affecting the process cost. Adiabatic reactor will be suitable if the concentration of CO in the feed gas is such that the inlet temperature to the reactor is above 700°F, or roughly less than 25% on dry basis.

5.6 The cold quenching system is the most economical system particularly for the gas with high CO concentration. This system not only increases the reaction rate but also reduces the steam cost.

5.7 A major part of the total conversion is achieved in the first stage, but both the first and the last stages of the reactor occupies the largest portion of the overall reactor system.

5.8 From the sensitivity study, the objective function appeared to be somewhat sensitive to the parameters related to the kinetic expression and the character of catalyst pellet, indicating that special care must be exercised in the determination of these parameters.

5.9 Although the steam to gas ratio used in this study is selected rather arbitrarily, its determination is extremely important in the water-gas shift conversion process. Therefore, a more extensive study should be made for the determination of steam to gas ratio in future work.

LITERATURE

1. Aris, R., "Optimal Design of Chemical Reactors," Academic Press, New York, 1961.

2. ASME Boiler and Pressure Vessel Code, Section VIII, Unfired Pressure Vessels, The Americal Society of Mechanical Engineers, New York, 1956.

3. Bellman, R., "Dynamic Programming," Princeton University Press, Princeton, N. J., 1957.

4. Bhavnani, K. H., Chen, K., "Optimization of Time-Dependent Systems by Dynamic Programming," Joint Automatic Control Conference Proceedings, 1966.

5. Bohlbro, H., Acta Chem. Scand. 15, 502 (1961).

6. Bohlbro, H., Acta Chem.,Scand. 17 7 (1963).

7. Chilton, C., "Cost Engineering in the Process Industries," McGraw-Hill, New York, p. 50, 1960.

8. Communication, Girdler Catalyst, Louisville, Ky., April, 1968.

9. Consolidation Coal Company, "Low Sulfur Boiler Fuel Using The Consol CO_2 Acceptor Process," p. B-6, November 1967.

10. Ergun, S., Chem. Eng. Progr. 48, 89 (1952).

11. Gamson, B. W., Chem. Eng. Progr. 47, 19 (1951).

12. Kern, D. Q., "Process Heat Transfer," McGraw-Hill, New York, 1950.

13. Knabel, S. J., Tsaros, C. L., "Process Design and Cost Estimate for a 258 Billion BTU/Day Pipeline Gas Plant-Hydrogasification Using Synthesis Gas Generated by Electrothermal Gasification of Spent Char," p. 20, Institute of Gas Technology, IIT Center, November, 1967.

14. Laupichler, F. G., Ind. Eng. Chem. 30, 578 (1938)

15. Levenspiel, O., "Chemical Reaction Engineering," John Wiley and Sons, Inc. New York, p. 274, 1962.

16. Mars, P., Chem. Eng. Sci. 14, 375 (1961).

17. McCabe, W. L. and Smith, J. C., "Unit Operations of Chemical Engineering," McGraw-Hill, New York, 1956.

18. Moe, J. M., Chem. Eng. Progr. 58, 33 (1962).

19. Norman, W. S., "Absorption, Distillation and Cooling Towers," Longmans, England, p. 327, 1961.

20. Page, J. S., "Estimators' Manual of Equipment and Installation Cost," Gulf , Houston, 1963.

21. Rossini, F. D., et al., "Selected Values of Hydrocarbons," U. S. Department of Commerce, National Bureau of Standards, Washington, D. C., 1947.

22. Ruthven, D. M., "The Activity of Commercial Water-Gas Shift Catalysts," Tripartite Conference, Montreal, Sept. 1968.

23. Seinfeld, J. H. and Lapidus, L., I & EC Process Design and Development, Vol. 7, No. 3, 475 (1968).

24. Ting, A. P. and Wan, S. W., Chem. Eng. May 19, 185 (1969).

25. Treybal, R. E., "Mass Transfer Operations," Second ed., McGraw-Hill, New York, p. 162, 1968.

26. Utility Gas Production General Accounting Procedure, Office of Coal Research, U. S. Department of the Interior, May 20, 1965.

27. Wen, C. Y. and Chang, T. M., Ind. Eng. Chem. Process Design Develop. 7, 49 (1968).

28. Wilke, C. R. and Hougen, O. A., Trans. A.I. Ch. E. 41, 445(1949)

29. Atwood,Kenton, Arnold, M. R., and Appel, E. G., I. & E. C., P. 1600, August, 1950.

NOTATION

a_i	Coefficient
A_1, A_2, A_3	Adiabatic paths in reaction zones of the first, second and third stages, respectively
A_h, A_v, A_T	Heat transfer areas of the heating zone, the vaporizing zone, and the total, respectively [sq.ft.]
B	Baffle spacing [ft.]
C_i, C_b, C_c	Concentration of component i [mole frac.] and concentrations of product gas in bulk of gas phase and at catalyst surface [lb mole/cu. ft.], respectively
C_f	Characterization factor of packing
C_L	Height of a unit compartment [ft.]
C_p, C'_p	Heat capacities of gases and water, respectively [BTU/(lb.°F)]
C_{pim}	Molar temperature-mean heat capacity of component i [BTU/(lb mole, °F)]
d	Characteristic length in the reactor [ft.]
D_a	Axial dispersion coefficient [sq. ft./hr.]
D_{e_1}, D_{e_p}	Effective diffusivity of CO in catalyst pores at 1 atm and at pressure p, respectively [sq.ft./hr]
D_i, D_o, D_s	Inside diameter of tube, equivalent diameter for heat transfer tube, and inside shell diameter of heat exchanger, respectively [ft.]
d_p	Diameter of catalyst pellet [ft.]
E	Activation energy in pseudo first order rate equation [BTU/lb mole]
E_1, E_2, E_3	Equilibrium curves obtainable in the first, second and third stages, respectively
f_i	Fugacity of component i [psi]
F_i^{n-1}, F_i^n	Molar flow rates of component i at (n-1) -th compartment and n-th compartment, respectively [lb mole/hr.]
F_N	Minimum objective function in N-stage process [$/yr]
f_s	Shell side friction factor [sq.ft./sq. in.]

g_c	Gravitational acceleration conversion factor [$(ft.lb_m)/(lb_f hr^2)$]
G	Superficial gas mass velocity [lb./(sq.ft.hr)]
G_i, G_s	Mass velocity in tube side and shell side, respectively [lb/(sq.ft.hr.)]
G_N	Objective function in N-th stage, [$/yr]
$\Delta H, \Delta H_{To}$	Heat of reaction at any temperature and at temperature T_o, respectively [BTU/lb mole CO]
h_i, h_o	Film heat transfer coefficient in inside and outside, respectively [BTU/lb mole CO]
h_p	Fluid-particle heat transfer coefficient [BTU/(sq.ft.hr.°F)]
J, $\bar{J}$	Objective function for a given value of parameter and that at the optimum condition, respectively.
J_H, J_M	Heat transfer factor and mass transfer factor, respectively
k	Reaction rate constant in second order rate equation [hr^{-1}]
k'	Constant related to the packings and fluid flow
k_o	Apparent first order rate constant based on the unit catalyst bed volume [hr^{-1})
k_{a_1}, k_{a_p}	Apparent catalyst activities at 1 atm and at pressure p, respectively [hr^{-1}]
k_c, k_e	Thermal conductivity of catalyst and effective thermal conductivity of catalyst particle, respectively [BTU/(ft.hr.°F)]
k_f	Fluid-particle mass transfer coefficient [ft./hr.]
k_g, k_w	Thermal conductivities of gas and water, respectively [BTU/(ft.hr.°F)]
k_s	Intrinsic catalyst activity based on unit surface area [ft.lb mole/(hr.BTU)]
k_{v_1}	Intrinsic rate constant at 1 atm [hr^{-1}]
K_y	Equilibrium constant based on mole fraction
L, L_H	Lengths of reactor and heat exchanger, respectively [ft.]

M_i	Chemical component of i
n	Constant related to the packings and fluid flow
N_{Pr}	Prandtl number
P	Pressure of the system [psi]
P_{CO}, P_{CO_e}	Partial pressure of CO at any time and at equilibrium, respectively [psi]
ΔP	Pressure drop [psi]
Q	Heat transfer rate in heat exchanger [BTU/hr]
r	Radial distance in catalyst particle [ft.]
R	Gas constant [BTU/(lb mole °R)]
r_{CO}, r'_{CO}	Reaction rate of CO, [lb mole CO/(hr.cu.ft.hr.)] and [cu.ft.CO/(hr.cu.ft.hr.)]
R_d	Dirt factor in heat exchanger
r_s	Reaction rate per unit catalyst particle [lb mole CO/(hr.unit cat.)]
s	Specific gravity
S	Steam flow rate [lb/hr]
S_e	Sensitivity
S_p	Specific surface area of catalyst [sq.ft./lb]
S_v	Space velocity at N.T.P. basis [hr^{-1}]
t	time [hr.]
t_1, t_2	Temperatures of tube side at inlet and outlet, respectively [°F]
T	Temperature [°F][°R]. The subscript denotes the stage number and and the subscript represents the status.
T_1, T_2	Temperatures of shell side at outlet and inlet, respectively [°F]
T_b, T_c	Bulk gas temperature in reactor and surface temperature of catalyst particle respectively [°F]
T_m	Shell side gas temperature at which vaporization of water starts to take place [°F]

T^{n-1}, T^n	Exit temperature of (n-1)-th compartment and n-th compartment, respectively [°F]
T_o	Standard temperature, 77°F
T_s	Temperature of steam [°F]
U	Overall heat transfer coefficient [BTU/(sq.ft.hr.°F)]
U_h, U_v, U_T	Overall heat transfer coefficients for heating zone, vaporizing zone, and whole heat exchanger, respectively [BTU/(sq.ft.hr.°F)]
v,V	Axial mean velocity [ft./hr.] and linear velocity of gas in empty tower [ft./sec.], respectively
V_c^n	Catalyst volume per unit compartment [cu.ft.]
$w, \bar{w}$	Parameters subject to variation and that at a specific value considered, respectively
W	Quenching water [lb/hr]. The subscript denotes the stage number.
W_s	Mass flow rate of gas in shell side [lb./hr.]
W_T	Mass flow rate of water in tube side [lb/hr]
X	Fractional conversion of CO. The subscript denotes the stage number and the superscript represents the status
X_{CO}, X_{CO_e}	Fractional conversion of CO at any time and at equilibrium, respectively
$\bar{Y}_N$	State vector in N-th stage
Z	Height of packing [ft.]

Greek Letters

ε	Voidage of catalyst bed
$\bar{\theta}_N$	Decision vector at N-th stage
η_1	Effectiveness factor at 1 atm
ζ	Internal porosity of catalyst
λ	Latent heat of water [BTU/lb]
μ, μ_w	Viscosity of gas and water, respectively, [lb/(ft.hr.)]
μ_o	Viscosity of water at tube-wall temperature [lb/(ft.hr.)]

ν_i	Stoichiometric coefficient for component i
ρ, ρ_p	Densities of gas and catalyst particle, respectively [lb/cu.ft.]
χ_i	Fugacity coefficient of component i
ϕ_1	Thiele modulus at 1 atm

Page Intentionally Left Blank